The effect of controlled rheology on the evolution of chemical composition distribution of commercial heterophasic ethylene propylene copolymers (HEPCs)

by

Sifiso Magagula

Thesis presented in partial fulfilment of the requirements for the degree of
Doctor of Philosophy (Polymer Science)

At the

University of Stellenbosch

Supervisor: Prof. A.J. van Reenen March 2020

Declaration

By submitting this thesis electronically, I declare that the entirety of the work contained therein is my own, original work, that I am the sole author thereof (save to the extent explicitly otherwise stated), that reproduction and publication thereof by Stellenbosch University will not infringe any third party rights and that I have not previously in its entirety or in part submitted it for obtaining any qualification.

Sifiso Innocent Magagula March 2020

Abstract

The vis-breaking of heterophasic ethylene-propylene copolymers (HEPCs) is an important industrial process. While the changes in molar mass properties are easy to track using high-temperature size exclusion chromatography (HT-SEC) before and after vis-breaking, changes in the chemical composition are much more challenging due to the complex chemical composition resulting from different ethylene contents and ethylene block lengths. The present work tracks the microstructural changes of three samples with 0 – 10.8 mol.% ethylene content before and after vis-breaking with the aid of molar mass and chemical composition sensitive chromatographic techniques. Bulk sample analyses indicated that the rubber phase, which is ethylene rich was essential in aiding peroxide mobility during vis-breaking as indicated by the narrower dispersities and lower peak molar masses with increasing ethylene content. Preparative temperature rising elution fractionation (p-TREF) and solvent gradient elution fractionation (SGEF) were used to fractionate the non vis-broken and vis-broken HEPC bulk samples into several fractions for further analyses. Upon vis-breaking, the SGEF fractions with high molar mass were observed to diminish after vis-breaking. Furthermore, the increase in ethylene content was observed to reduce the impact of the peroxide on the fraction quantities before and after vis-breaking implying that vis-breaking affects more the polyolefin chains with more PP segments and less those with more ethylene co-monomer. However, SGEF may not be suitable for the fractionation of mixtures of homopolymer and copolymers due to the different solubilities in the solvent/non-solvent mixtures. Furthermore, *in-situ* solid state NMR experiments revealed the greater sensitivity of copolymers containing short ethylene sequences to peroxide degradation. Long chain ethylene sequences were found to be resistant to radical degradation.

Acknowledgements

First and foremost, I would like to thank the almighty God for life and guidance throughout this study

My utmost gratitude also goes out to my supervisor, Prof. A.J. van Reenen for giving me the opportunity to study in his group, for financial support and encouragement throughout the course of this study.

My most sincere gratitude also goes out to the following individuals and organizations:

Drs Anthony Ndiripo and Paul Bungu for their help with HT-HPLC and HT-SEC analyses.

Dr Jaco Brand and Mrs Elsa Malherbe for their help with solution-state NMR analyses.

Miss Megan Matthews for help with room and variable temperature solid-state NMR analyses.

All members and staff of the Department of Chemistry and Polymer science.

Olefins group members.

Dr Divann Robertson for the educative and enlightening discussions we have had.

Dr Richard Thompson for hosting and giving me access to his lab during my visit at Durham University, UK.

Drs Carl Reynolds and Stephen Boothroyd at Durham University, UK for their help with rheometer measurements.

The Newton Fund PhD Exchange programme for giving me the opportunity to visit Durham University, UK.

SASOL for funding

Table of contents

List of figures

List of tables

List of abbreviations

2D-LC	2-dimensional-liquid chromatography
AFM	Atomic force microscopy
ATR	Attenuated total reflectance
A-TREF	Analytical temperature rising elution fractionation
ATR-FTIR	Attenuated total reflectance-Fourier transform infrared
BHT	Butylated hydroxytoluene
CEF	Crystallization elution fractionation
CPMAS	Cross polarization and magic angle spinning
CRYSTAF	Crystallization analysis fractionation
DMA	Dynamic mechanical analysis
DSC	Differential scanning calorimetry
ELSD	Evaporative light scattering detector
EPC	Ethylene-propylene copolymers
EPR	Ethylene-propylene rubber
FE-SEM	Field emission scanning electron microscopy
FTIR	Fourier transform infrared spectroscopy
GC	Gas chromatography
HDPE	High density polyethylene
HEPC	Heterophasic ethylene-propylene copolymer
HPLC	High performance liquid chromatography
HT-2D-LC	High temperature 2-dimensional liquid chromatography
HT-HPLC	High temperature high performance liquid chromatograph
ICP	Impact copolymer
iPP	Isotactic polypropylene
IR	Infra-red
LCB	Long chain branching
LDPE	Low density polyethylene
LLDPE	Linear low density polyethylene
MFR	Melt flow rate

MM	Molar mass
MMD	Molar mass distribution
M_n	Number average molecular weight
M_w	Weight average molecular weight
NMR	Nuclear magnetic resonance
Đ	Dispersity
PE	Polyethylene
PET	Poly(ethylene terephthalate)
PP	Polypropylene
PS	Polystyrene
P-TREF	Preparative temperature rising elution fractionation
PVC	Poly(vinyl chloride)
RI	Refractive index
SCALLS	Solution crystallization analysis by laser light scattering
SEC	Size exclusion chromatography
SEC-FTIR	Size exclusion chromatography coupled to Fourier transform infrared spectroscopy
SEM	Scanning electron microscopy
SGIC	Solvent gradient interaction chromatography
TCB	1,2,4 - Trichlorobenzene
TCE	Tetrachloroethylene
TCE-d_2	Deuterated 1,1,2,2 - tetrachloroethane
TEM	Transmission electron microscopy
TFA	Turbidity fractionation analysis
T_g	Glass transition temperature
T_m	Melting temperature
TREF	Temperature rising elution fractionation
XRD	X-ray diffraction
ZN	Ziegler-Natta

Chapter 1

Introduction and overview

This chapter gives a brief introduction on heterophasic copolymers, an outline of the chapters in this manuscript and a short description of what each chapter entails.

1.1 Introduction

Polyolefins are by far the biggest class of plastics world-wide. Among these, polypropylenes (PPs) and polyethylenes (PEs) have been reported as the world's leading polyolefins in terms of market size. Polyolefins account for more than 55 % of the global plastics in demand and the market grows by 5-6 % every year. The biggest contributors to this are the good physical and mechanical properties, non-toxicity, energy efficient production, low cost and availability of their raw materials [1, 2]. Over the years, the demand on these materials has led to an exponential increase in their world production. Between 1950 and 2015 alone, the world production of polyolefins increased from 1.5 million metric tonnes to 322 million metric tonnes with a recorded compound growth rate of 8.6 % per year [3].

Despite the widespread use of plastics, the greatest danger lies in their threat to the environment. Litter continues to be a major problem in our streets, roadsides, countryside and seas. The cost of cleaning is very high: the cost of sweeping one ton of litter from the streets is nine times more than that of collecting it from household bins. It has been reported that plastics account for about 7 % by mass and 11 % by volume of all waste. Other materials account for the bulk of the waste. Paper has been reported to account for about 38 % of the waste stream. Therefore, this shows that replacing plastics with other materials such as paper will only result in an increase of solid waste and food wastage since it will not be protected by plastic packaging. The use of biodegradable plastics in the place of conventional plastics such as polyethylene has also proven to be expensive. Polyolefins are generally non-toxic and unreactive if used properly. They do not generate any toxic substances during their manufacture. Even when they are discarded after use, these plastics do not form toxic substances that will affect groundwater or the atmosphere. However, the greatest danger that plastic pose to the environment is the accidental suffocation of young children and ingestion by livestock and marine animals [4-6]. The simplest remedy to this problem lies in education and awareness. Educating our society about disposing of plastics in an environmentally friendly manner where they can be re-used, recycled or otherwise safely landfilled. Thus creating awareness that it is the ultimate responsibility of every individual to create a safe environment for all is necessary [7].

Even though as a result of public sentiment, the polyolefin market is under a threat, PP has remains an important material and has the highest production rate of all the polyolefins. The reason for this is that PP has good stiffness, melts at high temperatures, has a high yield

strength, is resistant to chemicals and has excellent moisture barrier properties [1, 8, 9]. However, one major setback for PP is its limited impact resistance at low temperatures [9]. In order to counteract this major drawback, ethylene copolymers are usually added to the PP matrix and this gives rise to a class of polyolefins known as heterophasic ethylene-propylene copolymers (HEPCs). HEPCs are a class of in-reactor alloys which largely consists of a PP homopolymer phase interspersed with ethylene-propylene rubber (EPR) particles. However, due to the nature of the production process, HEPCs also contain small portions of PE homopolymers and amorphous PP. HEPCs are usually produced via a two-stage sequential polymerization procedure in the presence of a Ziegler-Natta catalyst. In the first stage, the PP homopolymer matrix is produced and then passed into the second stage where the EPR phase with different ratios of ethylene and propylene is introduced to produce the final product.

Ever since their discovery towards the end of the 1970s, HEPCs have experienced an exponential increase in terms of market size over conventional PPs. Over time HEPCs have gained usefulness in a wide range of applications ranging from trivial packaging uses to complex technical uses [9]. This is due to their good impact/stiffness performance properties, good aesthetic properties and a good creep resistance [10]. However, one major drawback has traditionally been that HEPCs could not be used for making injection moulded products like housewares, buckets, automotive parts and packaging material because of poor processability. In order to improve the processability of these materials, two methods are often used: in-reactor modification and post-reactor modification methods. In-reactor modification is when the polymer is modified whilst inside the reactors during production. This normally involves improvement of reactor technology and development of new catalysts to produce the desired product. Post-reactor modification on the other hand is when the polymer is modified outside the reactors after production. While both methods are effective, the in-reactor modification method is much more expensive than the post-reactor method. This leaves most industries with the option of the post-reactor method. This method encompasses a few technologies to choose from and one of the cheapest methods commonly used is chemical modification or degradation by the use of peroxides [9].

Peroxide-induced degradation, also known as vis-breaking or controlled rheology is a process often used to increase the flow properties of PP [9]. Due to the increasing demand on HEPCs, most industries have started using vis-breaking as a means of increasing the flow properties of HEPCs. However, the difference between PPs and HEPCs lies in the complexity of the chemical composition of the latter. It is a fact that vis-breaking leads to a significant loss of

impact properties in HEPCs and this therefore has led to a lot of interest in the investigation of how vis-breaking affects the chemical composition of HEPCs [11-13].

During the vis-breaking process, a suitable peroxide is added to the polymer in the presence of heat. The heat initiates the formation of radicals which will attack the polymer chains in a random fashion. The resultant polymer will have a higher MFR and a narrower molecular weight distribution (MWD) than the parent polymer. In addition to that, controlled rheology reactor grades have improved processing properties over conventional reactor grades in that [14]:

- they require less injection pressure to fill the mould due to their low viscosity,
- they require a lower melting temperature to achieve the same viscosity as the conventional grade,
- their cycle times are about 10 -15 % less,
- they have less warpage on de-moulding,
- they have improved pigment/colour mixing at any given temperature due to the decreased viscosity and better flow at that temperature,
- their narrower MWD shows minimal differences parallel to or across the flow direction, and
- due to their low injection pressure, a machine with a lower clamping force can be used on them.

HEPCs are commercially important materials, and the fundamental understanding of the processes and chemistry that affects the macroscopic properties of these materials needs to be expanded. Most of the work that has been done on the vis-breaking of HEPCs has been focused on the effect that the vis-breaking process has on the molecular characteristics of these complex materials [11-13]. From these studies, it has been reported that chemically similar yet structurally different peroxides affect the molecular make-up of HEPCs differently [10, 12, 15]. However, none of these studies have investigated how changing chemical composition distribution (CCD) affects the action of the peroxides used during the vis-breaking process.

1.2 Aims

The main aim of the project is to investigate the effect of cyclo-aliphatic peroxides on the various components of HEPCs at different ethylene contents and the effect that the changing CCD has on the action of the peroxides. The information obtained would help to correlate any changes in mechanical properties (especially hardness and impact resistance) to the changes in

chemical composition distribution of these complex copolymers (although the latter falls outside the scope of this study, but will shed additional light on previous studies [10, 15]).

1.3 Objectives

1. To vis-break HEPCs of different co-monomer content to the same degree using the same type of peroxide.
2. To investigate the effect of the degree of vis-breaking on molar mass, molar mass distribution and CCD using advanced analytical techniques such as high temperature-size exclusion chromatography (HT-SEC), differential scanning calorimetry (DSC), high temperature high performance liquid chromatography (HT-HPLC), carbon-13 nuclear magnetic resonance (^{13}C NMR) and Fourier transform infrared spectroscopy (FTIR).
3. To fractionate the HEPCs before and after vis-breaking using preparative temperature rising elution fractionation (p-TREF) and preparative molar mass fractionation (p-MMF).
4. To analyse the fractions for changes in molar mass and chemical CCD using the analytical tools mentioned in objective 2.
5. To use variable temperature solid-state ^{13}C NMR to investigate the reaction of the peroxide with the HEPCs *in-situ*.
6. Correlate all the results obtained with the analytical techniques mentioned in objective 2 with the changes observed in the solid-state ^{13}C NMR results.

1.4 Dissertation outline

Chapter 2

This chapter provides a more detailed background information on heterophasic copolymers, their vis-breaking and work done on the characterization of vis-broken heterophasic copolymers using different analytical techniques.

Chapter 3

This chapter focuses on providing detailed information about the materials analysed, the experimental procedures as well as the characterization techniques used in this study.

Chapter 4

Chapter 4 reports on the characterization of the bulk heterophasic copolymers before and after vis-breaking.

Chapter 5

The main emphasis of chapter 5 is to report results on the characterization of the heterophasic copolymer fractions obtained by molar mass fractionation (MMF) and preparative temperature rising elution fractionation (P-TREF).

Chapter 6

Chapter 6 reports mostly on the variable temperature solid-state ^{13}C-NMR results obtained before and after vis-breaking of the heterophasic copolymer bulk samples and fractions.

Chapter 7

This chapter gives an overall summary based on the results discussed in Chapters 4, 5 and 6.

1.5 References

1. Kaminsky, W., *Trends in polyolefin chemistry.* Macromolecular Chemistry and Physics, 2008. **209**(5): p. 459-466.

2. Hilken, G., *Zukunft der Kunststofferzeugung in Deutschland, Europa und in der Welt.* Kunststoffe, 2005. **10**: p. 34-40.

3. Group P.E.M.R., *Consultic Marketing & Industrieberatung GmbH.* World Plastics Production, 1950. **2011**.

4. Anderson, Z.T., Cundy, A. B., Croudace, I. W., Warwick, P. E., Celis-Hernandez, O., Stead, J. L., *A rapid method for assessing the accumulation of microplastics in the sea surface microlayer (SML) of estuarine systems.* Scientific Reports, 2018. **8**(1): p. 9428.

5. Maes, T., Jessop, R., Wellner, N., Haupt, K., Mayes, A. G., *A rapid-screening approach to detect and quantify microplastics based on fluorescent tagging with Nile Red.* Scientific Reports, 2017. **7**: p. 44501.

6. Sheavly, S., Register , K., *Marine debris & plastics: environmental concerns, sources, impacts and solutions.* Journal of Polymers and the Environment, 2007. **15**(4): p. 301-305.

7. Moffet, J., Bregha, F., Middelkoop, M. J., *Responsible care: a case study of a voluntary environmental initiative.* Voluntary codes: Private governance, the public interest and innovation, 2004: Carleton Research Unit for Innovation, Science and Environment, p. 177-208.

8. Razavi, A., Thewalt, U., *Site selective ligand modification and tactic variation in polypropylene chains produced with metallocene catalysts.* Coordination Chemistry Reviews, 2006. **250**(1-2): p. 155-169.

9. Gahleitner, M., Jääskeläinen, P., Ratajski, E., Paulik, C., Reussner, J., Wolfschwenger, J., Neißl, W., *Propylene–ethylene random copolymers: Comonomer effects on*

crystallinity and application properties. Journal of Applied Polymer Science, 2005. **95**(5): p. 1073-1081.

10. Swart, M., *The effect of controlled degradation with an organic peroxide on the molecular characteristics and properties of heterophasic propylene-ethylene copolymers (HECO)*. 2013, PhD Thesis, University of Stellenbosch.

11. Sheng, B.-R., Zhang, Y.-q., Xu, J.-t., Wang, H.-t., Feng, L.-x., *Influences of molecular weight and crystalline structure on fracture behavior of controlled-rheology-polypropylene prepared by reactive extrusion.* Polymer Degradation and Stability, 2008. **93**(1): p. 225-232.

12. Swart, M., Van Reenen, A. J, *The effect of controlled degradation on the molecular characteristics of heterophasic ethylene–propylene copolymers.* Journal of Applied Polymer Science, 2015. **132**(14).

13. Phiri M. J., Pasch, H., *Exploring the Compositional Heterogeneity of Vis-Broken Impact Poly(propylene) Copolymers by Advanced Fractionation Methods.* Macromolecular Chemistry and Physics, 2016. **217**(6): p. 783-793.

14. Kent, R., *Energy efficiency in plastics Processing*. *Practical worksheets for industry*. 2007, Tangram Technology Ltd.

15. Magagula, S. I., *The effect of organic peroxides on the molecular composition of heterophasic ethylene-propylene impact copolymers*. 2015, Masters Thesis, Stellenbosch University.

Chapter 2

Historical and literature review

This chapter gives a brief background information on heterophasic copolymers and the vis-breaking process. It further gives a brief overview on some of work done on heterophasic copolymers using different analytical techniques.

2.1 Introduction: A brief history of heterophasic copolymers

The revolutionary discovery of low pressure polymerization in the early 1950s led to the discovery of high density polyethylene (HDPE; by Hoechst in Germany) and isotactic polypropylene (iPP; by Montecatini in Italy) [1]. Even though these polymers showed good stiffness and heat resistance properties, their toughness and impact resistance were still an issue. Improving the toughness and impact resistance of HDPEs was easier because the glass-transition temperature (Tg) of polyethylene (PE) was not the limiting factor of their application range. Therefore the random copolymerization of HDPEs with higher α-olefins such as 1-butene or 1-hexene resulted in the desired improvement. However, for iPP, a different approach had to be found because the polymer's Tg of about 0 °C prevented its application in sub-zero environments. It was later discovered that the dispersion of certain amounts of elastomeric materials in the iPP matrix served the purpose. This led to a new revolution aimed at the development of polypropylene.

The first attempt towards the development of iPP used a post-reactor modification process called compounding. Here, different amounts of externally produced elastomers, such as ethylene-propylene rubbers (EPRs) or ethylene-propylene-diene elastomers (EPDMs) based on vanadium catalysts were mixed with the iPP homopolymers. The compounding process lasted until the mid-1960s [2, 3]. During this time, the slurry-type processes that were used made it difficult to produce propylene-based copolymers with low crystallinities. However, the introduction of multi-reactor gas-phase polymerization processes after the 1960s such as the Novolen [4], Spheripol [5] and Borstar [6] processes led to the production of efficient and performance-based copolymers, also referred to as heterophasic copolymers or PP impact copolymers. Figure 2.1 shows a simplified representation of a heterophasic copolymer. In these multi-reactor gas-phase polymerization processes, a crystalline PP matrix (produced in the first one or two reactors) was embedded with particles of EPR and PE (produced in one or more of the following reactors) to improve the low temperature impact resistance of PP [7].

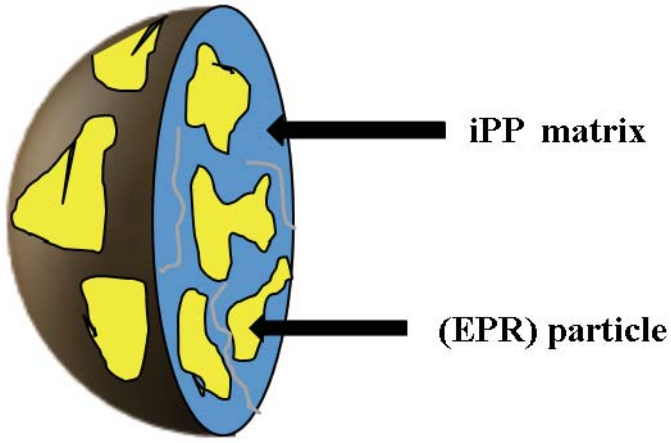

Figure 2.1 A simplified representation of a heterophasic copolymer.

Up to this time, it was very clear that the two decisive factors for the further development of heterophasic copolymers were both the flexible polymerization processes and continuously improved catalysts. For example, the use of second-generation Ziegler-Natta (ZN) catalysts which consisted of solid $TiCl_3$ and $Al(C_2H_5)_2Cl$ made the production of technical copolymers with a moderate EPR content possible. However, the introduction of third-generation ZN catalysts (*i.e* $MgCl_2$-supported $TiCl_3$ with ester-type internal donors), together with the breakthrough of solvent-free bulk polymerizations finally made the production of heterophasic copolymers with high impact strengths possible [8, 9].

2.2 Manufacture of heterophasic copolymers

Heterophasic copolymers are usually produced in a series of reactors in the presence of a ZN catalyst. A variety of reactor technologies can be used in the production of heterophasic copolymers and some of these include: Spherizone® (LyondellBasell), Unipol (Dow Plastics), Innovene® (Ineos), Novolen®, Spheripol (LyondellBasell) and Borstar (Borealis). Some of these technologies are gas-phase only and others are a combination of bulk and gas-phase. Figure 2.2 is an illustration of one of the reactor technologies (Novolen®) used in the production of heterophasic copolymers.

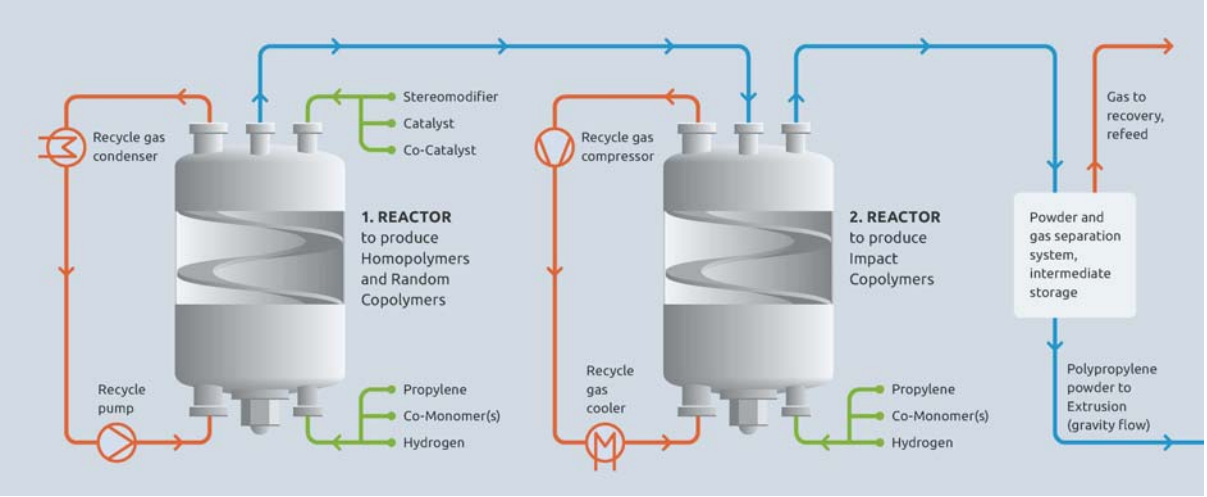

Figure 2.2 An illustation of the Novolen® technology used to produce heterophasic copolymers [10].

Regardless of the reactor technology used, the production of heterophasic copolymers requires at least two reactors. The reactors must be arranged in a specific in-series configuration. This is so that homopolymerization can take place in the first reactor and then copolymerization in the second reactor. This is also to facilitate the formation of a link between the homopolymer and copolymer phase produced. This link serves as a major contributor to the advanced properties of these in-reactor alloys. During the polymerization process, chain termination is usually achieved by introducing hydrogen into the system. This not only controls the average molar mass but the melt flow rate of the polymer as well.

For heterophasic copolymers, the ability to control the copolymer content is of utmost importance. Since the copolymer percentage in the final product depends on the production rate in the second reactor, it is usually controlled by the addition of an activity control agent. The control agent slows down the catalyst activity towards ethylene. This therefore controls the ethylene content and therefore the relative ratio of ethylene to propylene present in the second reactor.

2.2.1 Ziegler-Natta catalysis of heterophasic copolymers

Generally, a ZN catalyst is a multi-sited catalyst consisting of a metal compound which has a metal-carbon bond capable of allowing repeated insertions of an olefin unit [11]. A typical ZN catalyst system consists of: a $MgCl_2$ support, $TiCl_3$ or $TiCl_4$, aluminium alkyl co-catalyst (AlR_3), external and internal donors. The function of the external donors is to control the tacticity of PP whereas that of the internal donors is to control the distribution of $TiCl_3$ on the $MgCl_2$ support surface [12]. During polymerization, the exchange that occurs between the halogen atom of the $TiCl_3$ compound and the co-catalyst facilitates the formation of specific

active centres on the catalyst particle [13]. Such an exchange is illustrated by equation 2.1 below:

$$[TiCl_3] + [AlR_3] \rightarrow [Cl_2TiR] + AlR_2Cl \qquad \text{Eq 2.1}$$

When it comes to the mechanism of a ZN catalysed polymerization process, a number of models have been proposed [14-17]. However, the most common one up to now is the one proposed by Cossee [18, 19] and Arlman [20]. The model is divided into two steps. The first step involves the coordination of the monomer parallel to the metal-carbon bond (labelled as step (i) in Figure 2.3 below). The second step involves the chain migratory insertion of the monomer unit between the catalyst metal atom and the last carbon of the growing polymer chain (labelled as step (ii) in Figure 2.3 below).

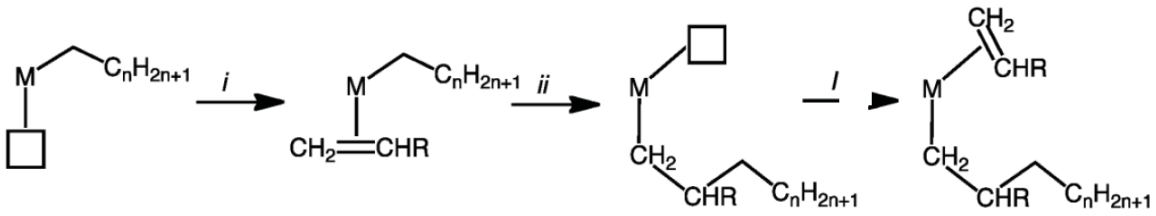

Figure 2.3 An illustration of the mechanism of a ZN catalysed polymerization process proposed by Cossee and Arlman[10, 21].

During ZN catalysis of heterophasic copolymers, tacticity, stereoregularity, co-monomer distribution and molar mass in the PP and EPR microstructures are usually governed by the interactions between components of the ZN catalyst system. As far as co-monomer and molar mass distributions are concerned, copolymers produced by means of a ZN catalyst exhibit a homogenous intramolecular sequence distribution as well as a heterogenous intermolecular distribution [22]. In any particle-forming polymerization process, the morphology of the polymer particles produced replicate the morphology of the catalyst used. The catalyst particle morphology is usually described in terms of particle shape, size, distribution and porosity. Uniform globular or spherically shaped catalyst particles are usually used because of their ability to produce free-flowing polymer particles. For PP catalysts, like ZN catalysts, active catalytic components are mobilized on spherical aggregates of a microcrystalline $MgCl_2$ support material which offers a spherical, porous structure with a large surface area [5, 7]. The amount of elastomer that can be in the polymer particle is governed by the porosity of the catalyst particle. This shows that the porosity and therefore the morphology of the ZN catalyst plays a crucial role in the production of heterophasic copolymers.

2.3 Proposed particle growth models of heterophasic copolymers

During any polyolefin polymerization, every single polymer granule obtained is a product of each catalyst particle fed at the beginning of the reactor train. However, the mechanism through which these polymer granules are made is still a mystery. Over the years, numerous studies have been conducted on the polymerization kinetics [23-25] and morphological developments of PP [26-35], which has led to the evolution of a number of particle growth models. However, the mechanisms involved and number of active catalyst sites for polymerization differ from model to model. In spite of all the disagreements, there is still some common ground of agreement in each model. They all agree that the morphology of the PP particle is a replica of that of the original catalyst. It is also agreed that the iPP granules are porous. They consist of firmly bonded small polymeric structures called “micro-particles”. Each of these micro-particles contains a fragment of catalyst inside and are separated by micro-pores (See Figure 2.4).

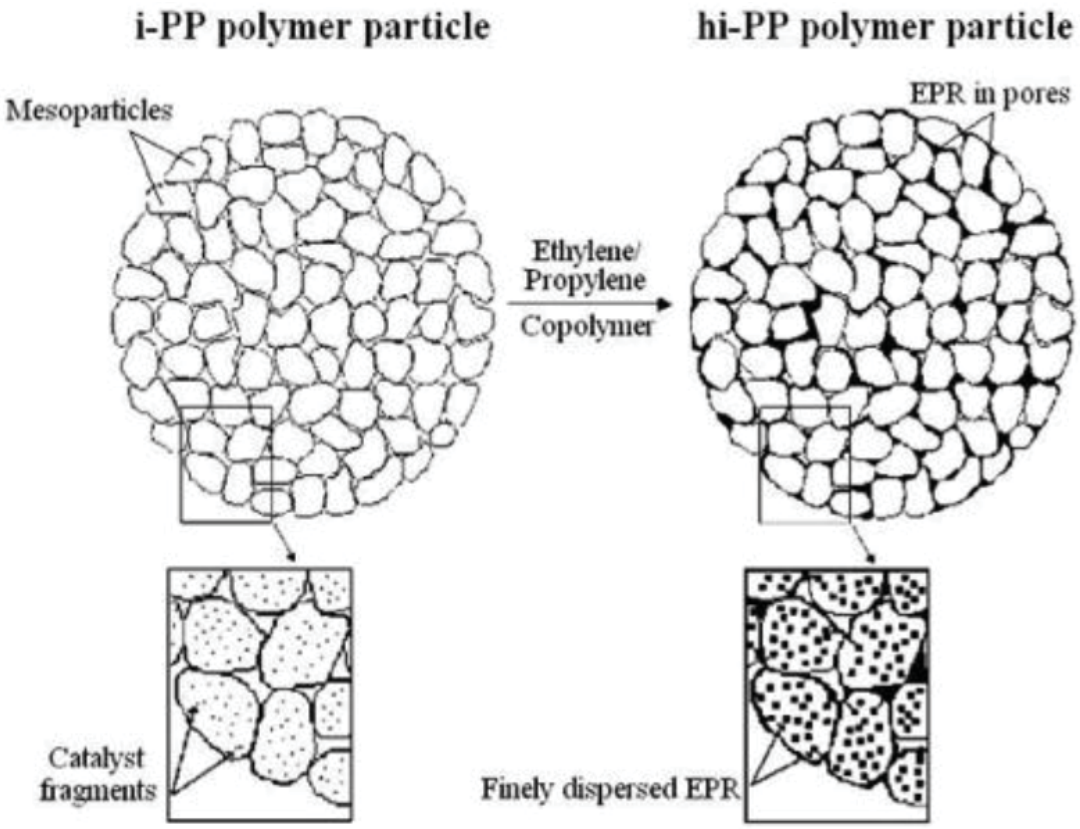

Figure 2.1 A graphic representation of the heterophasic copolymer particle growth model as described by Urdampilleta et al [36]

In addition to the PP studies, a few other studies were also conducted on the morphological developments of heterophasic copolymers [10, 36-40]. These studies had the same agreements and disagreements as the PP studies with regards to the mechanism behind the development of

the PP granule. However, their main focus was on the development and distribution of the copolymer phase. From these studies, it was established that the porosity of the iPP granules before the introduction of ethylene plays a crucial role in the development and distribution of the copolymer phase. It was reported that upon addition to the PP homopolymer matrix, the copolymer phase is dispersed within the pre-existing voids of the PP homopolymer particles (See Figure 2.4). However, it was discovered that for a PP homopolymer of low porosity, the copolymer phase prefers external surface coverage over internal pore filling. On the other hand, for a homopolymer with sufficient porosity, the copolymer phase was found to prefer internal pore filling over external surface coating, resulting in the appearance of grainy structures throughout the homopolymer particle. For the first time Botha *et al* [10] showed that the reactor technology also has an effect on the morphological development of heterophasic copolymers. Even though their technologies used the same ZN catalysts, products with different characteristics were obtained. This shows that the catalyst morphology and the morphology of the homopolymer prior to the introduction of ethylene are not the only factors affecting the development and dispersion of the copolymer phase. The type of reactor technology used has a crucial role to play as well.

2.4 Vis-breaking or controlled degradation

The flexibility of product design during the multi-stage polymerization processes combined with the possibility of post-reactor modification has led to the production of heterophasic copolymers with a wide range of application segments, such as in packaging, automotive, or infrastructure. In the packaging industry, injection moulding and cast or blown films are very important and these require the use of polymers with very high MFRs. Nowadays, the automotive industry also requires the use of polymers with very high MFRs to produce parts with a reduced weight and thickness for the production of light weight vehicles [41].

In order to get heterophasic polymers with a high MFR, two methods can be implemented. One is to modify the polymer whilst in the reactors (in-reactor modification) and the other could be to modify it after the polymerization process outside the reactors (post-reactor modification). In-reactor modification is a bit of a challenge, partly because heterophasic copolymers with high MFRs e.g MFR > 40 g/10 mins are difficult to produce directly by polymerization with a ZN catalyst system. This is because the matrix polymer (the PP homopolymer) of the heterophasic copolymer needs to have a MFR that is 50 to 100 % higher than that of the final heterophasic copolymer. This means very high hydrogen concentrations have to be used in the

polymerization of the matrix polymer resulting in higher costs. A matrix polymer with a high MFR is also brittle and this could have a negative impact on the final properties of the product [36]. The best way to achieve high MFRs is by post-reactor modification which usually requires chemical treatment with an organic peroxide *i.e* vis-breaking or controlled rheology of a molten heterophasic copolymer. In this case, the effect of the vis-breaking process on the properties of the polymer is controlled by two main factors, the residence time and half-life of the peroxide [42].

Residence time is the time taken by the material in the extruder or processing chamber and is determined by the extruder's throughput and free volume. Half-life on the other hand is defined as the time taken for 50 % of the peroxide to be consumed and is controlled by the specific temperature at which the extruder is operated and the type of peroxide used. Longer half-lives and higher or lower decomposition temperatures improve the control of the reaction and at the same time have an influence on the product quality and safety. It is, therefore, important to understand the effect of a specific peroxide on the molecular properties of the polymer. This will help in predicting the amount of peroxide needed to achieve specific properties.

2.4.1 Vis-breaking of PP

The vis-breaking of PP can either be done by heat or with the use of organic peroxides. In both cases, the long molecular chains are broken down into shorter ones (β–scission) resulting in a narrow MMD and a decrease in molar mass (see Figure 2.5 below). The narrow MMD and decrease in molar mass improves the flowability and increases the MFR of the final product. In the case of peroxide induced vis-breaking, the MFR is linearly dependent on the concentration of the peroxide used hence the term controlled rheology is used. The changes in MMD and molar mass experienced during vis-breaking have an effect on the mechanical properties of the final PP product. Vis-broken PP or PP random copolymers tend to exhibit lower stiffness (tensile and flexural modulus) and slightly better impact properties when compared to a non vis-broken PP or PP random copolymer with the same MFR [43].

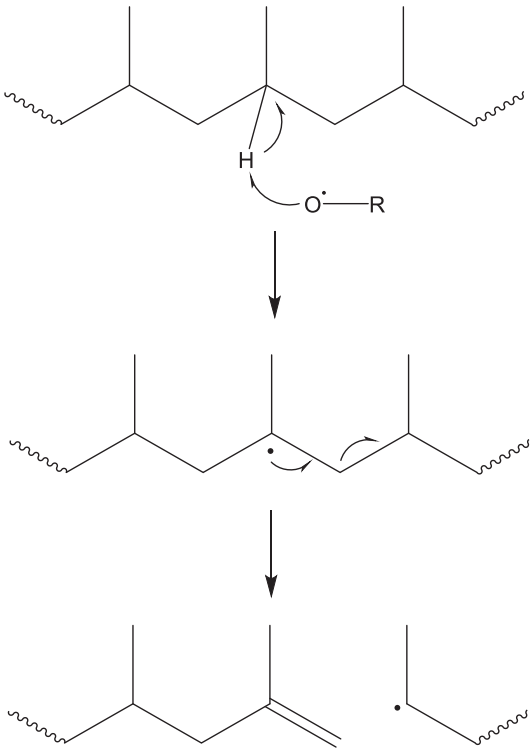

Figure 2.2 An illustration of the mechanism pathway followed by the vis-breaking of PP.

2.4.2 Vis-breaking of PE

During vis-breaking, PE or PE random copolymers are usually crosslinked by the peroxide (as illustrated in Figure 2.6). This leads to an increase in molar mass and therefore a drop in MFR. It is usually defined either in terms of gel formation or lack of flowability [43].

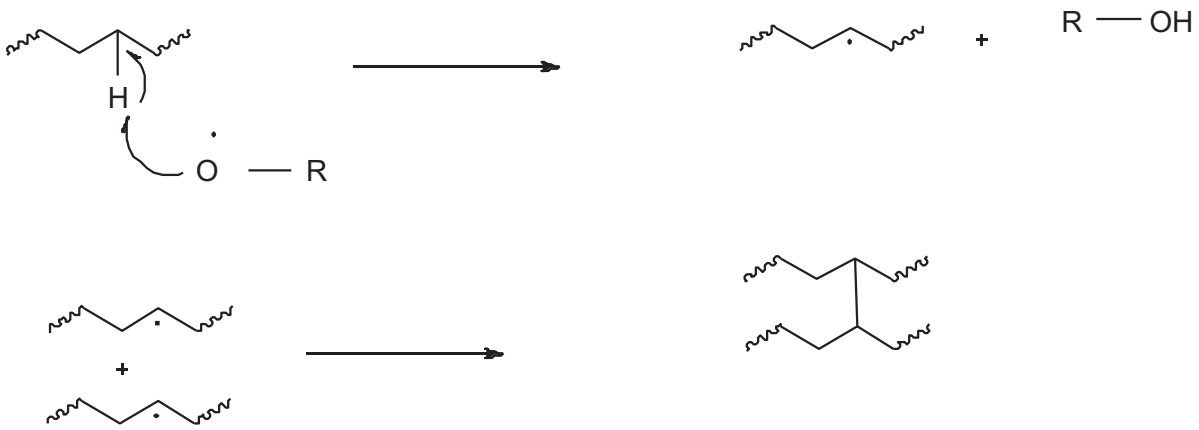

Figure 2.3 A scheme of the mechanism for polyethylene peroxide crosslinking [44].

2.4.3 Vis-breaking of heterophasic copolymers

Vis-breaking of heterophasic copolymers is much more complicated because of their complex CCD comprising of amorphous rubber, semi-crystalline ethylene-propylene copolymers and PP homopolymer components. In order to achieve a higher MFR, both the matrix polymer and

rubber should decrease in molar mass. However, this is not possible as some of the PE random copolymers may undergo crosslinking, resulting in flow problems and gel formation. This will in turn have adverse effects on the mechanical properties, resulting to a decrease in stiffness and impact resistance.

The vis-breaking of heterophasic copolymers to a given MFR requires more peroxide than during the vis-breaking of homopolymers. This is to counteract the crosslinking reactions encountered by the ethylene copolymers present in the polymer. Increasing the amount of peroxides used has an effect on the CCD of heterophasic copolymers. This increases the amount of amorphous material in the final product [43]. Therefore, more research needs to be done to study the exact effects of peroxides on the molecular properties of heterophasic copolymers. This could be a solution to the problems encountered in balancing the need for high melt flow polymers with the necessary properties required.

2.5 Temperature rising elution fractionation (TREF) of heterophasic copolymers

Temperature rising elution fractionation (TREF) is an analytical technique that fractionates semi-crystalline polymers based on their chain crystallizabilities [45-47]. The polymer chain crystallizability is usually influenced by the chain's microstructure. Therefore, TREF can be useful in predicting the CCD of copolymers and tacticity distributions of homopolymers [48]. This information is crucial for understanding polymerization mechanisms and constructing structure-property relationships.

The principle of polymer fractionation by crystallizability is best defined by the Flory-Huggins equation. This equation accounts for the decrease in equilibrium melting temperature of the polymer which is influenced by the type of solvent used and the number of chain segments present as shown by equation 2.2 below [49, 50]:

$$\frac{1}{T_m} - \frac{1}{T_m^0} = \frac{R}{\Delta H_u}\frac{V_u}{V_1}\left[-\frac{\ln v_2}{x} + \left(1 - \frac{1}{x}\right)v_1 - x_1 v_1^2\right], \qquad \text{Eq 2.2}$$

where T_m^0 is the melting temperature of the pure polymer, T_m is the equilibrium melting temperature of the polymer in solution, ΔH_u is the heat of fusion per repeating unit, V_u and V_1 are the molar volumes of the polymer repeating unit and diluent, v_1 and v_2 are the volume fractions of the diluent and polymer, x is the number of segments, and x_1 is the Flory-Huggins thermodynamic interaction parameter.

The TREF experiment involves two main steps: crystallization and elution and can be operated in either of two modes: analytical (A-TREF) or preparative (P-TREF) modes. These two modes

differ in the elution step and the size of sample used [48]. Table 2.1 below gives a comparison of the characteristics of both modes.

Table 2.1 Comparisons between analytical and preparative temperature rising elution fractionation (A-TREF and P-TREF) [47]

A-TREF	P-TREF
1. Fractions are continuously collected by gradually increasing the elution temperature.	1. Fractions are collected at predetermined temperature intervals. Continuous operation is less commonly used.
2. Information on macromolecular structure is obtained on-line by means of a calibration curve.	2. Information on macromolecular structure is obtained off-line by additional analytical techniques such as ^{13}C-NMR, DSC, HT-SEC, HT-HPLC etc.
3. Requires smaller columns and smaller sample sizes.	3. Requires larger columns and larger polymer sample sizes.
4. Faster than P-TREF but generates less information about polymer microstructure.	4. Time-consuming but can generate detailed information about polymer microstructure.

During the TREF experiment, the polymer is first dissolved in a good solvent at high temperature. The polymer solution is then transferred into glass reactors containing an inert support, such as glass beads or sea sand. The temperature in the column is then decreased at a slow, constant cooling rate (CR) by means of a programmed temperature controlling unit. In both A-TREF and P-TREF, the CR has to be slow enough to ensure efficient polymer fractionation. This allows the polymer chains to crystallize on the inert support in an “orderly” fashion, from higher to lower crystallizabilities i.e from lower to higher co-monomer contents. Consequently, an onion-like layered polymer structure forms around the inert support (see Figure 2.7) and this concludes the crystallization step. The crystallization step is the most important step because most of the polymer fractionation occurs here. After the crystallization step, the polymer-coated support is introduced into the TREF elution column (see Figure 2.9) for the elution step to begin. During the elution step, pure solvent is pumped through the column as the temperature is increased at predetermined temperature intervals. The solvent dissolves back each layer on the onion-like structure depending on the dissolution temperature reached at each predetermined temperature interval for each polymer layer (see Figure 2.8) [48]. The elution step follows the reverse order of the crystallization step.

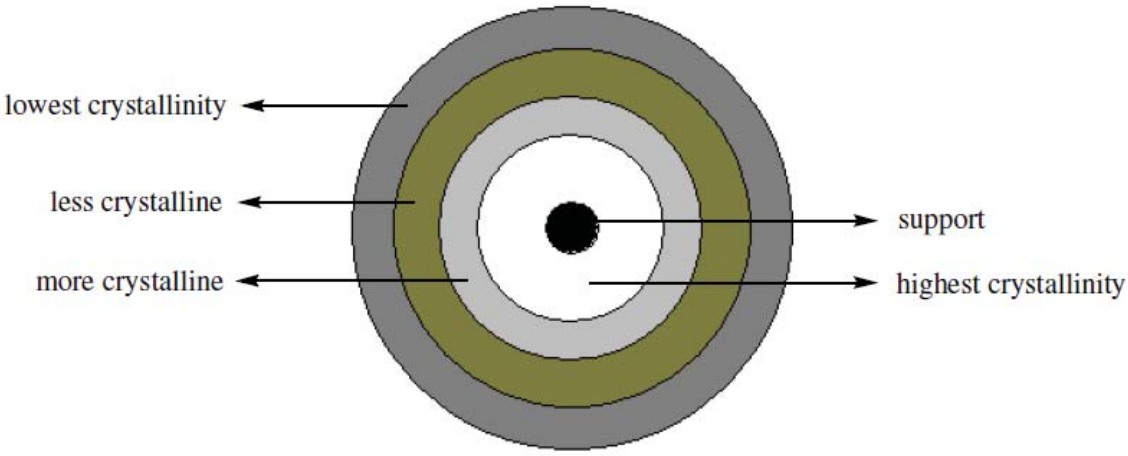

Figure 2.4 The onion-like layered structure formed around the inert support after the crystallization step [51].

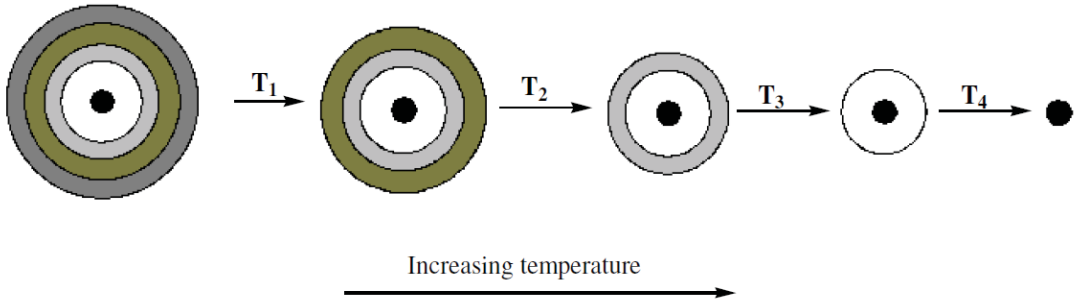

Figure 2.5 A simple representation of the dissolution process during the elution step [51].

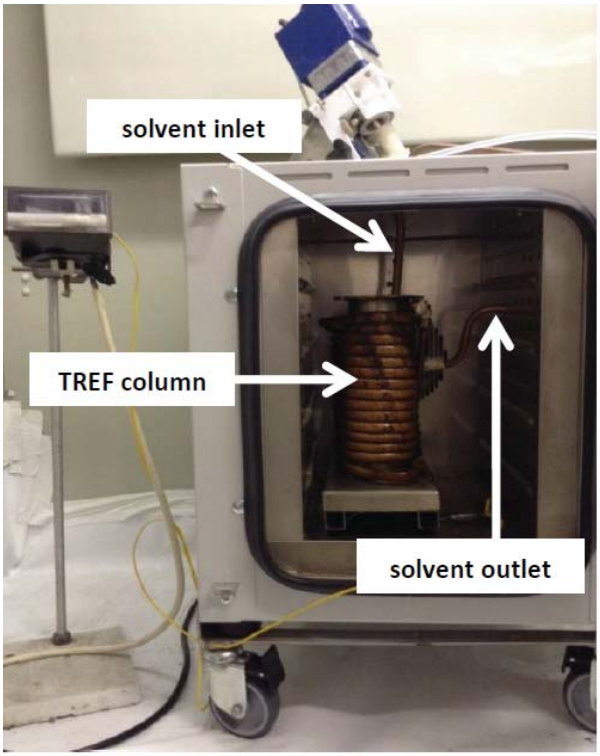

Figure 2.6 A picture showing the TREF elution column used during the elution step [51].

One of the main applications of TREF is to determine the CCD of copolymers. However, one major setback is that TREF analyses cannot be used to obtain quantitative CCD data because the TREF results can be affected by several operating conditions and material type. TREF results can be affected by solvent type, CR, co-monomer type, co-monomer content, and co-monomer sequence length distribution [48]. Therefore, it is important to clearly understand how chain microstructural characteristics and operating conditions influence TREF results in order to avoid data misinterpretation. For example, in HEPCs co-monomer content has a significant effect on TREF profiles. The co-monomer units reduce the chain regularity of long PP sequences and thus lowering their chain crystallizability [52, 53]. Longer chain branches were also reported to lower chain crystallizability [54] which shows that the TREF profiles are not only affected by the co-monomer content but the co-monomer type as well. Processes such as vis-breaking have been reported to reduce chain crystallizability in HEPCs [55, 56]. Lowering the crystallizability of a polymer usually shifts the TREF elution profile towards lower elution temperatures. Operating conditions such as cooling rate (CR), heating rate and solvent flow rate can also significantly affect TREF profiles. For example, a fast CR can significantly reduce the fractionation efficiency thus reducing the time taken by the polymer chains to efficiently separate according to their microstructures. Slow solvent flow rates increase the residence time of the polymer solution and axial dispersion in the column thus

causing a broadening of the TREF profiles and an increase of the TREF peak temperature. Fast heating rates will cause a given volume of solvent to elute polymer over a wide range of crystallinities thus broadening the TREF profiles [48].

In-spite of the good characteristics that the TREF technique has, it has limitations. One of the limitations is that TREF is less sensitive to molar mass effects of polymers with molar masses of more than 10 000 g/mol. The TREF results become independent of chain length for samples with higher molar masses [57]. Therefore, for polymers with higher molar masses, the effects of vis-breaking on molar mass cannot be detected via TREF. An alternative fractionation method which fractionates according molar mass is needed for this purpose.

2.6 Molar mass fractionation (MMF) or solvent gradient fractionation (SGF) of heterophasic copolymers

Molar mass fractionation (MMF) is a fractionation technique that fractionates polyolefins based on molar mass difference. Most polyolefin materials exhibit a broad molar mass distribution (MMD).Therefore, MMF is used to fractionate these polymers in order to obtain fractions with a narrow MMD. The narrow MMD is crucial in understanding the polymer's structure-property relationship [58].

MMF can be performed in either of two methods: preparative molar mass fractionation (P-MMF) [59-62] and solvent gradient fractionation (SGF) [58, 63-66]. Both methods use a solvent/non-solvent gradient but the difference is mostly in the elution step. In both cases, an appropriate solvent system (good and poor solvents) is selected and fractions with varying molar masses are obtained depending on the solvent/non-solvent ratio used. Therefore, this serves as an indicator that the solvent/non-solvent ratio is crucial for facilitating proper fractionation. For instance, the SGF method allows dissolved polymer to crystallize on an inert support such as sand. The solvent/non-solvent mixture with increasing solvent kept at constant temperature is then passed through the polymer/sand mixture to obtain fractions with increasing molar masses (see Figure 2.11 below) [58, 66]. On the contrary, during the P-MMF method, the non-solvent in the solvent/non-solvent mixture is increased until a stable cloud point is observed. The formed precipitate (i.e first fraction) is then given enough time to settle and then carefully removed using a suction device (see Figure 2.10 below) [60]. The obtained fractions are usually further analysed by high temperature size exclusion chromatography (HT-SEC) and carbon-13 nuclear magnetic resonance spectroscopy (^{13}C-NMR) [58].

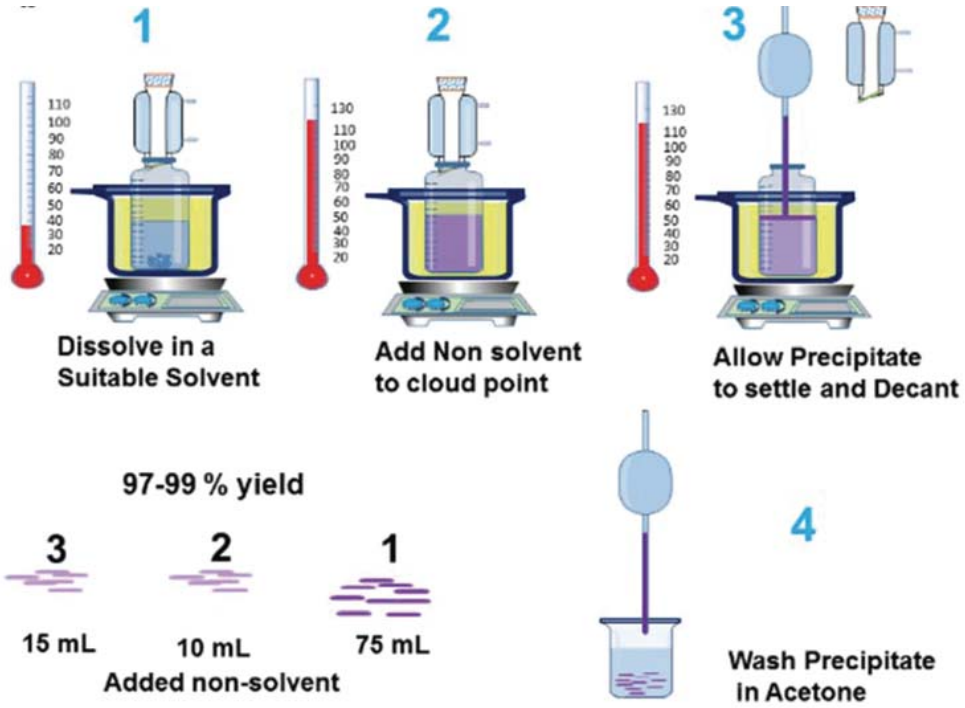

Figure 2.7 A schematic representation of the P-MMF method [60]

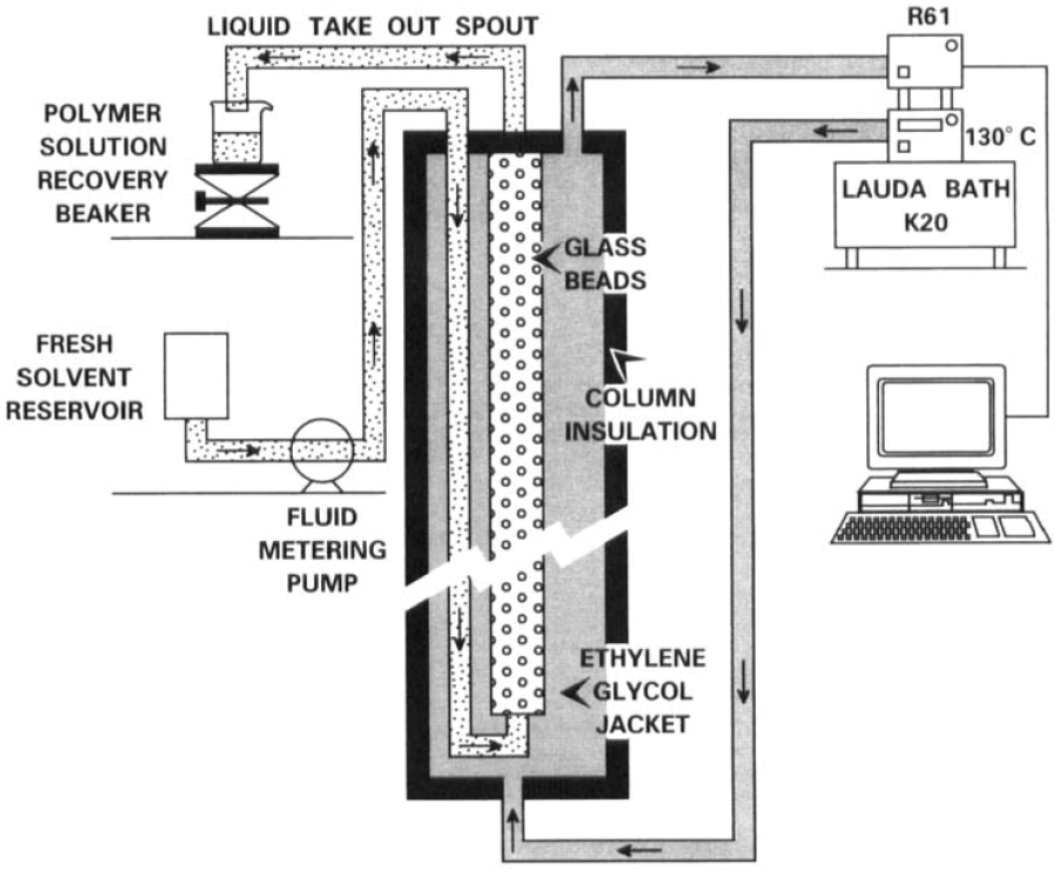

Figure 2.8 Fractionation setup of the SGF method [66]

Work done on the fractionation of polyolefins according to molar mass difference using the P-MMF [59-62] or SGF [58, 63-66] has been extensively reported in literature. All this work was aimed at understanding the relationship that exists between the structures and properties of different kinds of PE and ethylene-based copolymers. So far, no work has been reported on the MMF of HEPCs. Results show that both methods are the best except that SGF fractions exhibited broad MMD curves at high molar masses [58, 66]. This could be due to co-monomer influencing the fractionation in this region.

2.7 Characterization techniques of heterophasic copolymers

2.7.1 High temperature size exclusion chromatography (HT-SEC)

Size exclusion chromatography (SEC), also known as gel permeation chromatography (GPC), is a column-based chromatographic technique that separates according to the hydrodynamic volume (V_h) of the polymer species in solution. Therefore SEC is the most widely accepted and used analytical method for the measurement of molecular size, MMD and molar mass averages of biopolymers and synthetic polymers [67, 68].

The basic principle by which SEC works is simple. It involves the injection of a sample solution which is carried through the column by a suitable solvent. Depending on the V_h, the polymer molecules permeate the pores of the stationary phase. The smaller molecules permeate the porous packing material more readily and deeper than the larger ones. This interaction results in the larger molecules being eluted first and the smaller ones last [67]. Therefore, this means that retention time increases with decreasing chain sizes. For proper separation, it is imparative to select the pore sizes of the column packing based on the molar masses of the polymers to be separated. If the polymers to be separated have broad molar mass distributions, a series of SEC columns is used [69]. Figure 2.12 below is a schematic representation of how a typical SEC setup looks like.

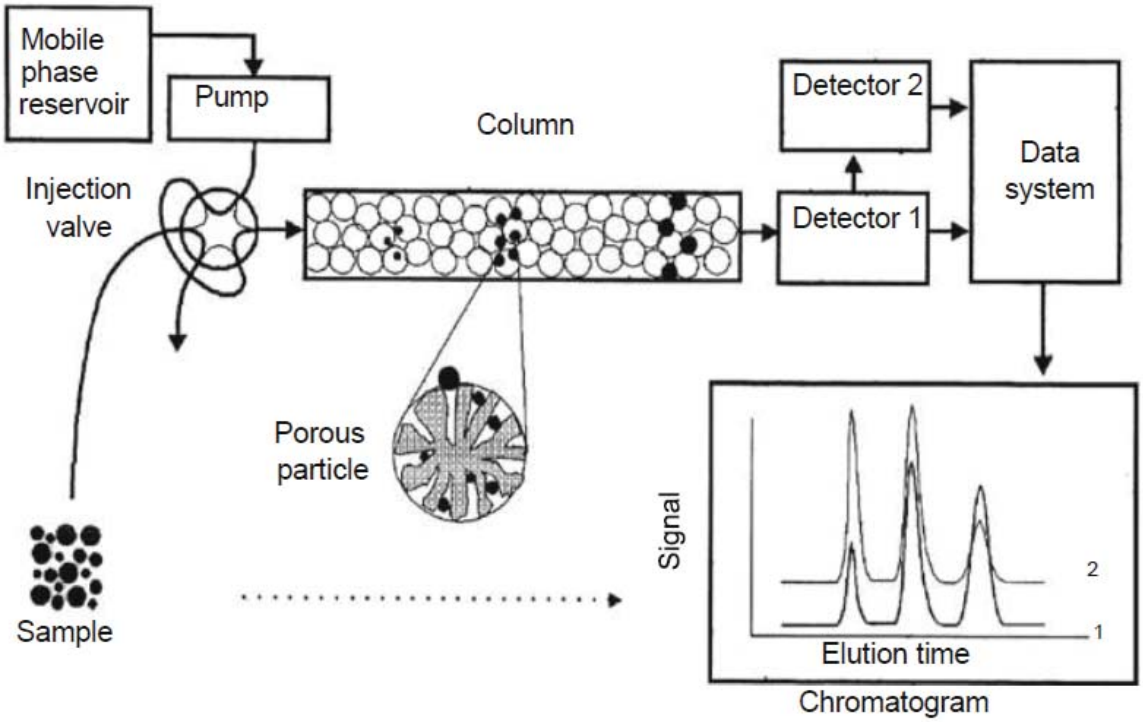

Figure 2.9 A schematic diagram showing the operation of SEC [67].

Since polyolefins are soluble at temperatures above their melting point, accurate SEC analyses of these materials can only be carried out at high temperatures (between 110 °C and 160 °C). Therefore thermodynamically stable high boiling point solvents such as 1,2,4-trichlorobenzene (TCB), ortho-dichlorobenzene (o-DCB), decalin, methylcyclohexane, ∝ −chloronaphthalene and tetrachloroethane are usually used for the analyses [70, 71]. However, operating at high temperatures introduces problems such as degradation. Degradation may occur during sample dissolution or during the SEC separation itself [72, 73]. This degradation problem is usually combated by adding phenolic antioxidants (e.g 0.2 mg/ml to 1.5 mg/ml of butylated hydroxytoluene, BHT) to the mobile phase [74, 75].

Over the years, HT-SEC has been used to trace the effect of vis-breaking on the molar mass averages and MMDs of HEPCs [21, 55, 56, 76]. In these studies, a decrease of molar mass and narrowing of MMD was observed with increasing the degree of vis-breaking. This was a direct indication of an increase in retention time and therefore a decrease in V_h. In this study, HT-SEC will also be used to trace the effect of vis-breaking on the molar masses and MMDs of HEPCs with varying CCDs.

2.7.2 High temperature high performance liquid chromatography (HT-HPLC)

High temperature high performance liquid chromatography (HT-HPLC) is a column based chromatographic technique used to separate complex polyolefins according to chemical

composition [77-79]. HT-HPLC was developed in 2004 by the group of Pasch and Macko in collaboration with Polymer Laboratories, Ltd (Church, Stretton, England) [80]. Their idea was to develop an instrument that could operate at high temperatures as well as in a solvent gradient mode. HPLC separates polyolefins based on either their adsorption/desorption or precipitation/re-dissolution behaviour. However, gradient HPLC, which is used in this study separates polyolefins that have both the precipitation and adsorption behaviour [81]. One advantage that HPLC has over TREF is that it can be used for the analysis of both semi-crystalline and amorphous polyolefin samples.

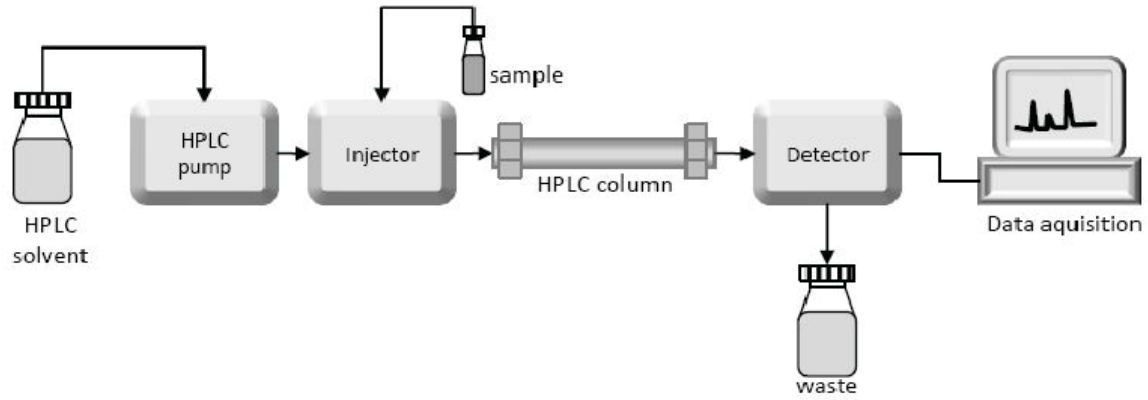

Figure 2.10 A schematic diagram of the HPLC instrumentation [82]

The HT-HPLC work done by Macko and Pasch proved that highly selective separations of polyolefins can be achieved by using a carbon based stationary phase such as a Hypercarb column. It was also shown that iPP in 1-decanol is partially retained on the porous graphite carbon (PGC) stationary phase. Through coupling of HPLC to SEC it was shown that the peak eluting between 1.0 – 1.4 ml has a lower molar mass than that eluting at 3.0 ml [81]. Macko *et al.* also discovered that the separations in the Hypercarb column were highly dependent upon the crystallizability of the methylene sequences of the polymer in the stationary phase. The longer methylene sequences tend to interact more with the stationary phase as compared to the shorter ones and hence their elution at higher retention volumes (V_r) [83, 84]. Figure 2.13 above is a schematic representation of the HPLC instrumentation. It includes a pump, injector, column, detector and integrator or acquisition and display system. The column is the heart of the instrument because this is where separation takes place. Work done by Pasch *et al.* also showed that HPLC can be used to identify and separate resin components according to chemical composition [85]. It has also been shown that the online coupling of HPLC to HT-SEC and proton nuclear magnetic resonance spectroscopy (^{1}H-NMR) provides a wealth of information on the constitutional composition of both new and established polyolefin resins.

In the current study, HT-HPLC will be used to trace the effect of vis-breaking on the chemical composition of HEPCs.

2.7.3 Fourier transform infra-red spectroscopy (FTIR)

Fourier transform infra-red spectroscopy (FTIR) is a spectroscopic technique that has been widely used to determine the composition, crystallinity, tacticity as well as molecular chain conformation of polymeric materials [86]. FTIR has also been useful in the structural identification of organic molecules and polymeric materials because of its sensitivity towards the constitution and folding manner of molecular chains [87-89].

The theory with which FTIR works is based on the fact that most molecules absorb light in the infra-red region of the electromagnetic spectrum. The absorption of each molecule specifically depends on the bonds present in that molecule. Therefore, the resultant absorption spectrum reflects the presence of chemical bonds and functional groups that are specific to that molecule. The absorbed frequency is usually measured in wavenumbers over the range of 4000 – 600 cm^{-1} [86].

Useful bands in the structural identification of PP were found at 940, 997, 998, 900, 840, 841, 808, 1100 and 973 cm^{-1}. The bands at 973, 998, 840, 841 and 1220 cm^{-1} were reported to correspond to 5, 10, 12, 13-15 and 14 monomer units in helical sequences of iPP [90-96]. However, Kessin and co-workers argued that the band at 998 cm^{-1} corresponds to 11-12 monomer units instead of 10 [89, 90, 97]. Moreover, a study by Miyamoto and Inagaki showed that a sequence length of less than 10 monomer units resulted in the disappearance of the 997 cm^{-1} band [91]. This was a confirmation that the sequence length represented by this band was strictly 10 monomer units. Furthermore, Kobayashi *et al.* observed that for sequence lengths shorter than 10 monomer units, all the regularity bands disappear except for the bands at 841 and 998 indicating that these bands represented sequence lengths of more than 10 monomer units [88]. All these studies prove that FTIR is sensitive to chemical structure and can therefore be used to detect any structural changes. In the current study, FTIR will be used to diagnose any structural changes induced by vis-breaking on the HEPC samples.

2.7.4 Differential scanning calorimetry (DSC)

Differential scanning calorimetry (DSC) is the most popular thermal analysis technique when it comes to thermal analysis. DSC is often fondly referred to as the “workhorse” of thermal

analysis [98]. The DSC technique was developed in 1962 by Watson and O'Neill [99]. However, the name DSC was first introduced in 1963 when Perkin-Elmer introduced their first DSC (called DSC-1) into the market. Moreover, the term DSC came from the DSC instrument's ability to obtain quantitative calorimetric information with increasing or decreasing temperature [98].

During the DSC experiment, the difference between the heat flow into the sample analysed and reference is measured as a function of temperature under a controlled temperature programme [98]. The furnace of the DSC instrument is kept under inert conditions by the continuous purging with nitrogen gas to avoid oxidative decomposition of the sample [69]. Therefore, DSC can be used to determine the glass transition temperature (T_g), heat capacity jump at glass transition, melting and crystallization temperatures etc [98]. Figure 2.14 is an illustration of a typical DSC furnace.

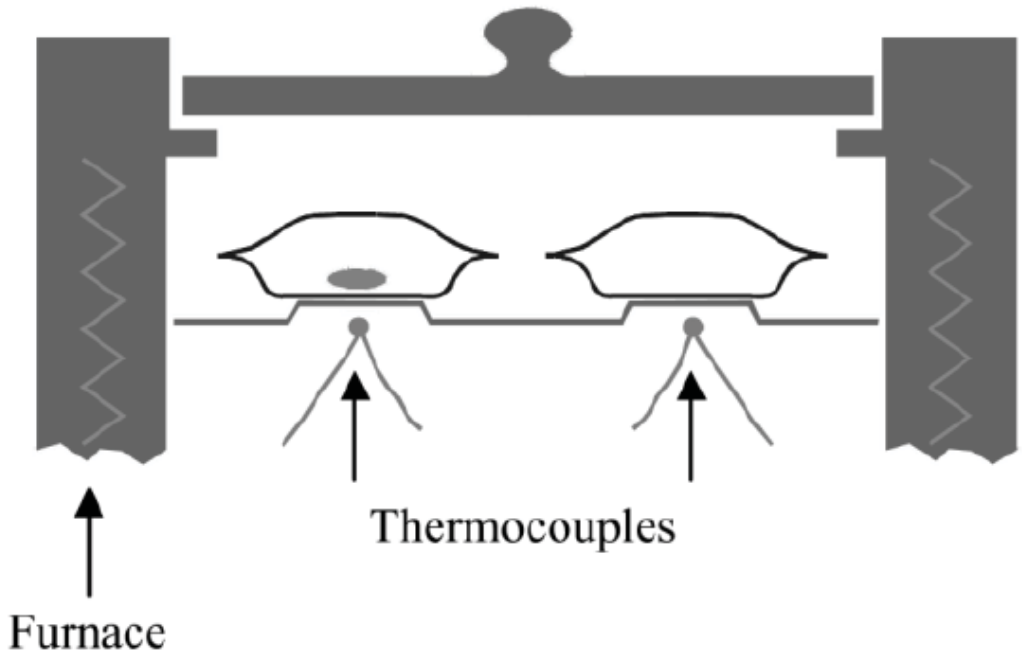

Figure 2.11 An illustration of a typical DSC furnace with a sample and reference. The pan with a grey pellet on the right represents the sample and the empty pan on the left represents the reference [69].

DSC has also been used to obtain information on the degradation behaviour of polymers [100-102]. The effect of degradation on melting and crystallization temperatures, the shape of melt endotherms as well as overall percentage crystallinity has been traced using DSC [102]. This provides useful information about the susceptibility of certain crystalline phases or conformations to degradation. Crystallinity in polymers is highly dependent on chain length,

composition as well as sequence distribution of monomers. Therefore, DSC has been used to show that reducing the sequence length of monomer blocks as is the case during vis-breaking, decreases the crystallization temperature (T_c) and enthalpy of crystallization (ΔH_c). Using DSC, it has also been proven that the introduction of ethylene reduces the T_g of a PP homopolymer from 262K to the region of 214-222K [103]. This shows that a disturbance in the monomer sequence, which is likely to happen during vis-breaking causes a drop in the T_g of the polymer.

2.7.5 Solid state carbon-13 nuclear magnetic resonance spectroscopy (^{13}C NMR)

Solid-state ^{13}C-NMR spectroscopy is an analytical technique commonly used to investigate the morphology and molecular dynamics of solid polymers [104-109]. The advantages of using solid state NMR are that the polymers are studied in their native state under conditions that are similar to their application environment [110]. Furthermore, during the analysis, different phases (amorphous, crystalline, semi-rigid, etc) of the polymer can be selectively probed based on differences in molecular dynamics e.g cross-polarization dynamics or relaxation behaviour [111].

Unlike solution-state ^{13}C-NMR, solid-state ^{13}C-NMR enables the evaluation of the actual chain structure instead of the averaged microstructure obtained from solution NMR. Solid state NMR can be used to study localised as well as longer range interactions over various time scales. However, one major drawback that solid-state ^{13}C-NMR has is that it has a lower resolution as compared to solution-state ^{13}C-NMR. Therefore complementary results from solution NMR are still required to make conclusions on the average chain composition of the polymers [110, 111].

With a few exceptions, solid state NMR has not been widely applied in understanding the nature of complex polymers such as HEPCs. However, most recently, variable temperature solid-state ^{13}C-NMR was used to study the temperature-dependent development of segmental mobility within HEPCs of varying chemical composition distribution. During this study, the development of amorphous PP signals was observed with increasing temperature and this was attributed to the presence of ethylene defects within the HEPCs. It was also observed that the PP components with high rigidity did not disappear at high temperatures for all the HEPCs except for the homopolymer [112]. The latter will be expanded on in Chapter 6.

In this study, for the first time, variable temperature solid-state ^{13}C-NMR will be used to investigate the *in situ* (in the NMR instrument) vis-breaking of HEPCs.

2.7.6 Solution-state ^{13}C NMR

Solution-state ^{13}C-NMR spectroscopy is a technique that has been extensively used in investigating the chain microstructure of polymers. It is often used for polyolefin identification, determining co-monomer sequence distributions and co-monomer content through signal integration [69, 113]. The experiments are carried out in solution. This is because segmental motion in solutions is rapid enough to obtain an average of the dipole-dipole interactions present and this is depicted by the narrow NMR lines obtained [111, 114]. It is for this reason that solution-state NMR is referred to as a high resolution technique.

The principle through which solution-state NMR operates is based on the fact that the magnetic properties of atomic nuclei can be harnessed to obtain chemical information [115]. The atomic nuclei exists in two spin states (i.e excited or higher and lower energy states). Excitement of the nuclei from a higher to a lower energy state is achieved through irradiation of the nuclei with the energy that corresponds to the energy difference of their spin state. The spin charge on the nuclei generates a magnetic field and therefore a magnetic moment that corresponds to the spin state [115, 116]. Atomic nuclei can absorb and re-emit electromagnetic radiation. Therefore, the energy of absorption and intensity of the NMR signals are proportional to the strength of the magnetic field [117].

In solution-state NMR, the chemical shifts of the signals obtained are usually reported relative to those of the reference used. In our case, we used 1,1,2,2-tetrachloroethane (TCE-d_2) and it has a chemical shift of 74.3 ppm [118]. The observed chemical shifts give information about the structure of the sample analysed. Furthermore, the chemical shifts of protons are much easier to predict as compared to those of heavier nuclei. This is because the chemical shifts of protons are primarily determined by simpler shielding effects such as electron density whereas those of heavier nuclei are influenced by more than one factor [69].

Solution-state NMR can be used to trace the effect of vis-breaking on the microstructure of HEPCs. In a study by Swart *et al.* on the vis-breaking of a HEPC, it was shown that vis-breaking affected segmented ethylene-propylene copolymers with long ethylene sequences (PEE) resulting in a decrease in the low temperature impact strength of the HEPC used [21, 55]. In the current study, solution-state NMR will also be used to study the effect that vis-breaking has on the chain microstructure of HEPCs except that HEPCs with different chemical composition distributions will be used.

2.8 References

1. Mülhaupt, R., *Catalytic polymerization and post polymerization catalysis fifty years after the discovery of Ziegler's catalysts.* Macromolecular Chemistry and Physics, 2003. **204**(2): p. 289-327.

2. Galli, P., Danesi, S, Simonazzi, T, *Polypropylene based polymer blends: fields of application and new trends.* Polymer Engineering & Science, 1984. **24**(8): p. 544-554.

3. Liang, J. Z., Li, R. K. Y., *Rubber toughening in polypropylene: A review.* Journal of Applied Polymer Science, 2000. **77**(2): p. 409-417.

4. Schwager, H., *Polypropylen-Reaktorblends: Werkstoffe mit aussergewöhnliche Zähigkeit.* Kunststoffe, 1992. **82**(6): p. 499-501.

5. Cecchin, G., Morini, G., Pelliconi, A., *Polypropene product innovation by reactor granule technology*. in Macromolecular Symposia. 2001. Wiley Online Library.

6. Borealis. *Borstar Polypropylene Process and Catalyst Technology - Pushing the Boundaries of Polypropylene Performance*. [cited 2019 10 April]; Available from: http://www.eiseverywhere.com/docs/5555/165999.

7. Ramsteiner, F., Kanig, G., Heckmann, W., Gruber, W., *Improved low temperature impact strength of polypropylene by modification with polyethylene.* Polymer, 1983. **24**(3): p. 365-370.

8. Galli, P., Haylock, J. C., *Advances in Ziegler-Natta polymerization-unique polyolefin copolymers, alloys and blends made directly in the reactor*. in Makromolekulare Chemie. Macromolecular Symposia. 1992. Wiley Online Library.

9. Galli, P., Vecellio, G., *Technology: driving force behind innovation and growth of polyolefins.* Progress in Polymer Science, 2001. **26**(8): p. 1287-1336.

10. Botha, L., *The effect of in-process ethylene incorporation on the evolution of particle morphology and molecular characteristics of commercial heterophasic ethylene propylene copolymers (HEPCs)*. 2014, PhD Thesis. Stellenbosch University.

11. Soga, K., Shiono, T., *Ziegler-Natta catalysts for olefin polymerizations.* Progress in Polymer Science, 1997. **22**(7): p. 1503-1546.

12. Andoni, A., *A flat model approach to Ziegler-Natta olefin polymerization catalysts.* 2009, PhD Thesis, Technische Universiteit Eindhoven.

13. Harding, G., *The structure-property relationships of polyolefins*. 2009, PhD Thesis, University of Stellenbosch.

14. Natta, G., Mazzanti, G., *Organometallic complexes as catalysts in ionic polymerizations.* Tetrahedron, 1960. **8**(1): p. 86-100.

15. Ystenes, M., *The trigger mechanism for polymerization of α-olefins with Ziegler-Natta catalysts: A new model based on interaction of two monomers at the transition state and monomer activation of the catalytic centers.* Journal of Catalysis, 1991. **129**(2): p. 383-401.

16. Patat, F., Sinn, H. J., *Zum Ablauf der Niederdruckpolymerisation der α-Olefine. Komplexpolymerisation I.* Angewandte Chemie, 1958. **70**(16): p. 496-500.

17. Rodriguez, L., Van Looy, H. M., *Studies on Ziegler-Natta catalysts. Part V. Stereospecificity of the active center.* Journal of Polymer Science Part A-1: Polymer Chemistry, 1966. **4**(8): p. 1971-1992.

18. Cossee, P., *Ziegler-Natta catalysis I. Mechanism of polymerization of α-olefins with Ziegler-Natta catalysts.* Journal of Catalysis, 1964. **3**(1): p. 80-88.

19. Cossee, P., *The formation of isotactic polypropylene under the influence of Ziegler-Natta catalysts.* Tetrahedron Letters, 1960. **1**(38): p. 17-21.

20. Arlman, E., *Ziegler-Natta catalysis II. Surface structure of layer-lattice transition metal chlorides.* Journal of Catalysis, 1964. **3**(1): p. 89-98.

21. Swart, M., *The effect of controlled degradation with an organic peroxide on the molecular characteristics and properties of heterophasic propylene-ethylene copolymers (HECO)*. 2013, PhD Thesis, University of Stellenbosch.

22. Pasquini, N., Addeo, A., *Polypropylene handbook*. 2005: Hanser.

23. Rincon-Rubio, L., Wilen, C. E., Lindfors, L. E., *A kinetic model for the polymerization of propylene over a Ziegler-Natta catalyst.* European Polymer Journal, 1990. **26**(2): p. 171-176.

24. Rotzinger, B., *Polymerisation und copolymerisation von propylen und ethylen mit Ziegler-Natta trägerkatalysatoren auf Magnesiumchloridbasis der arten MgCl-2/TiCl-4/Al (i-Bu)-3, MgCl-2/TiCl-4/Al (i-Bu)-3/Lewisbase und MgCl-2/TiCl-4-TMEDA/Al (i-Bu)-3*. 1984, PhD Thesis, ETH Zurich.

25. Tait, P., Jaber, I. A., Loontjens, A. J., *2. Studies on the polymerization of propylene using highly active Magnesium Chloride supported Ziegler-Natta catalysts: Effects of alkyl concentration on the polymerization rate and on the active centre concentration,* in *Studies in Surface Science and Catalysis*. 1990, Elsevier. p. 11-27.

26. Bukatov, G., Zaikovskii, V. I., Zakharov, V. A., Kryukova, G. N., Fenelonov, V. B., Zagrafskaya, R. V., *The morphology of polypropylene granules and its link with the titanium trichloride texture.* Polymer Science USSR, 1982. **24**(3): p. 599-606.

27. Ferrero, M., Sommer, R., Spanne, P., Jones, K. W., Conner, W. C., *X-ray microtomography studies of nascent polyolefin particles polymerized over magnesium chloride-supported catalysts.* Journal of Polymer Science Part A: Polymer Chemistry, 1993. **31**(10): p. 2507-2512.

28. Galli, P., Haylock, J. C., *Continuing initiator system developments provide a new horizon for polyolefin quality and properties.* Progress in Polymer Science, 1991. **16**(2-3): p. 443-462.

29. Hutchinson, R., Chen, C. M., Ray, W. H., *Polymerization of olefins through heterogeneous catalysis X: Modeling of particle growth and morphology.* Journal of Applied Polymer Science, 1992. **44**(8): p. 1389-1414.

30. Hock, C. W., *How $TiCl_3$ Catalysts Control the Texture of As-Polymerized Polypropylene.* Journal of Polymer Science Part A-1: Polymer Chemistry, 1966. **4**(12): p. 3055-3064.

31. Kakugo, M., Sadatoshi, H., Yokoyama, M., Kojima, K., *Transmission electron microscopic observation of nascent polypropylene particles using a new staining method.* Macromolecules, 1989. **22**(2): p. 547-551.

32. Noristi, L., Marchetti, E., Baruzzi, G., Sgarzi, P., *Investigation on the particle growth mechanism in propylene polymerization with $MgCl_2$-supported ziegler–natta catalysts.* Journal of Polymer Science Part A: Polymer Chemistry, 1994. **32**(16): p. 3047-3059.

33. Vermel, Y. Y., Zakharov, V. A., Fenelonov, V. B., Zaikovskii, V. I., Zagrafskaya, R. V., *EM Moroz and GD Bukatov*, Kinetika i Kataliz, 1981. **22**: p. 480.

34. Wristers, J., *Nascent polypropylene morphology: Polymer fiber.* Journal of Polymer Science: Polymer Physics Edition, 1973. **11**(8): p. 1601-1617.

35. Wristers, J., *Direct examination of polymerization catalyst by electron scanning microscopy.* Journal of Polymer Science: Polymer Physics Edition, 1973. **11**(8): p. 1619-1629.

36. Urdampilleta, I., González, A., Iruin, J. J., de La Cal, J. C., Asua, J. M. *Morphology of high impact polypropylene particles.* Macromolecules, 2005. **38**(7): p. 2795-2801.

37. Kakugo, M., Hashimoto, M, Isobata, J., *Sumitomo's liquid-phase and gas-phase processes for polypropylene production*. in Paper Presented at the 1987 AIChE Annual Meeting. 1987.

38. Kakugo, M., Sadatoshi, H., Sakai, J., *27. Morphology of nascent polypropylene produced by $MgCl_2$ supported Ti catalyst*, in *Studies in Surface Science and Catalysis*. 1990, Elsevier. p. 345-354.

39. Simonazzi, T., Cecchin, G., Mazzullo, S., *An outlook on progress in polypropylene-based polymer technology.* Progress in Polymer Science, 1991. **16**(2-3): p. 303-329.

40. Debling, J. A., Ray, W. H., *Morphological development of impact polypropylene produced in gas phase with a $TiCl_4/MgCl_2$ catalyst.* Journal of Applied Polymer Science, 2001. **81**(13): p. 3085-3106.

41. Gahleitner, M., Jääskeläinen, P., Ratajski, E., Paulik, C., Reussner, J., Wolfschwenger, J., Neißl, W., *Propylene–ethylene random copolymers: Comonomer effects on crystallinity and application properties.* Journal of Applied Polymer Science, 2005. **95**(5): p. 1073-1081.

42. Dutta, S., *More efficient manufacture of controlled-rheology polypropylene.* Society of Plastics Engineers, Plastics Research Online, 2010.

43. Malm, B., Jääskeläinen, P., Vestberg, T., *Heterophasic copolymers.* 2004, Google Patents.

44. Campus, A., Mateu, G., *The influence of temperature on he properties of crosslinked LDPE.* Wire Journal International, 1985. **18**(5): p. 57-&.

45. Wild, L., Glöckner, G., *Temperature rising elution fractionation*, in *Separation Techniques Thermodynamics Liquid Crystal Polymers*. 1990, Springer. p. 1-47.

46. Fonseca, C., Harrison, I. R., *Temperature rising elution fractionation.* Modern Techniques for Polymer Characterization, 1999: p. 1-13.

47. Soares, J., Hamielec, A. E., *Modern techniques for polymer characterization.* RA Pethrick, Ed, 1999: p. 15-55.

48. Anantawaraskul, S., Soares, J. B. P., Wood-Adams, P. M., *Fractionation of semicrystalline polymers by crystallization analysis fractionation and temperature rising elution fractionation*, in Polymer Analysis Polymer Theory. 2005, Springer. p. 1-54.

49. Flory, P. J., *Principles of Polymer Chemistry*. 1953: Cornell University press.

50. Mandelkern, L., *Equilibrium Concepts.* 2002: Cambridge University Press.

51. Robertson, D., *Studying crystallization kinetics using solution crystallization analysis by laser light scattering (Scalls)*. 2012, Masters Thesis, University of Stellenbosch

52. Shirayama, K., Kita, S., Watabe, H., *Effects of branching on some properties of ethylene/α-olefin copolymers.* Die Makromolekulare Chemie: Macromolecular Chemistry and Physics, 1972. **151**(1): p. 97-120.

53. Burfield, D. R., Kashiwa, N., *DSC studies of linear low density polyethylene. Insights into the disrupting effect of different comonomers and the minimum fold chain length of the polyethylene lamallae.* Die Makromolekulare Chemie: Macromolecular Chemistry and Physics, 1985. **186**(12): p. 2657-2662.

54. Savitski, E. P., Caflisch, G. B., Killian, C. M., Meadows, M. D., Merkley, J. H., Huff, B. J., *Influence of the short-chain branch length on the calibration of temperature rising elution fractionation systems.* Journal of Applied Polymer Science, 2003. **90**(3): p. 722-728.

55. Swart, M., Van Reenen, A. J. *The effect of controlled degradation on the molecular characteristics of heterophasic ethylene–propylene copolymers.* Journal of Applied Polymer Science, 2015. **132**(14).

56. Phiri, M. J., Pasch, H., *Exploring the compositional heterogeneity of vis-broken impact poly(propylene) copolymers by advanced fractionation methods.* Macromolecular Chemistry and Physics, 2016. **217**(6): p. 783-793.

57. Wild, L., Ryle, T. R., Knobeloch, D. C., Peat, I. R., *Determination of branching distributions in polyethylene and ethylene copolymers.* Journal of Polymer Science: Polymer Physics Edition, 1982. **20**(3): p. 441-455.

58. Xue, Y., Bo, S., Ji, X., *Solvent gradient fractionation and chain microstructure of complex branched polyethylene resin.* Journal of Polymer Research, 2016. **23**(7): p. 131.

59. Bungu, P. E., Pasch, H., *Comprehensive analysis of branched polyethylene: the multiple preparative fractionation concept.* Polymer Chemistry, 2017. **8**(31): p. 4565-4575.

60. Bungu, P. E., Pasch, H., *Branching and molar mass analysis of low density polyethylene using the multiple preparative fractionation concept.* Polymer Chemistry, 2018. **9**(9): p. 1116-1131.

61. Ndiripo, A., Eselem Bungu, P. S., Pasch, H., *Comprehensive branching analysis of polyethylene by combined fractionation and thermal analysis.* Polymer International, 2018.

62. Jørgensen, J. K., Larsen, Å., Helland, I., *Study on LLDPE molecular structure characterization by preparative and analytical cross-fractionation.* e-Polymers, 2010. **10**(1).

63. Tarasova, E., Poltimäe, T., Krumme, A., Lehtinen, A., Viikna, A., *Triple crystallization behavior of fractionated ethylene/α-olefin copolymers of different catalyst type.* Journal of Polymer Research, 2011. **18**(2): p. 207-216.

64. Hosoda, S., *Structural distribution of linear low-density polyethylenes.* Polymer journal, 1988. **20**(5): p. 383.

65. Schouterden, P., Groeninckx, G., Van der Heijden, B., Jansen, F., *Fractionation and thermal behaviour of linear low density polyethylene.* Polymer, 1987. **28**(12): p. 2099-2104.

66. Hsieh, E. T., Tso, C. C., Byers, J. D., Johnson, T. W., Fu, Q., Cheng, S. Z. D., *Intermolecular structural homogeneity of metallocene polyethylene copolymers.* Journal of Macromolecular Science, Part B: Physics, 1997. **36**(5): p. 615-628.

67. Pasch, H., Trathnigg, B., *Multidimensional HPLC of polymers*. 2013: Springer.

68. Kostanski, L. K., Keller, D. M., Hamielec, A. E., *Size-exclusion chromatography—a review of calibration methodologies.* Journal of Biochemical and Biophysical Methods, 2004. **58**(2): p. 159-186.

69. Ndiripo, A., *Comparative study on the molecular structure of ethylene/1-octene, ethylene/1-heptene and ethylene/1-pentene copolymers using advanced analytical methods*. 2015, Masters Thesis, Stellenbosch University.

70. Rao, B., Balke, S. T., Mourey, T. H., Schunk, T. C., *Methyl cyclohexane as a new eluting solvent for the size-exclusion chromatography of polyethylene and polypropylene at 90° C.* Journal of Chromatography A, 1996. **755**(1): p. 27-35.

71. Ibhadon, A., *Gel permeation chromatography of isotactic polypropylene using the cyclohexane–decalin solvent system.* Journal of Applied Polymer Science, 1991. **42**(7): p. 1887-1890.

72. Parth, M., Aust, N., Lederer, K., *Molecular characterization of ultrahigh molar mass and soluble fractions of partially cross-linked polyethylenes.* International Journal of Polymer Analysis and Characterization, 2003. **8**(3): p. 175-186.

73. Mes, E., De Jonge, H., Klein, T., Welz, R. R., Gillespie, D. T., *Characterization of high molecular weight polyethylenes using high temperature asymmetrical flow field-flow fractionation with on-line infrared, light scattering, and viscometry detection.* Journal of Chromatography A, 2007. **1154**(1-2): p. 319-330.

74. Pasti, L., Melucci, D., Contado, C., Dondi, F., Mingozzi, I., *Calibration in thermal field flow fractionation with polydisperse standards: Application to polyolefin characterization.* Journal of Separation Science, 2002. **25**(10-11): p. 691-702.

75. Sun, T., Brant, P., Chance, R. R., Graessley, W. W., *Effect of short chain branching on the coil dimensions of polyolefins in dilute solution.* Macromolecules, 2001. **34**(19): p. 6812-6820.

76. Magagula, S. I., *The effect of organic peroxides on the molecular composition of heterophasic ethylene-propylene impact copolymers*. 2015, Masters Thesis, Stellenbosch University.

77. Heinz, L.-C., Macko, T., Pasch, H., Weiser, M.-S., Mülhaupt, R., *High-temperature liquid chromatography at critical conditions: Separation of polystyrene from blends with Polyethylene and ethylene-styrene block copolymers.* International Journal of Polymer Analysis and Characterization, 2006. **11**(1): p. 47-55.

78. Pasch, H., Heinz, L.-C., Macko, T., Hiller, W., *High-temperature gradient HPLC and LC-NMR for the analysis of complex polyolefins.* Pure and Applied Chemistry, 2008. **80**(8): p. 1747-1762.

79. Pasch, H., Malik, M. I., Macko, T., *Recent advances in high-temperature fractionation of polyolefins*, in *Polymer Composites–Polyolefin Fractionation–Polymeric Peptidomimetics–Collagens*. 2012, Springer. p. 77-140.

80. Heinz, L.-C., Pasch, H., *High-temperature gradient HPLC for the separation of polyethylene–polypropylene blends.* Polymer, 2005. **46**(26): p. 12040-12045.

81. Macko, T., Pasch, H., *Separation of linear polyethylene from isotactic, atactic, and syndiotactic polypropylene by high-temperature adsorption liquid chromatography.* Macromolecules, 2009. **42**(16): p. 6063-6067.

82. Laboratoryinfo. *High performance liquid chromatography*. [cited 2019 04 February]; Available from: http://laboratoryinfo.com/hplc/

83. Macko, T., Brüll, R., Alamo, R. G., Stadler, F. J., Losio, S., *Separation of short-chain branched polyolefins by high-temperature gradient adsorption liquid chromatography.* Analytical and Bioanalytical Chemistry, 2011. **399**(4): p. 1547-1556.

84. Macko, T., Brüll, R., Alamo, R. G., Thomann, Y., Grumel, V., *Separation of propene/1-alkene and ethylene/1-alkene copolymers by high-temperature adsorption liquid chromatography.* Polymer, 2009. **50**(23): p. 5443-5448.

85. Pasch, H., Albrecht, A., Bruell, R., Macko, T., Hiller, W., *High temperature interaction chromatography of olefin copolymers*. 2009. Wiley Online Library.

86. Koenig, J. L., *Spectroscopy of polymers*. 1999: Elsevier.

87. Zerbi, G., Ciampelli, F., Zamboni, V., *Classification of crystallinity bands in the infrared spectra of polymers*. in Journal of Polymer Science Part C: Polymer Symposia. 1964. Wiley Online Library.

88. Kobayashi, M., Akita, K., Tadokoro, H., *Infrared spectra and regular sequence lengths in isotactic polymer chains.* Die Makromolekulare Chemie: Macromolecular Chemistry and Physics, 1968. **118**(1): p. 324-342.

89. Kissin, Y. V., Rishina, L. A., *Regularity bands in the IR spectra of C_3H_6/C_3D_6 copolymers.* European Polymer Journal, 1976. **12**(10): p. 757-759.

90. Kissin, Y. V., Tsvetkova, V. I., Chirkov, N. M., *Nature of the infrared absorption bands disappearing during the melting of polypropylene.* Polymer Science. Series A, 1968. **10**(5): p. 1265-1270.

91. Miyamoto, T., Inagaki, H., *Structural and steric isomerism of polypropylenes.* Journal of Polymer Science Part A-2: Polymer Physics, 1969. **7**(6): p. 963-981.

92. Su, Z., W., Hongying, D., Jinyong, Z., Xiuqin, D., Xia, Z., Ying, Y., Jian, H., Charles C., Xu, D., Wang, D., *Conformation transition and crystalline phase variation of long chain branched isotactic polypropylenes (LCB-iPP).* Polymer, 2007. **48**(3): p. 870-876.

93. Zhu, X., Yan, D., Yao, H., Zhu, P., *In situ FTIR spectroscopic study of the regularity bands and partial-order melts of isotactic poly (propylene).* Macromolecular Rapid Communications, 2000. **21**(7): p. 354-357.

94. Zhu, X., Yan, D., Fang, Y., *In situ FTIR spectroscopic study of the conformational change of isotactic polypropylene during the crystallization process.* The Journal of Physical Chemistry B, 2001. **105**(50): p. 12461-12463.

95. Zhu, X., Yan, D., *In situ FTIR spectroscopy study on the melting process of isotactic poly (propylene).* Macromolecular Chemistry and Physics, 2001. **202**(7): p. 1109-1113.

96. Zhu, X., Li, Y, Yan, D, Zhu, P., Lu, Q., *Influence of the order of polymer melt on the crystallization behavior: I. Double melting endotherms of isotactic polypropylene.* Colloid and Polymer Science, 2001. **279**(3): p. 292-296.

97. Kissin, Y. V., Tsvetkova, V. I., Chirkov, N. M., *The stereoregularity of polypropylene from IR and NMR data.* European Polymer Journal, 1972. **8**(4): p. 529-546.

98. Menczel, J. D., Judovits, L., Prime, R. B., Bair, H. E., Reading, M., Swier, S., *Differential scanning calorimetry (DSC).* Thermal Analysis of Polymers: Fundamentals and Applications, 2009: Wiley, p. 7-239.

99. Watson, E., O'neill, M. J., Justin, J., Brenner, N., *A Differential scanning calorimeter for quantitative differential thermal analysis.* Analytical Chemistry, 1964. **36**(7): p. 1233-1238.

100. Olivares, N., Tiemblo, P., Gómez-Elvira, J. M., *Physicochemical processes along the early stages of the thermal degradation of isotactic polypropylene I. Evolution of the γ relaxation under oxidative conditions.* Polymer Degradation and Stability, 1999. **65**(2): p. 297-302.

101. Rosa, D., Sarti, J., Mei, L. H. I., Silveira, S., *A study of parameters interfering in oxidative induction time (OIT) results obtained by differential scanning calorimetry in polyolefin.* Polymer Testing, 2000. **19**(5): p. 523-531.

102. Elvira, M., Tiemblo, P., Gómez-Elvira, J. M., *Changes in the crystalline phase during the thermo-oxidation of a metallocene isotactic polypropylene. A DSC study.* Polymer Degradation and Stability, 2004. **83**(3): p. 509-518.

103. Gan, S. N., Burfield, D. R., Soga, K., *Differential scanning calorimetry studies of ethylene-propylene copolymers.* Macromolecules, 1985. **18**(12): p. 2684-2688.

104. Schmidt-Rohr, K., Spiess, H. W., *Multidimensional Solid-state NMR and Polymers.* 2012: Elsevier.

105. Spiess, H. W., *Nuclear magnetic resonance spectroscopy in macromolecular science.* Macromolecular Chemistry and Physics, 2003. **204**(2): p. 340-346.

106. Spiess, H. W., *Multidimensional NMR methods for elucidating structure and dynamics of polymers,* in *Annual Reports on NMR Spectroscopy*. 1997, Elsevier. p. 1-37.

107. Hedesiu, C., Demco, D. E., Kleppinger, R., Buda, A. A., Blümich, B., Remerie, K., Litvinov, V. M., *The effect of temperature and annealing on the phase composition, molecular mobility and the thickness of domains in high-density polyethylene.* Polymer, 2007. **48**(3): p. 763-777.

108. Horii, F., Kaji, H., Ishida, H., Kuwabara, K., Masuda, K., Tai, T., *Solid-state NMR analyses of the structure and dynamics of polymers in the different states.* Journal of Molecular Structure, 1998. **441**(2-3): p. 303-311.

109. Klein, P. G., Driver, M. A. N., *Chain diffusion in ultralong n-alkane crystals studied by ^{13}C NMR.* Macromolecules, 2002. **35**(17): p. 6598-6612.

110. Agarwal, V., van Erp, T. B.,Balzano, L., Gahleitner, M., Parkinson, M., Govaert, L. E., Litvinov, V., Kentgens, A. P. M., *The chemical structure of the amorphous phase of propylene–ethylene random copolymers in relation to their stress–strain properties.* Polymer, 2014. **55**(3): p. 896-905.

111. Bovey, F.A., Mirau, P. A., *NMR of Polymers*. 1996: Academic Press.

112. Botha, L., Sinha, P., Duveskog H., Van Reenen Albert J., *The use of solid-state NMR to investigate the development of segmental mobility in commercial heterophasic ethylene propylene copolymers (HEPCs).* Macromolecular Reaction Engineering, 2015. **9**(4): p. 313-324.

113. Hsieh, E. T., Randall, J. C, *Monomer sequence distributions in ethylene-1-hexene copolymers.* Macromolecules, 1982. **15**(5): p. 1402-1406.

114. Bovey, F. A., Mirau, P. A., Gutowsky, H. S., *Nuclear magnetic resonance spectroscopy*. 1988: Elsevier.

115. Stothers, J., *Carbon-13 nuclear magnetic resonance spectroscopy*. Quarterly Reviews, Chemical Society, 1965. **19**(2): p. 144-167.

116. Levy, G. C., Lichter, R. L., Nelson, G. L., *Carbon-13 nuclear magnetic resonance spectroscopy*. 1992: Krieger Publishing Company.

117. Hayashi, S., Hayamizu, K., *Chemical shift standards in high-resolution solid-state NMR (1) 13C, 29Si, and 1H nuclei.* Bulletin of the Chemical Society of Japan, 1991. **64**(2): p. 685-687.

118. Cheruthazhekatt, S., Harding, G. W., Pasch, H., *Comprehensive high temperature two-dimensional liquid chromatography combined with high temperature gradient chromatography-infrared spectroscopy for the analysis of impact polypropylene copolymers.* Journal of Chromatography A, 2013. **1286**: p. 69-82.

Chapter 3

Experimental

This chapter provides details on the origin of samples used, sample selection, sample preparation as well as the analytical techniques used in this study.

3.1 Origin of HEPCs

The three different heterophasic ethylene-propylene copolymers (HEPCs) used in this study were originally produced by SASOL Polymers, Secunda, South Africa.

The HEPCs were obtained from the same commercial gas phase process. Figure 3.1 is an illustration of a typical commercial gas phase process for the production of heterophasic copolymers. The first reactor is responsible for the production of the polypropylene homopolymer and the second reactor allows for the introduction of ethylene and propylene in a specific ratio to the existing polypropylene homopolymer for copolymerization to occur. The ratio between the ethylene and propylene monomers determines the ethylene distribution in the copolymer.

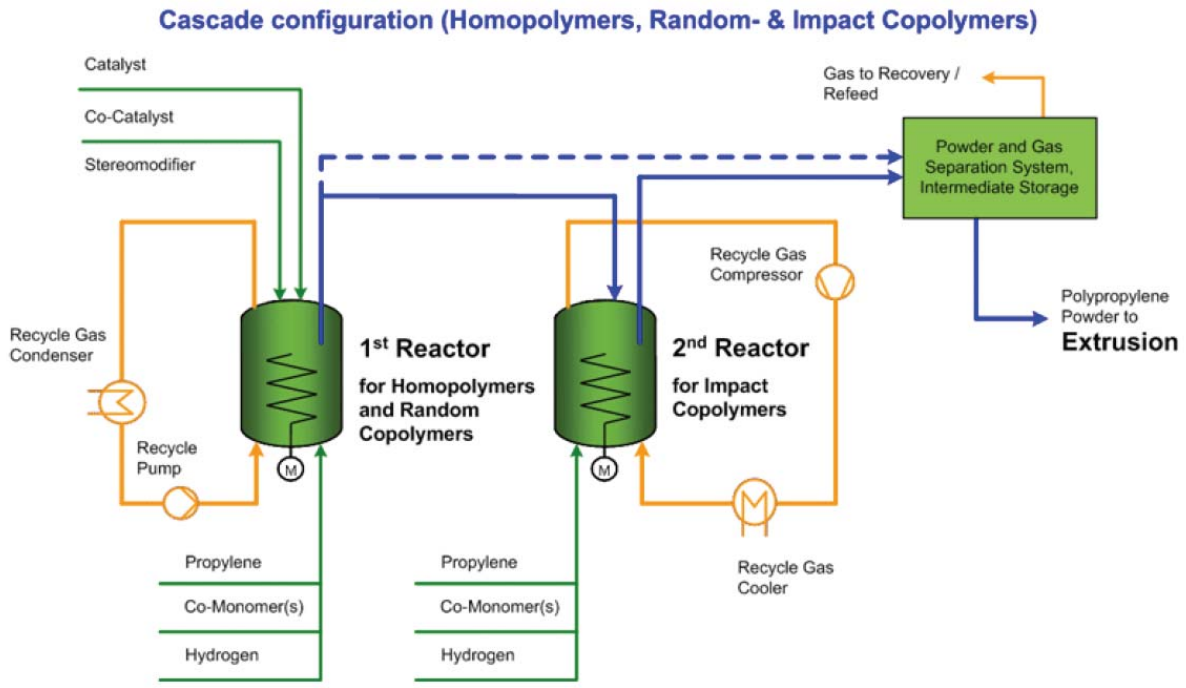

Figure 3.1 An illustration of the sequential arrangement of reactors in the Novolene gas phase process for the production of heterophasic copolymers [1]

3.1 Sampling of HEPCs

The HEPCs samples used in this study were sampled at different times during the transition from homopolymer to copolymer. They, therefore, comprise different copolymer compositions. It must be noted that the transition to copolymer can occur at different rates depending on the plant conditions. Therefore, the samples obtained during each transition will differ in terms of the rate of ethylene introduction and development of ethylene content, thus the samples obtained for this study are representative of this particular transition only.

Samples representing the polypropylene homopolymer in the first reactor (denoted T0) were sampled (from the second reactor) 0 mins after the introduction of ethylene into the second reactor. The other samples were removed at 30 mins intervals after the ethylene introduction and therefore follow the series T30, T60, T90 etc. However, in order to account for the broad range of ethylene contents from low to high ethylene contents, a few samples were selected from the series for the purposes of this study (T0, T180, and T300). Table 3.1 shows the properties of the samples used in this study as reported by Botha *et al*.[1, 2].

Table 3.1 Properties of samples used in this study [1, 2].

Sample	Time [min][a]	Ethylene content [mol%][b]	Ethylene content [mol%][c]	Copolymer content [mol%][c]	Copolymer ethylene content [mol%][c]
T0	0	0	0	0	0
T180	180	5.2	2.8	10.1	28.2
T300	300	10.8	6.5	17.6	36.8

[a] Time of sampling after ethylene introduction
[b] Determined by ^{13}C NMR
[c] Determined by FTIR

3.2 Vis-breaking of the HEPCs

The vis-breaking experiment used involved developing a methodology that will mimic the reactions that will occur during extrusion vis-breaking. This methodology used a melt flow indexer to blend and react small amounts of the HEPCs with peroxide.

Trigonox®301 or 3,6,9-trimethyl-1,4,7-triperoxonane (Akzo Nobel Polymer Chemicals, Amersfoort, Netherlands) was used as the peroxide of choice. It has a molecular weight of 264.3 g/mol and a total active oxygen content of 7.3-7.6%. Figure 3.2 shows the structure of Trigonox®301. The reactivity of organic peroxides varies with temperature and is often given in terms of half-life. Therefore, the half-life of the Trigonox®301 peroxide at a specific temperature can be calculated from the equation below:

$$k_d = Ae^{-Ea/RT} \quad \text{(Eq 3.1)}$$

$$t_{1/2} = \frac{\ln 2}{k_d} \quad \text{(Eq 3.2)}$$

Where,

$t_{1/2}$ = time required to reduce the original initiator content of a peroxide by 50 %, at a given temperature
K_d = initiator decomposition rate at a given temperature
Ea = 150.23 kJ/mol

A = 1.02 x 10^{15}
R = 8.3124 J/(mol.K)
T = (273.15 + °C) K

and the total active oxygen content is calculated from the equation below:

$$Total\ active\ oxygen\ content = \frac{16 \times number\ of\ peroxide\ bonds}{molecular\ weight} \times 100 \qquad \text{Eq 3.3}$$

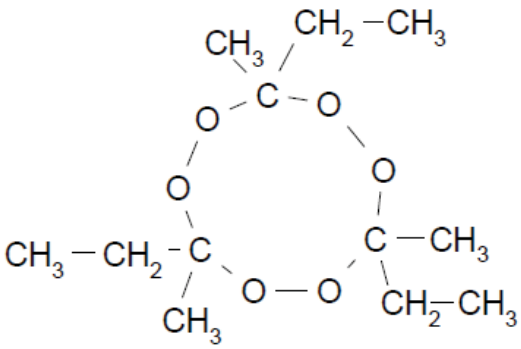

Figure 3.2 Molecular structure of Trigonox®301 [3]

During each vis-breaking experiment, the melt flow indexer (Wirsam Scientific, South Africa) was set to 190 °C and kept at this temperature throughout the experiment. 10 g of each HEPC sample was premixed with 0, 0.025, 0.2 and 0.5 wt. % of Trigonox®301 in a beaker. The mixture was then transferred into the pre-heated melt flow indexer and allowed a residence time of 30 minutes in the instrument's barrel. Once the polymer/peroxide was fully melted, it was pushed out of the melt flow indexer using 2.16 kg weight. Figure 3.3 below is an illustration of a typical melt flow indexer.

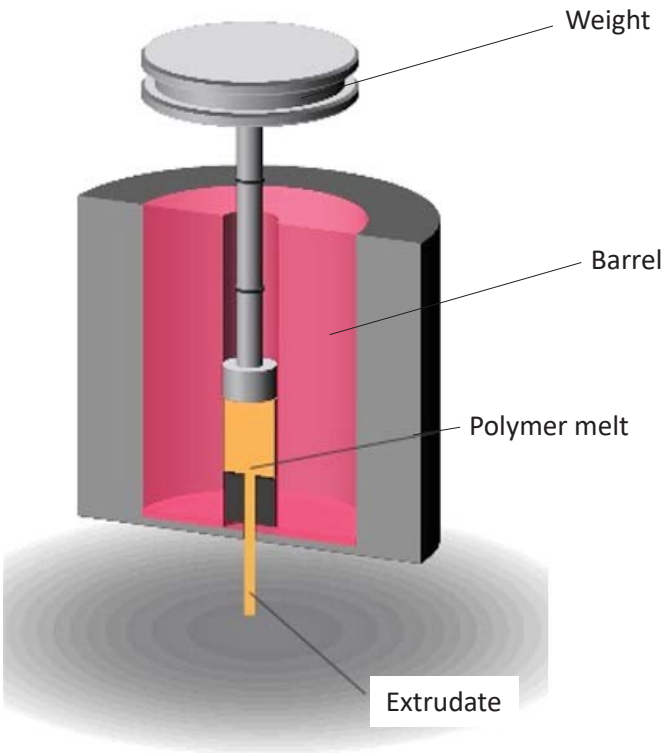

Figure 3.3 A schematic diagram of a typical melt flow indexer [4]

3.3 Fractionation techniques

3.3.1 Preparative temperature rising elution fractionation (p-TREF)

Vis-broken and non vis-broken HEPC fractions were obtained via an in-house built p-TREF instrument. The p-TREF procedure is divided into two consecutive steps: crystallization and elution, which are described in detail below.

3.1.1.1 Crystallization step

In the crystallization step, 3 g of either the vis-broken or non vis-broken HEPCs was dissolved in 300 ml of xylene at 130 °C in a glass reactor. Once the polymer samples were completely dissolved, pre-heated silica sand (white quartz, 50-70 mesh particle size, Sigma Aldrich) was added to the polymer solution to act as a crystallization support. The glass reactor was then placed in an oil bath pre-heated at 130 °C. After that, the oil bath was cooled at 1 °C/hour from 130 °C to 25 °C to facilitate crystallization of the polymer from solution onto the silica sand support. Due to the differences in crystallizability of the polymer chains, the polymers crystallize in several layers around the sand particles. The layers grow outwards in an orderly fashion according to decreasing crystallizability. Figure 3.4 is an illustration of the crystallization step setup.

3.3.1.2 Elution step

During the elution step, the crystallized polymer was transferred to a steel column placed in a modified GC oven. After that, xylene was passed through the column while the temperature in the oven and column was increased to 130 °C in a stepwise manner for the fractions to be collected at predetermined temperatures. The xylene solvent was pumped at 40 ml/min using a FMI “Q” Model QG150 pump and fractions were collected at pre-determined intervals per temperature increment. The eluted fractions were transferred to a round bottomed-flask and a rotary evaporator was used to remove the solvent. After the solvent was mostly evaporated, the fractions were recovered by precipitation with acetone. The recovered fractions were then dried to a constant weight in a vacuum oven. Figures 3.5 and 3.6 are illustrations of the modified GC oven and steel column used during the elution step.

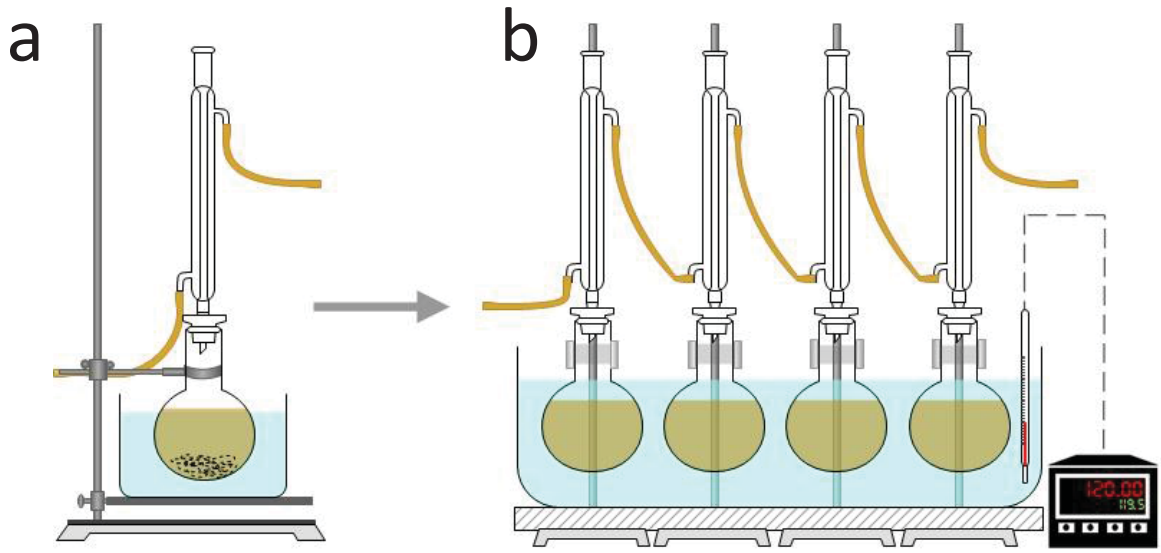

Figure 3.4 An illustration of the dissolution (a) and cooling (b) setups during the crystallization step

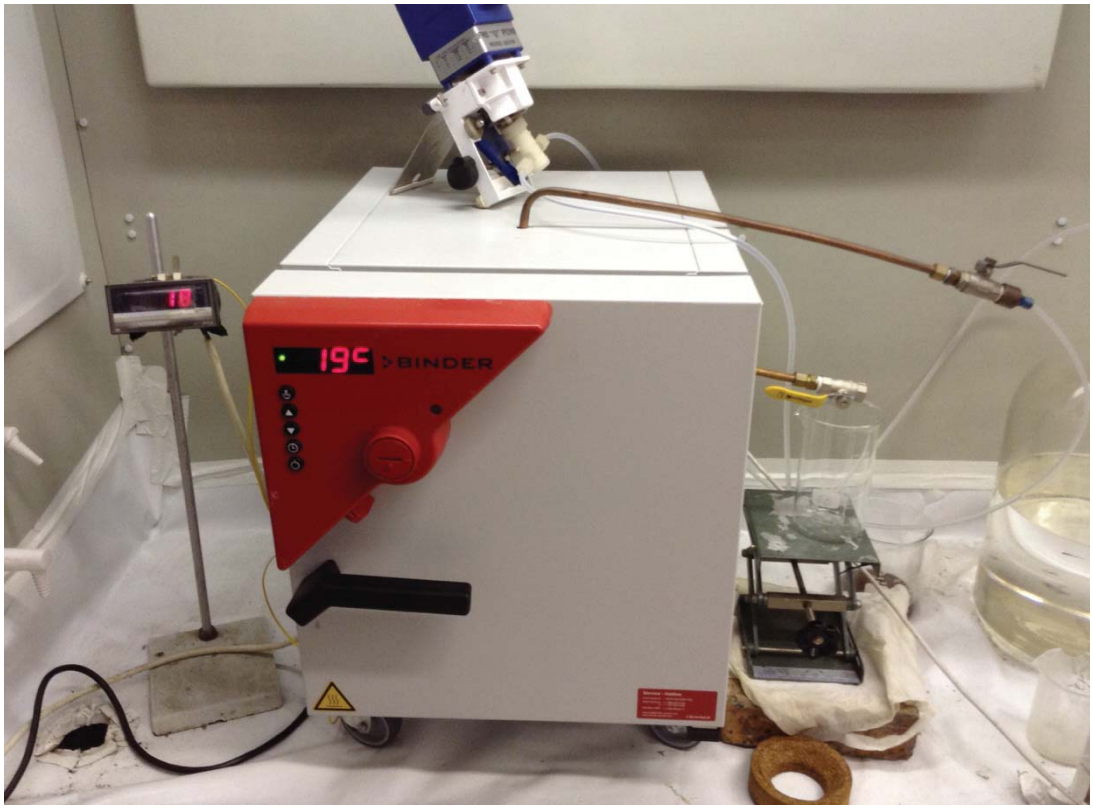

Figure 3.5 An illustration of the modified GC oven used during the elution step setup

Figure 3.6 A picture of the steel column used in this study

3.3.2 Solvent gradient elution fractionation (SGEF)

Xylene and 2-ethoxyethanol were used as solvent and non-solvent, respectively. 3 g of the HEPC sample and 0.06 g of Irganox1010 phenolic antioxidant were dissolved in 100 ml of xylene at 130 °C. 700 ml of 2-ethoxyethanol (non-solvent) was then added dropwise into the solution. After that, the xylene/ 2-ethoxyethanol solvent mixture was transferred into a column consisting of sand particles (white quartz, 50-70 mesh particle size, Sigma Aldrich) pre-heated to 130 °C. The solvent mixture was allowed a residence time of 45 mins in the column before it was eluted to collect the first fraction. For the rest of the fractions, the solvent mixture was varied in stepwise increments by increasing the volume percent of xylene (solvent). The temperature was kept constant at 130 °C throughout the fractionation except for the last fraction where it was increased to 150 °C to ensure a 100 % recovery of the fractionated sample. The eluted solvent mixture was cooled, precipitated with acetone, filtered and dried in a vacuum oven. Figure 3.7 is an illustration of the SGEF setup used in this study.

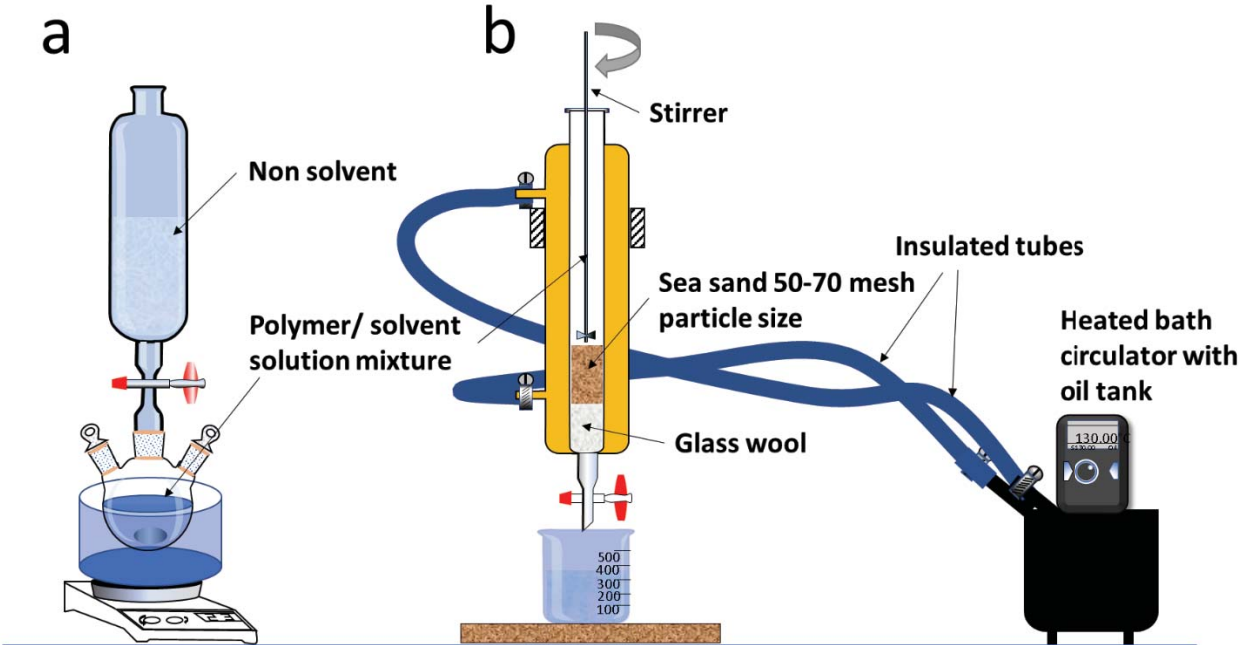

Figure 3.7 An illustration of the SGEF setup used in this study where (a) is the dropwise addition of the non solvent into polymer/solvent solution and (b) is the elution of the solvent/non solvent mixture.

3.4 Characterization techniques

3.4.1 Fourier transform infrared spectroscopy (FTIR)

A Thermo Nicolet iS10 spectrometer (Thermo Electron, Waltham, USA) was used for the attenuated reflectance (ATR) measurements of the bulk HEPCs and their P-TREF fractions. The samples were used in their solid form without any prior modifications. Spectra were

collected between 4000 and 650 cm^{-1} at 64 scans with a 4 cm^{-1} resolution and an automatic background subtraction. Data collection and processing was achieved via a Thermo Scientific OMNIC software (version 8.1).

3.4.2 Solid-state carbon-13 nuclear magnetic resonance spectroscopy (^{13}C-NMR)

All the solid-state NMR experiments in this study were performed in a Varian VNMS 500 MHz two-channel spectrometer using 4 mm zirconia rotors and a 4 mm Chemagnetics™ T3 HX MAS probe. For the CP-MAS (cross-polarization magic angle spinning) experiments, ^{13}C cross-polarization spectra were obtained at variable temperatures under the following conditions: proton decoupling, a 3.5 µs 90 ° pulse and a recycle delay of 5 s. Magic-angle-spinning was performed at 5 KHz with adamantine used as an external chemical shift standard and the downfield peak was referenced to 38.3 ppm. The power parameters were optimized for the Hartmann-Hahn match; the radio frequency fields were $\gamma_C B_{1C} = \gamma_H B_{1H} \approx 57\ KHz$. Cross-polarization contact time was 1 ms. The free induction decay had 442 complex points and was Fourier transformed with 20 Hz line broadening.

3.4.3 Solution-state carbon-13 nuclear magnetic resonance spectroscopy (^{13}C-NMR)

A 600 MHz Varian^{unity} INOVA NMR spectrometer situated at the Central Analytical Facility (CAF) at Stellenbosch University was used for all the solution-state ^{13}C-NMR experiments in this study. The solution NMR instrument was set to the following operating conditions: a 90 ° flip angle of ~ 7.4 µs with inverse gated proton decoupling as well as an acquisition time of 1.8 s and a pulse delay of 15 s. For all the analyses, 60 mg of the HEPC samples were dissolved in 0.6 ml deuterated tetrachloromethane (d-TCE, Aldrich, South Africa) to a final concentration of 100 mg/ml. In order to completely homogenise the sample in solution, 0.3 ml of the solvent was first added to the sample in an NMR tube and then heated with a heat gun to facilitate melting. Another 0.3 ml of the solvent was finally added to the tube. The tube was then sealed and then placed in an oil bath at 130 °C for at least an hour for it to homogenise. Spectra obtained from the NMR experiments was considered to be 99 % quantitative because only the carbon atoms with T_1 relaxation delays of < 3 s were taken into account. Integrals of the obtained spectra were obtained according to the spectral assignments reported in literature [5-8]. Monomer contents and dyad monomer sequences were calculated according to the method by Ray *et al.* [7] and number average sequence lengths according to Zhang *et al.* [8]. PEP, PEE and EEE triads were determined using the method by Ray *et al.* [7] and the PPP, PPE and EPE triads were calculated according to a method by Kakugo *et al.* [9]. Figure 3.8 below is a ^{13}C-

NMR spectra of an ethylene-propylene impact copolymer showing the ^{13}C-NMR peak assignments in this polymer and Figure 3.9 is an illustration of the carbon assignments used in solution NMR.

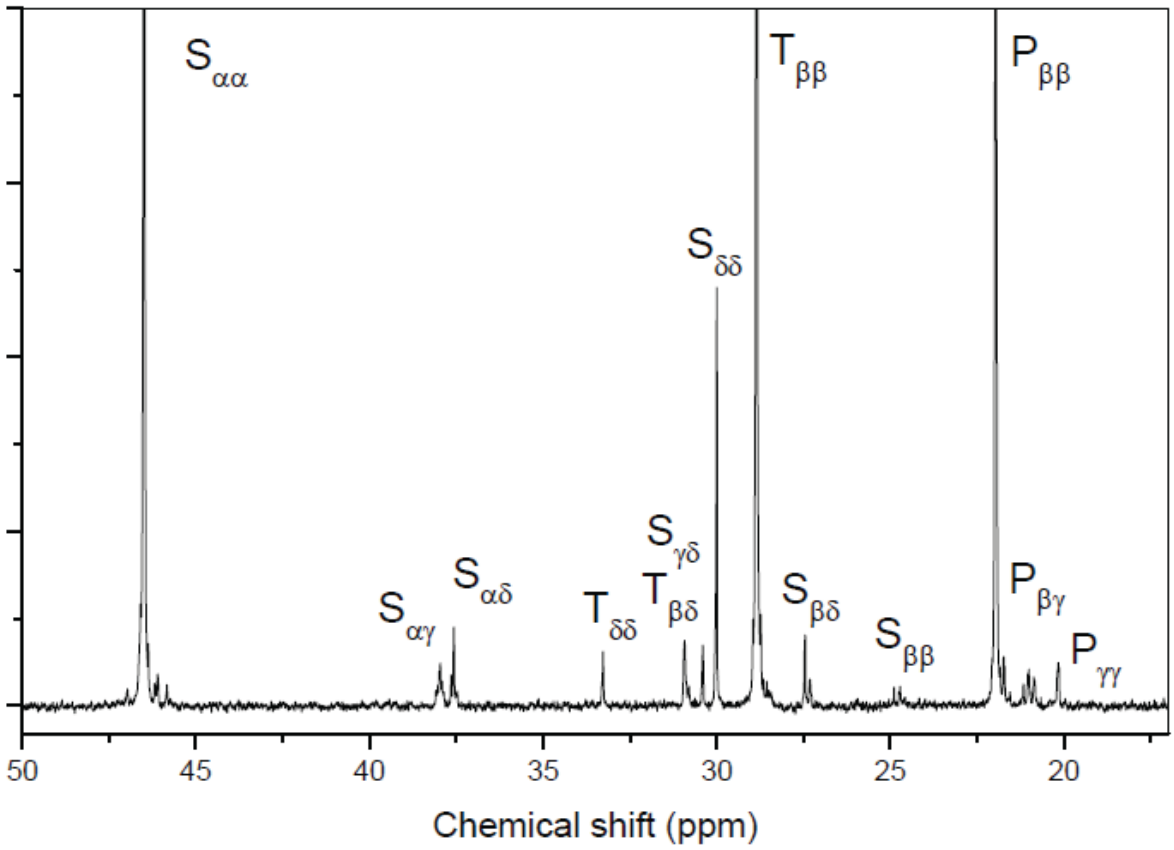

Figure 3.8 Solution-state ^{13}C-NMR of an ethylene-propylene impact copolymer with a low ethylene content [3].

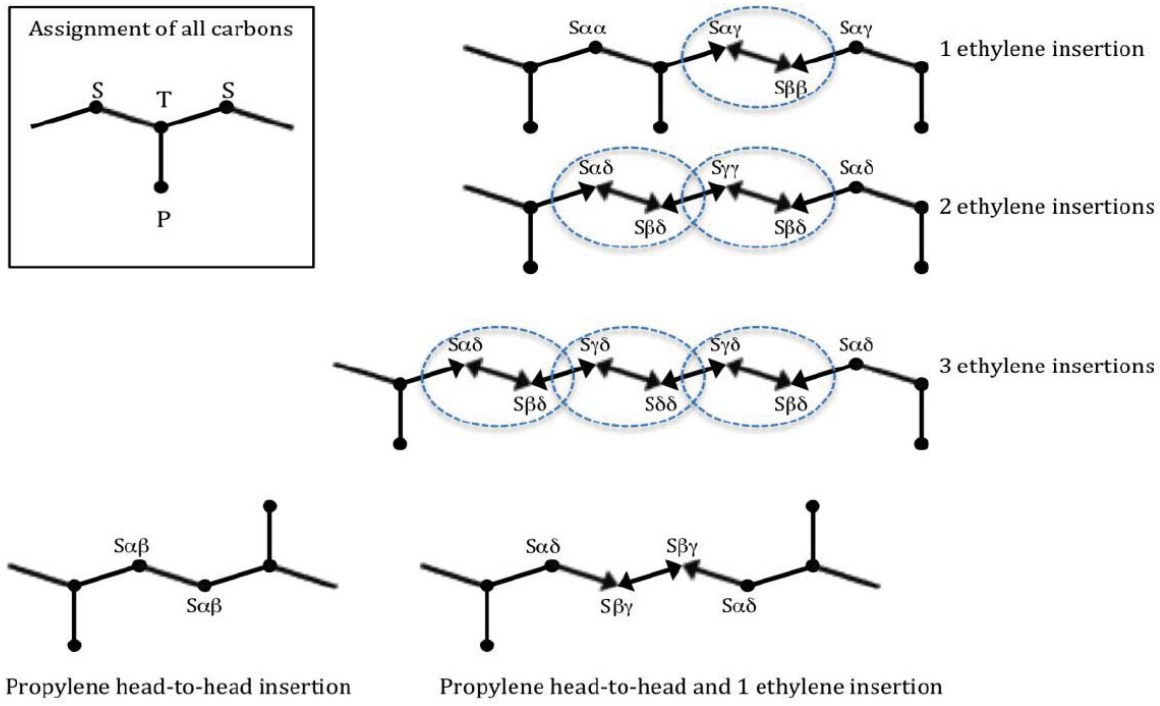

Figure 3.9 Solution NMR carbon assignments as proposed by Carman and Wilkes [6] and Ray *et al*. [7]

3.4.4 Differential scanning calorimetry (DSC)

A TA instruments Q100 calorimeter calibrated with Indium metal was used to determine the melting and crystallization behaviour of the HEPC samples used in this study. 4 mg of the HEPC sample was weighed in an aluminium pan with a flat lid and then placed in the furnace of the calorimeter for analysis. An empty aluminium pan with a flat lid was also placed in the furnace as a reference. The samples were subjected to 3 cycles at a heating/cooling rate of 10 °C/min and a temperature range of 0-200 °C. The thermal history of each HEPC sample was erased in the first cycle (first heating). Qualitative and quantitative information was obtained from the second and third cycles (first cooling and second heating). The temperature at the end of each cycle was kept constant for 2 mins. All the measurements were conducted in an inert nitrogen atmosphere set at a purge gas flow rate of 50 ml/min.

3.4.5 High temperature size exclusion chromatography (HT-SEC)

A PL-GPC 220 High temperature chromatograph (Polymer Laboratories, Church Stretton, UK) equipped with a refractive index (RI) detector was used for all the molar mass and molar mass dispersity measurements of the HEPCs used in this study. 4 mg of each HEPC sample was dissolved in 2 ml of TCB with 0.025 % BHT stabilizer to prevent sample decomposition/ degradation. The samples were left to dissolve for 3 hours in the TCB. Three 300 x 75 mm PLgel Olexis columns (Polymer Laboratories, Church Stretton, UK) together with a 50 x 7.5

mm PLgel Olexis guard column were used for all measurements. TCB with 0.025 % BHT was used as a mobile phase at a flow rate of 1 ml/min. 200 µl of each sample was injected for all measurements and each experiment was carried out at 150 °C. Narrowly distributed polystyrene standards (Polymer Laboratories, Church Stretton, UK) were used to calibrate the HT-SEC instrument.

3.4.6 High temperature high performance liquid chromatography (HT-HPLC)

A solvent gradient interaction chromatograph (SGIC) manufactured by Polymer Char (Valencia, Spain) was used for all the chromatographic experiments in this study. The chromatograph instrument used consisted of an auto sampler, two separate ovens, switching valves, two pumps equipped with vacuum degassers (Agilent, Waldbromm, Germany) and an evaporative light scattering detector (ELSD, model PL-ELS 1000, Polymer Laboratories, Church Stretton, England). The ELSD detector was used under the following conditions: a gas flow rate of 1.5 l/min, a nebulizer temperature of 160 °C and an evaporative temperature of 270 °C. All the chromatographic experiments were performed in a Hypercarb column (Hypercarb®, Thermo Scientific, Dreieich, Germany) with the following specifications: a 100 x 4.6 mm internal diameter packed with porous graphite particles with a particle diameter of 5 µm, a surface area of 120 m^2/g and a pore size of 250 Å. The column was placed in an oven and the temperature maintained at 160 °C. Separation was achieved by applying a linear gradient from 100 % 1-decanol to 100 % TCB within 10 mins of sample injection at a mobile phase flow rate of 0.5 ml/min [10]. The above experimental conditions were held constant for 20 minutes before re-establishing 1-decanol to 100 %. For all the experiments, a high pressure binary gradient pump (Agilent, Waldbromm, Germany) was used. The HEPCs were injected at a concentration of 1-1.2 mg/ml, with 20 µl of each sample injected. Figure 3.8 below is an illustration of the gradient profile of the mobile phase used during the HPLC experiments.

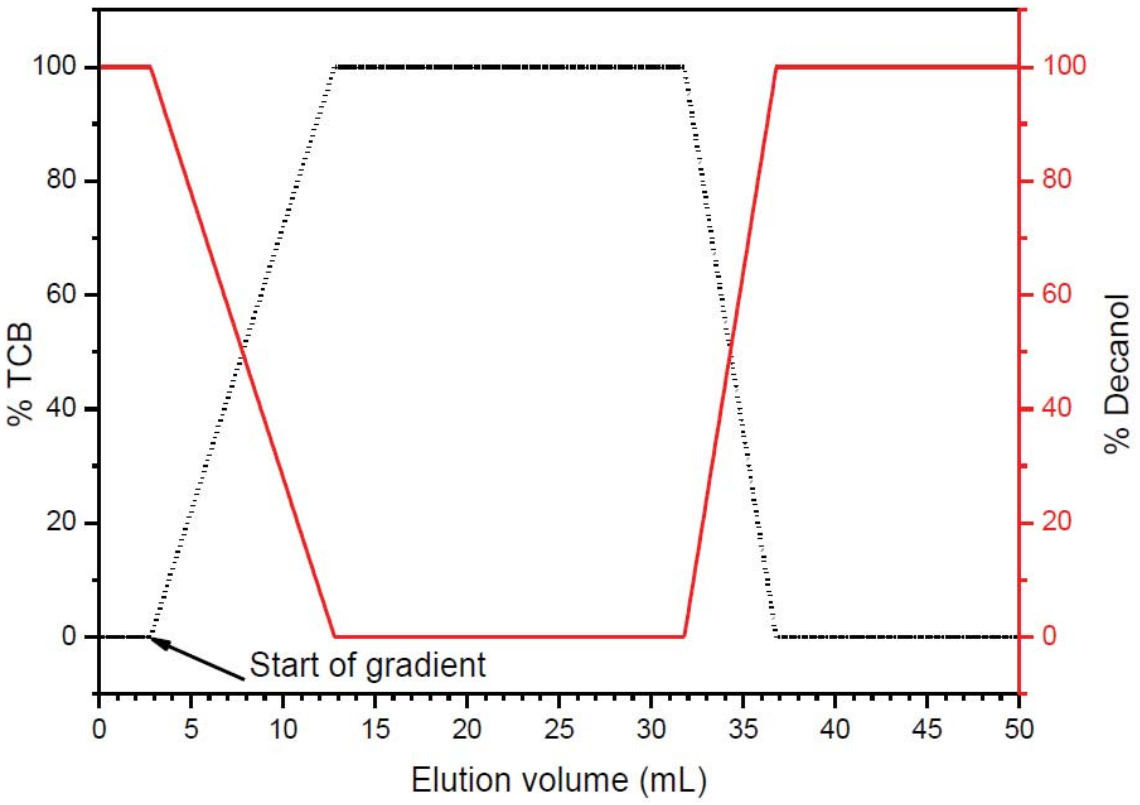

Figure 3.10 An illustration of the solvent gradient profile during a typical HPLC experiment [11]

3.5 Mechanical testing

3.5.1 Dynamic mechanical analysis (DMA)

For all the dynamic mechanical analyses in this study, a Q800 dynamic mechanical analyser (TA Instruments Ltd, Herts, United Kingdom) was used. DMA is a wonderful tool in determining the viscoelastic behaviour of polymers. It works by applying a sinusoidal stress on the polymer sample and then measuring the subsequent strain. This makes it easier to determine the complex modulus of your polymer samples. Varying the temperature in DMA analyses gives variations in complex modulus which in turn allows for the determination of the glass transition temperature (T_g) as well as other transitions which correspond to other molecular transitions [12].

In preparation for the DMA analyses, the HEPC samples were first melt pressed in rectangular moulds at 180 °C. The rectangular moulds were then measured three times along their length and width for accurate calculations. The HEPCs were then covered in foil and inserted into the DMA instrument for analyses. During the analyses, the HEPC samples were cooled from 50 °C to -100 °C by 1 °C/min and then kept isothermal at -100 °C for 5 mins. Temperatures were

then increased to 180 °C by 1 °C/min. Finally, the samples were cooled down again to room temperature (25 °C) at 1 °C/min. The frequency used for the analyses was 1 Hz.

3.5.2 Rheology measurements

3.5.2.1 Parallel plate rheology measurements

A TA instruments Discovery HR2 rheometer was used for all the parallel plate rheology measurements in this study. The HEPC samples were prepared by melt pressing them into disc moulds at 170 °C. Frequency sweeps were performed on the samples at temperatures ranging from 150 °C to 230 °C and angular oscillation frequencies ranging from 0.1 rad/s to 600 rad/s. In order to stay within the linear response region of all the HEPC samples, a 2.5 % strain was used throughout. A 25 mm parallel plate geometry with a 1 mm thickness was used in all the measurements. The rheology curves of all the HEPC samples were time-temperature superposition (TTS) shifted to 180 °C.

3.6 References

1. Botha, L., *The effect of in-process ethylene incorporation on the evolution of particle morphology and molecular characteristics of commercial heterophasic ethylene propylene copolymers (HEPCs)*. 2014, PhD Thesis. Stellenbosch University.

2. Botha, L., van Reenen, A., *The effect of in-process ethylene incorporation on the evolution of particle morphology and molecular characteristics of commercial heterophasic ethylene propylene copolymers (HEPCs).* European Polymer Journal, 2013. **49**(8): p. 2202-2213.

3. Swart, M., *The effect of controlled degradation with an organic peroxide on the molecular characteristics and properties of heterophasic propylene-ethylene copolymers (HECO)*. 2013, PhD Thesis, University of Stellenbosch.

4. Instron, melt flow,Heat Deflection Temperature and Impact, viewed on 26 February 2019, https://www.slideshare.net/Instron/3-challenges-in-plastics-testing-melt-flow-hdt-impact. [cited 2019 26 February 2019].

5. Randall, J. C., *Methylene sequence distributions and number average sequence lengths in ethylene-propylene copolymers.* Macromolecules, 1978. **11**(1): p. 33-36.

6. Carman, C., Wilkes, C., *Monomer sequence distribution in ethylene propylene elastomers. I. Measurement by carbon-13 nuclear magnetic resonance spectroscopy.* Rubber Chemistry and Technology, 1971. **44**(3): p. 781-804.

7. Ray, G. J., Johnson, P. E., Knox, J. R., *Carbon-13 nuclear magnetic resonance determination of monomer composition and sequence distribution in ethylene-propylene copolymers prepared with a stereoregular catalyst system.* Macromolecules, 1977. **10**(4): p. 773-778.

8. Zhang, X., Chen, H., Zhou, Z., Huang, B., Wang, Z., Jiang, M., Yang, Y., *DSC and carbon-13 nuclear magnetic resonance spectroscopy studies of ethylene-propene copolymers prepared by a highly active and stereospecific catalyst.* Macromolecular Chemistry and Physics, 1994. **195**(3): p. 1063-1073.

9. Kakugo, M., Naito, Y., Mizunuma, K., Miyatake, T., *Carbon-13 nuclear magnetic resonance spectroscopy determination of monomer sequence distribution in ethylene-propylene copolymers prepared with δ-titanium trichloride-diethylaluminum chloride.* Macromolecules, 1982. **15**(4): p. 1150-1152.

10. Cheruthazhekatt, S., Pijpers, T. F. J., Harding, G. W., Mathot, V. B. F., Pasch, H., *Compositional analysis of an impact polypropylene copolymer by fast scanning DSC and FTIR of TREF-SEC cross-fractions.* Macromolecules, 2012. **45**(15): p. 5866-5880.

11. Ndiripo, A., *Comparative study on the molecular structure of ethylene/1-octene, ethylene/1-heptene and ethylene/1-pentene copolymers using advanced analytical methods*. 2015, Masters Thesis, Stellenbosch University.

12. Menard, K. P., *Dynamic mechanical analysis: a practical introduction*. 2008: CRC press.

Chapter 4

Bulk analysis of vis-broken and non vis-broken HEPCs

In this chapter, the results obtained from the characterization of the vis-broken and non vis-broken bulk HEPCs are discussed.

4.1 Introduction

The first part of this study involve the analyses of non vis-broken and vis-broken (bulk) HEPCs. The T0, T180 and T300 bulk HEPC samples, with 0, 5.2 and 10.8 mol % ethylene content were first vis-broken at various degrees (0, 0.025, 0.2 and 0.5 wt. %) with Trigonox®301. The extent of the vis-breaking was then tracked by high temperature size exclusion chromatography (HT-SEC). Attenuated total reflectance-infrared spectroscopy (ATR-FTIR) was used to investigate any chemical changes induced by the vis-breaking. Differential scanning calorimetry (DSC) was used to investigate the effect that the degree of vis-breaking has on the thermal behaviour of bulk HEPCs. Finally, dynamic mechanical analyses (DMA) and rheological studies were then used to study the mechanical and rheological behaviour of the bulk HEPCS at the highest degree of vis-breaking (0.5 wt. % peroxide).

4.2 Results and discussion

4.2.1 High temperature size exclusion chromatography (HT-SEC)

In general, vis-breaking causes a decrease of the molar mass and a narrowing of the molar mass distribution (MMD) in a polymer sample [1]. Therefore, HT-SEC was used to investigate the degree of vis-breaking.

Figures 4.1 (a) - (c) below show MMD curves of the bulk HEPCs at various degrees of vis-breaking. From the results, a significant shift of the MMD curves towards lower molar masses and a narrowing of the MMD curves was observed at 0.5 wt. % for all the samples. However, the most significant shifts were observed for the T180 and T300 samples (Figures 4.1 b and c). This shift seemed to be related to the increase in ethylene content. One explanation for this is that the “soft” copolymer phase could be acting as an aid in the mixing/dispersion of the peroxide within the “hard” iPP matrix resulting in a more efficient vis-breaking process. Therefore, it was suspected that the copolymer (rubbery phase) could be acting as a transport system in the melt during vis-breaking. Alternatively, the ethylene-propylene copolymers could be more susceptible to vis-breaking than the iPP matrix.

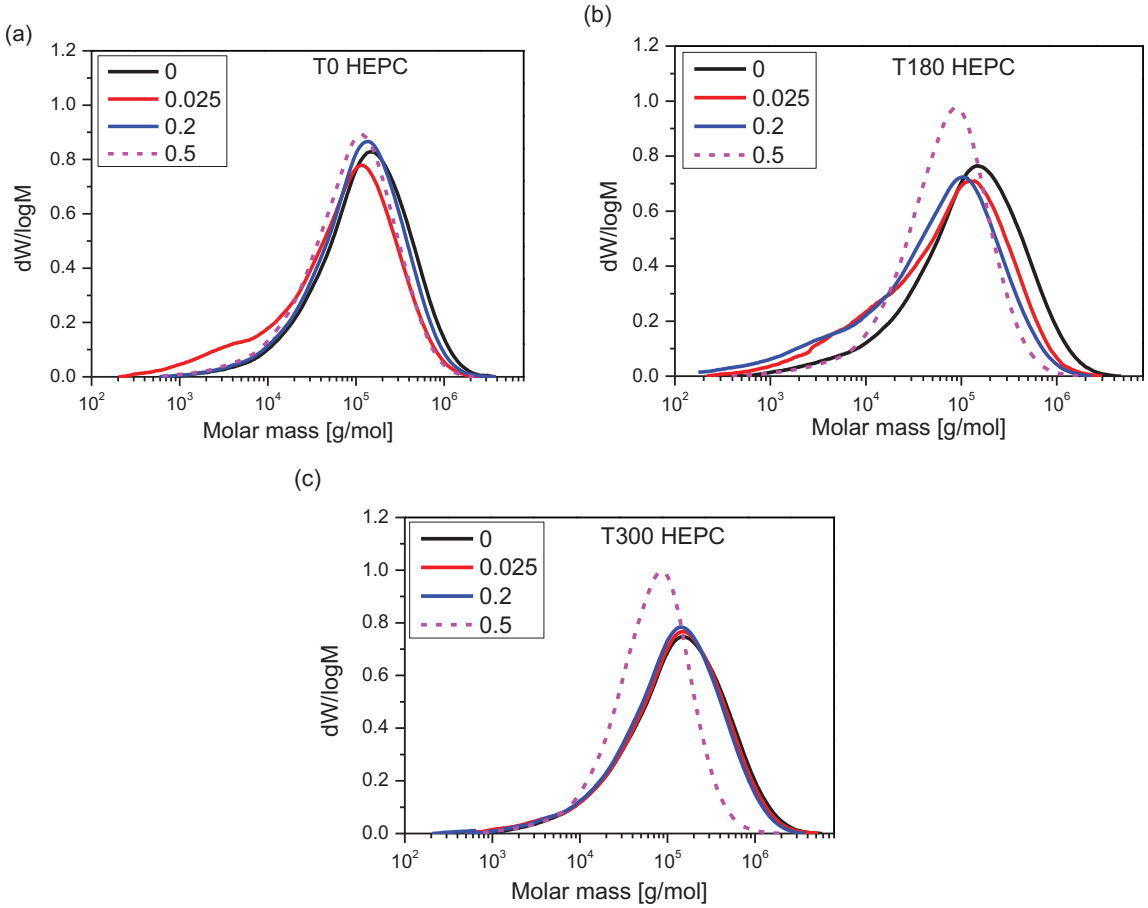

Figure 4.1 HT-SEC curves of (a) T0, (b) T180 and (c) T300 vis-broken at 0, 0.025, 0.2 and 0.5 wt. % Trigonox®301

In addition to the MMD curves, more data was extracted from the HT-SEC results in order to understand the degree of the vis-breaking. Tables 4.1 to 4.3 below show the HT-SEC data of the HEPCs with increasing peroxide used. The data shows a decrease of Mp, Mw and Đ with increasing peroxide concentration for all the HEPCs. Again, the decrease was more significant for the T180 and T300 samples at 0.5 wt. % of peroxide. The Mz value, which is sensitive to the high molar mass chains present, was seen to decrease with increasing the vis-breaking step. This confirmed that the peroxide was breaking down the long chains in the polymer samples (as would be expected).

Table 4.1 HT-SEC data of T0 at 0, 0.025, 0.2 and 0.5 wt. % Trigonox®301

% Trigonox®301	Mp [x10^{-5}] g/mol	Mn [x10^{-4}] g/mol	Mw [x10^{-5}] g/mol	Mz [x10^{-5}] g/mol	Đ
0.000	1.837	4.620	2.498	6.336	5.410
0.025	1.790	5.060	2.543	6.309	5.020
0.200	1.411	4.300	1.828	4.303	4.250
0.500	1.176	3.610	1.464	3.277	4.060

Table 4.2 HT-SEC data of T180 at 0, 0.025, 0.2 and 0.5 % Trigonox®301

% Trigonox®301	Mp [x10^{-5}] g/mol	Mn [x10^{-4}] g/mol	Mw [x10^{-5}] g/mol	Mz [x10^{-5}] g/mol	Đ
0.000	1.948	6.500	2.950	7.855	4.540
0.025	1.384	1.630	1.496	4.159	9.180
0.200	1.381	4.570	1.859	4.428	4.060
0.500	8.800	3.040	1.046	2.223	3.440

Table 4.3 HT-SEC data of T300 at 0, 0.025, 0.2 and 0.5 % Trigonox®301

% Trigonox®301	Mp [x10^{-5}] g/mol	Mn [x10^{-4}] g/mol	Mw [x10^{-5}] g/mol	Mz [x10^{-5}] g/mol	Đ
0.000	1.771	5.290	3.122	9.677	5.900
0.025	1.573	3.530	2.290	6.440	6.490
0.200	1.464	3.800	2.108	5.534	5.550
0.500	8.670	3.290	1.005	2.140	3.050

4.2.2 Attenuated total reflectance-Fourier transform infrared spectroscopy (ATR-FTIR)

From the HT-SEC results, it was established that vis-breaking had occurred in the HEPCs. Vis-breaking introduces chemical changes which could involve the formation of various functional groups that are strongly dependant on the structure of the polymer studied [2]. Therefore, ATR-FTIR is normally used in the identification of such functional groups.

Figures 4.2 (a) to (f) below show the FTIR spectra of the HEPCs at various degrees of vis-breaking. In literature, functional groups such as carbonyls, carboxylic groups and hydroperoxide groups are referred to as degradation products. During chain scission in the presence of oxygen, functional groups may be inserted into the polymer chains and these functional groups could be detected by FTIR. These functional groups indicate autoxidation products that may also involve chain scission. All the FTIR spectra showed bands that are representative of vis-breaking or degradation products (i.e carbonyls, carboxylic groups, and hydroperoxide groups) [3-7]. The C=O peaks were more pronounced at 0.5 wt. % for the T0 sample. However, for the T180 and T300 samples, the C=O peaks were more pronounced at 0.2 wt. %. These C=O peaks were confirmation that degradation had occurred in these samples. Note that oxygen needs to be present for these groups to form. Chain scission may take place without oxidative degradation occurring (see Figure 2.5). The experimental set-up limits the amount of oxygen available during vis-breaking.

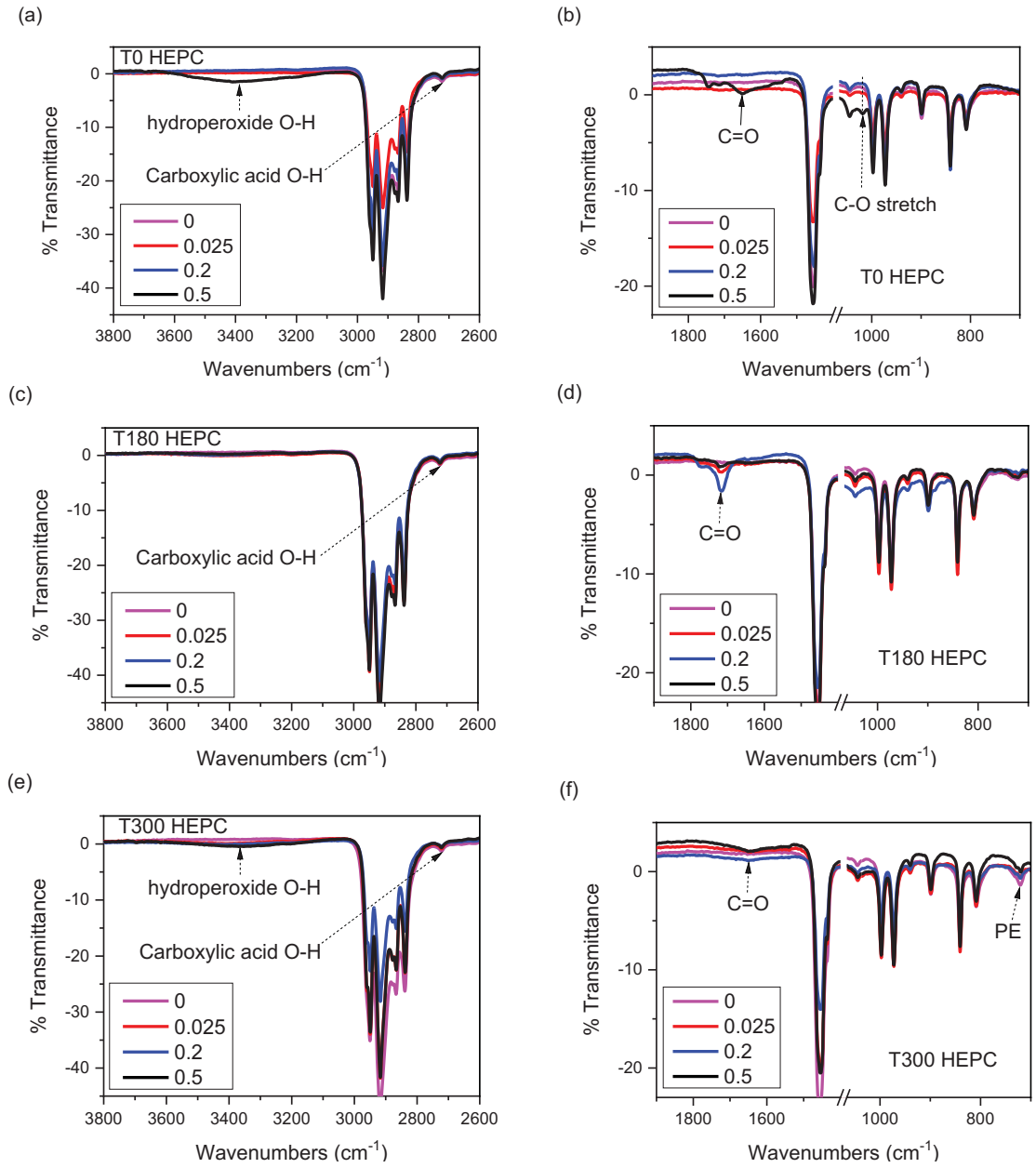

Figure 4.2 FTIR spectra showing the 3800-2600 (a, c, e) and 1900-700 (b, d, f) regions of the HEPCs at various degrees of vis-breaking (0, 0.025, 0.2, 0.5 wt. % peroxide)

4.2.3 Differential scanning calorimetry (DSC)

The effect of vis-breaking on the crystallization and melting behaviour of the HEPC samples was investigated by DSC. Figures 4.3 (a) to (f) below show the crystallization and melting curves of the HEPCs at various degrees of vis-breaking. The melting curves were all collected during the second heating cycle after all the thermal history of the samples was erased. This is because the influence of degraded molecules on crystallization is best reflected by the melting temperature obtained during the second heating cycle [8].

Looking at Figures 4.3 (a), (c) and (e) below, we see an initial increase in crystallization peak temperature with increasing peroxide concentration for T0 and T180. However, the crystallization peak temperatures remained the same for the T300 sample with increasing peroxide concentration. Figures (b), (d) and (f) show a significant splitting and broadening of the melt endotherms with increasing the vis-breaking step. The splitting and broadening became more significant at 0.5 wt % especially for samples T180 and T300. Rabello and White [8] observed similar splitting in photodegraded PP and ascribed this to chain scission reactions and functional group insertions (insertion of carbonyl and hydroxyl groups). These scission reactions and group insertions lead to the formation of defective crystals with low melting temperatures. As the extent of degradation during the vis-breaking is very low (Figure 4.2) it is more likely that the splitting observed for the HEPCs in this study could be due to presence of different crystalline forms of PP resulting from the vis-breaking. It is important to note that the melting and crystallization peaks only represent the iPP fraction, so any changes in the peaks after vis-breaking means that the iPP was affected by the vis-breaking, yet it is also possible that the change in CCD of other species during vis-breaking may affect the crystallization of iPP.

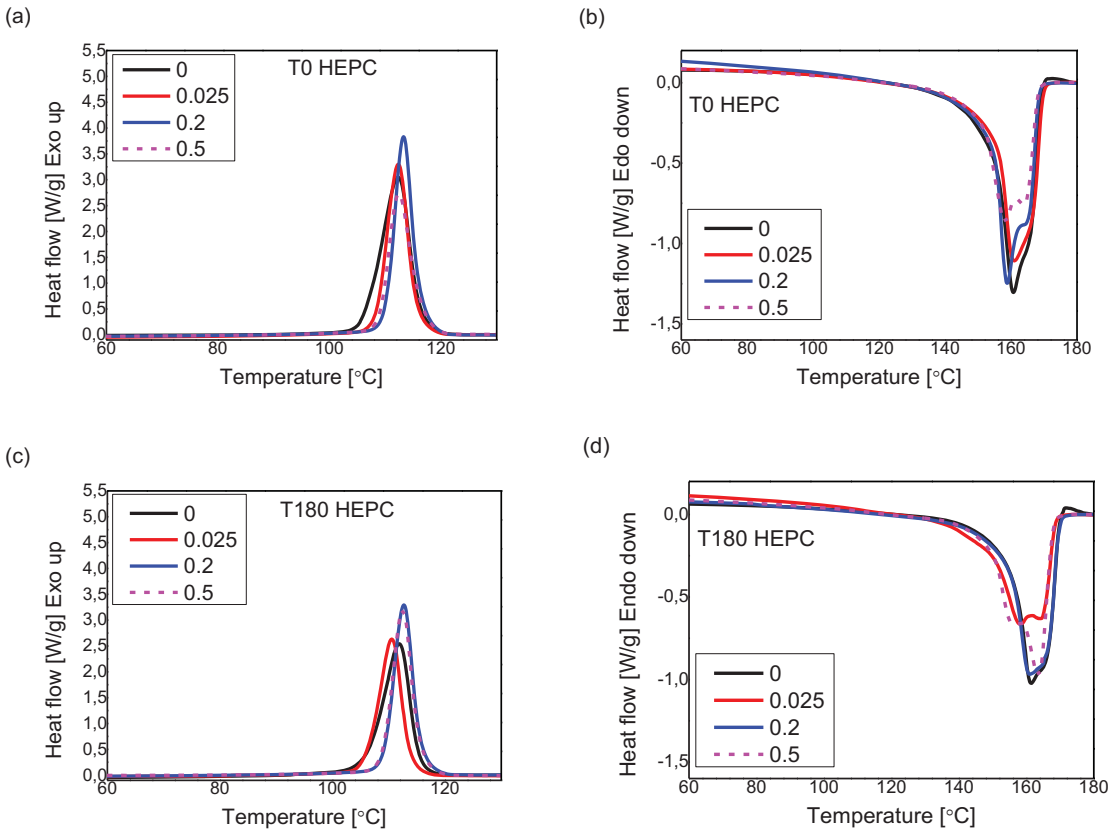

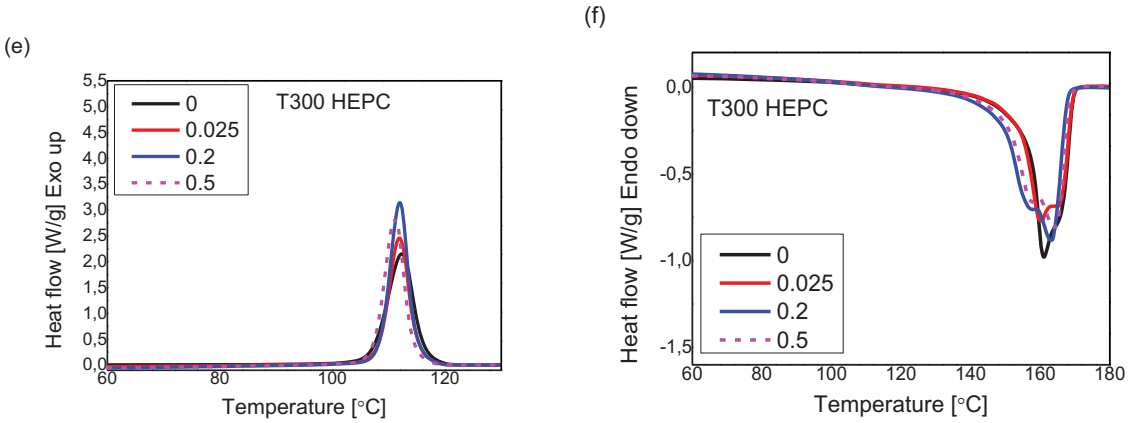

Figure 4.3 DSC crystallization (a,c,e) and melting (b,d,f) curves obtained from the second heating cycle of the HEPCs at various degrees of vis-breaking (0, 0.025, 0.2 and 0.5 wt. % peroxide)

Tables 4.4 to 4.6 are a representation of the thermal data for each of the HEPCs with increasing vis-breaking step. The T_m values in parenthesis represent the melting temperatures of the higher melting component of the endotherm splitting. We see an initial increase of T_c up to 0.2 wt. % with increasing peroxide concentration. However, T_c remained almost the same in all the peroxide concentrations for the T300 sample. The melting temperatures (T_m) and melt enthalpies (ΔH_m) decreased significantly at 0.5 wt. %, for all samples indicating a decrease in lamellae thickness [1]. This decrease at 0.5 wt. % was less significant in the polymers with higher ethylene incorporation. In the T180 and T300 samples, there was a more significant decrease of the melting enthalpy at 0.025 wt. % than at 0.5 wt. %. The decrease in melting enthalpy (ΔH_m) was not expected to occur at the same extent at low peroxide concentrations than at high peroxide concentrations where more peroxide radicals are available to induce vis-breaking. Therefore, the more significant decrease in melting enthalpy at 0.025 wt. % is somewhat puzzling, particularly as this was more pronounced for the sample with the lower ethylene content (T180 vs T300). This may be indicative of the effect of differing CCD as ethylene content decreases.

Table 4.4 DSC thermal data of the T0 sample at various degrees of vis-breaking [0, 0.025, 0.2, 0.5 wt. %]

T0 HEPC	T_c [°C]	T_m [°C]	ΔH_m [J/g]
0.000	112.3	160.7 (166.1)	109.7
0.025	112.4	161.0 (166.1)	86.8
0.200	113.3	158.8 (165.6)	81.2
0.500	112.5	158.1 (164.5)	67.3

Table 4.5 DSC thermal data of the T180 sample at various degrees of vis-breaking (0, 0.025, 0.2, 0.5 %)

T180 HEPC	T_c [°C]	T_m [°C]	ΔH_m [J/g]
0.000	111.9	161.5 (166.0)	80.2
0.025	110.5	158.3 (164.9)	59.3
0.200	112.7	161.1 (166.6)	71.8
0.500	112.5	155.1 (163.5)	66.2

Table 4.6 DSC thermal data of the T300 sample at various degrees of vis-breaking (0, 0.025, 0.2, 0.5 %)

T300 HEPC	T_c [°C]	T_m [°C]	ΔH_m [J/g]
0.000	112.3	160.9 (167.8)	65.2
0.025	111.9	160.2 (166.0)	57.0
0.200	112.0	155.9 (163.2)	67.7
0.500	111.1	157.1 (163.9)	61.5

4.2.4 Dynamic mechanical analysis (DMA)

At this stage, it was quite clear that the effect of the 0.5 wt. % vis-breaking step on the molecular characteristics of the HEPCs was significant. Therefore, the physical properties of the HEPCs were studied after this vis-breaking step.

In this section, the DMA results of the HEPCs after vis-breaking are discussed. DMA gives information on the storage and loss moduli (damping) of the material and these properties are normally reported as elastic modulus and tan δ. During material testing in DMA, a sinusoidal force is applied to the material in order to measure its deformation and phase shift (phase angle) (refer to Figure 4.4). Therefore the response of the material can be expressed as an in-phase (storage modulus) and out-phase response (loss modulus). The storage modulus is a measure of the stored energy and therefore represents the elastic portion of the material whereas the loss modulus is a measure of the energy dissipated and therefore represents the viscous portion of the material. Tan δ is a ratio of the loss modulus to the storage modulus. It measures the energy

dissipated by the material upon applying stress or strain. Tan δ can therefore be used as an indirect indication of the material's impact response.

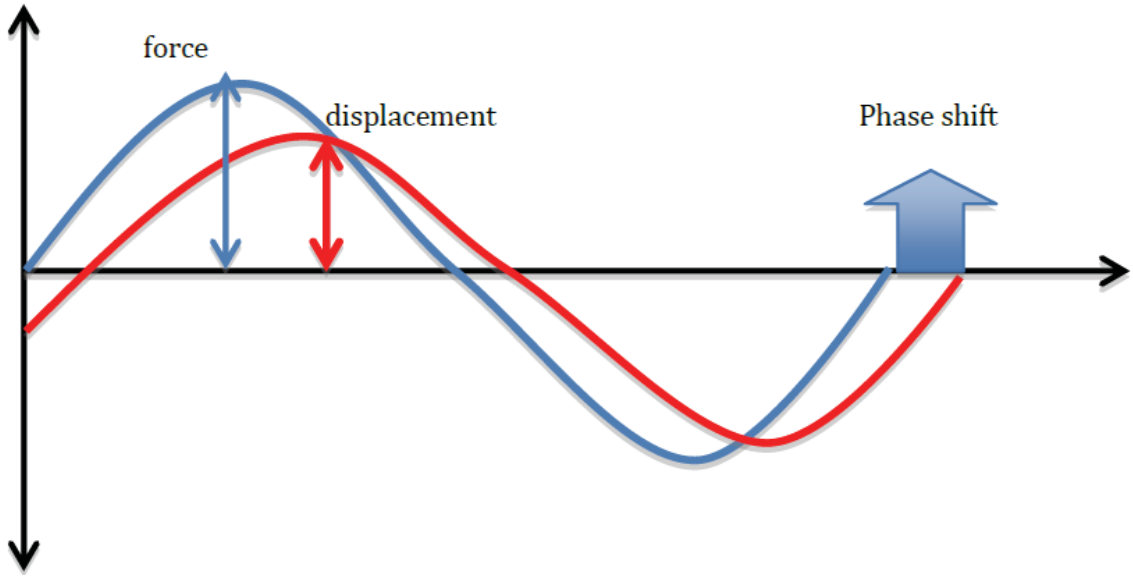

Figure 4.4 The relationship between the applied DMA force (in blue) and the measured deformation (in red) [9]

Varying the temperature changes the modulus values of the samples. These changes, which include changes in glass transition temperatures (Tg) are often reflected by changes in the storage modulus or tan δ curves. For instance, a decrease in Tg can be reflected by a decrease in storage modulus curves when viewed on a log scale against a linear temperature scale. Moreover, the Tg of a particular sample is also reflected by a peak on the tan δ curve. In addition to that, the areas under the tan δ peak and storage modulus curves can be related to the impact strength of the material [1, 9, 10].

Figures 4.5 (a) and (b) below show the tan δ curves of the HEPCs before and after vis-breaking at 0.5 wt. % peroxide. The T300 sample shows two peaks before and after vis-breaking. In literature, two major transitions have been previously reported on the tan δ curves of HEPCs and these are: the α_m (amorphous copolymer phase relaxation) above -50 °C and the β_{PP} (relaxation of PP homopolymer phase) between 15 – 20 °C [11]. Therefore, the two peaks observed in the T300 samples are an indication of the presence of these two molecular transitions. This clear separation of peaks was not observed for the non vis-broken T180 sample.

Upon comparison of Figure 4.5 (b) to Figure 4.5 (a), we see the appearance of the α_m peak in the T180 sample after vis-breaking. This was indicative of the appearance of a new phase in this sample after vis-breaking. In Figure 4.5 (b), we see that the α_m peak of the T180 appears

at significantly lower temperatures when compared to that of the T300, indicating that the species in this phase had a lower Tg. We also see that the β_{PP} peak of the T180 was slightly shifted towards lower temperatures compared to that of the T0 and T300 samples which might be due to the vis-breaking affecting high molar mass species in the PP homopolymer phase. Again comparing Figure 4.5 (a) to Figure 4.5 (b), we see something interesting with the T300 sample. Before vis-breaking, the α_m peak appears around -34 °C whilst the β_{PP} peak appears around 10 °C, while after vis-breaking, the β_{PP} peak remains at 10 °C, but the α_m peak shifts lower to about -38 °C. This increase in the difference between the α_m and β_{PP} peaks after vis-breaking indicates that there was increased phase separation between ethylene-propylene and PP homopolymer sequences in the T300 sample after vis-breaking. The results show that the vis-breaking clearly affects the "rubbery" or copolymer phase (in T300) more than the iPP phase. This gives more clarity to the molar mass changes observed for the T180 and T300 samples after vis-breaking.

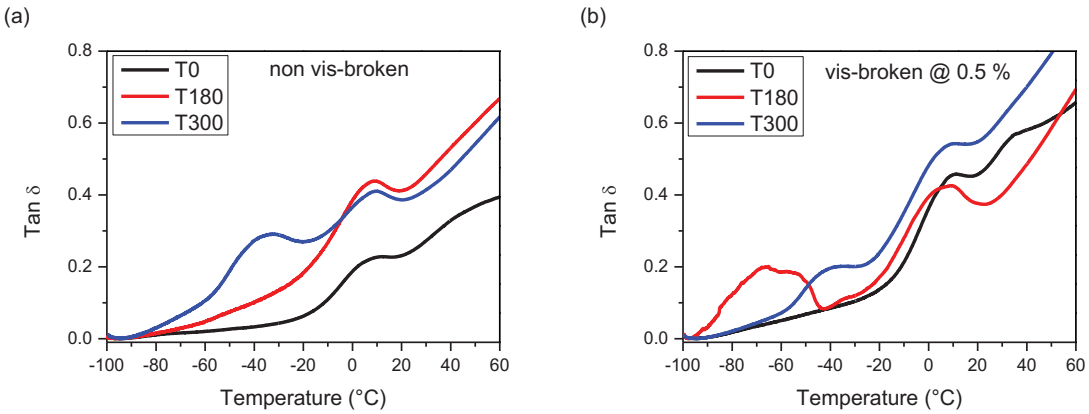

Figure 4.5 Tan σ curves of the (a) non vis-broken and (b) vis-broken @ 0.5 wt. % HEPCs as measured by DMA

Figures 4.6 (a) to (c) below show the storage modulus of the HEPCs before and after vis-breaking at 0.5 wt. % with increasing temperature. As expected, we see a decrease of the storage modulus after ethylene incorporation in both the non vis-broken and vis-broken samples. The PP sequences are there before the ethylene is introduced. Therefore, this was due to the ethylene sequences disturbing the crystalline PP sequences. Vis-breaking affects the iPP as well, and a combination of chain scission in the iPP and the copolymer phase leads to a change in the crystallizability of the material in total.

The large drop in G' of the T0 sample when compared to T180 and T300 might be due to crystallinity differences which are as a result of the ethylene co-monomer incorporation. The increase in G' observed after vis-breaking could also be attributed to differences in crystallinity

which were induced by the peroxide during vis-breaking (which is backed up by the DSC data). However, all these statements are inconclusive. Further investigation is required.

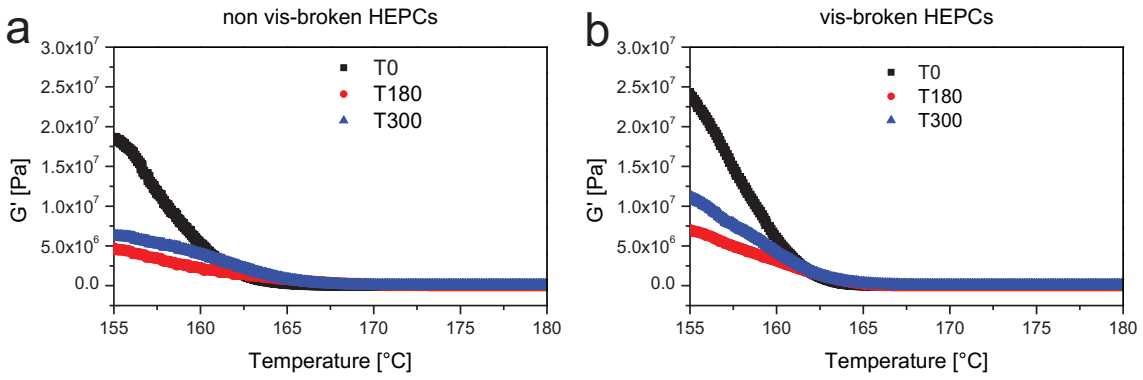

Figure 4.6 Storage modulus of (a) non vis-broken and (b) vis-broken (at 0.5 wt %) HEPCs measured between 155 and 180 °C

4.2.5 Rheology

The science of flow and deformation of matter is termed rheology. Rheology is important because it measures the relationship between the stress and deformation of a material. Most rheology measurements are done in the linear viscoelastic region (LVR) to get properties like G', G'', tan δ and η^*. This is because measurements done in the LVR help to bridge the gap between molecular structure and product performance. During experiments in the LVR, a small or slow deformation is applied on the material, this causes the molecular arrangements in the sample to be similar to the molecular arrangements of the sample if it was at equilibrium. Therefore, in the LVR, the mechanical response of the material is a reflection of the dynamic processes that would normally happen at molecular level [10].

In rheology, the frequency of modulus crossover correlates to relaxation time. Therefore, when relating the crossover frequency and crossover modulus to molar mass and molar mass distribution, a higher crossover frequency would mean a decrease in molar mass and a higher crossover modulus would be indicative of a narrower molar mass distribution [10].

Figures 4.7 (a) to (c) below show frequency sweep curves of the non vis-broken and vis-broken HEPCs. Tables 4.7 and 4.8 below show the dynamic data of the non vis-broken and vis-broken HEPCs obtained from a parallel plate rheometer. Looking at Figures 4.7 (a) to (c), we see an increase of the crossover frequency after vis-breaking for all the HEPCs. From Figure 4.7, as expected, a decrease in G' and G" was observed after vis-breaking. However, Figure 4.7 (a) showed two sets of G' data at low frequencies. Since the G' and G" curves were obtained from

overlays of G' and G" curves from different temperatures, these two sets of G' data were an indication of inconsistency in the data obtained at low frequencies after vis-breaking.

Upon comparison of the two tables, we also saw that the increase in crossover frequency was much more significant in the T180 and T300 samples, which was indicative of a significant decrease in molar mass after vis-breaking. This correlates well with the significant decrease in molar mass shown by Tables 4.2 and 4.3 at 0.5 wt. %. However, there was a decrease of the crossover modulus and this did not correlate well with the narrow MMD curves. This is proof that the crossover modulus was not a true representation of the narrowing of the MMD curves. In conclusion, all these results confirmed vis-breaking within these samples.

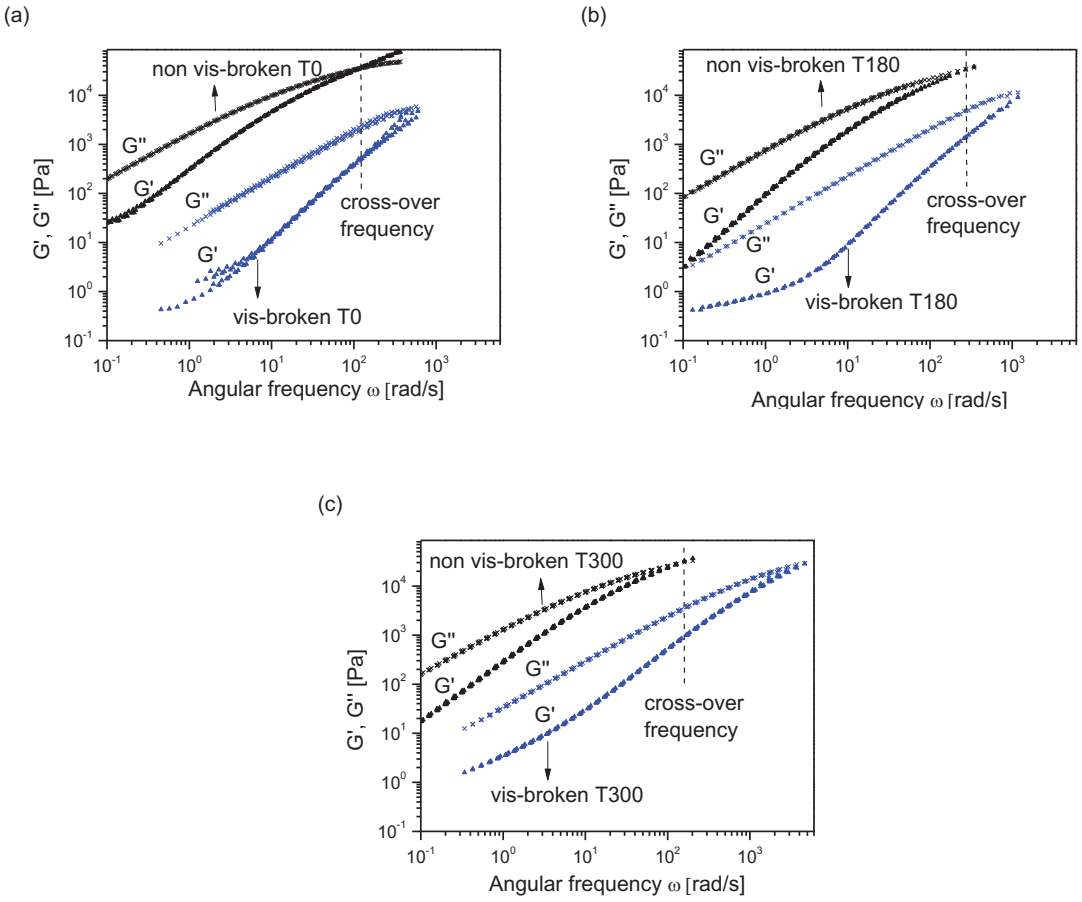

Figure 4.7 Frequency sweep curves of the non vis-broken and vis-broken (at 0.5 wt. %) of the (a) T0, (b) T180 and (c) T300 HEPCs (all TTS shifted to 180 °C)

Table 4.7 Dynamic data for the non vis-broken HEPCs collected from a parallel plate rheometer

Sample ID	Crossover modulus (Pa)	Crossover frequency (rad/s)
T0	34641	115
T180	33290	272
T300	32198	160

Table 4.8 Dynamic data for the vis-broken (at 0.5 wt. %) HEPCs collected from a parallel plate rheometer

Sample ID	Crossover modulus (Pa)	Crossover frequency (rad/s)
T0	5186	599
T180	11404	1172
T300	29140	4633

Figures 4.8 (a) and (b) below show the complex viscosity curves of the HEPCs before and after vis-breaking. The complex viscosity was determined from the frequency sweep experiment data using the equations below:

$$G^* = \sqrt{G'^2 + G''^2} \quad \text{Eq. 4.1}$$

$$\eta^* = \frac{G^*}{\omega} \quad \text{Eq. 4.2}$$

Where,

η^* = Complex viscosity

G^* = Modulus

G' = Elastic (Storage) modulus

G'' = Viscous (Loss) modulus

ω = Frequency

Upon comparing Figure 4.8 (b) to Figure 4.8 (a), we see a significant drop of the complex viscosity after vis-breaking which was an indication of decrease in molar mass. When comparing the HEPCs in Figure 4.8 (b) with each other, we saw that the T0 sample had the lowest complex viscosity whilst the T300 sample had the highest viscosity at lower frequencies. From these results, it appeared as though the vis-breaking affected the samples with low ethylene content (T0 and T180) more than those with high ethylene content (T300).

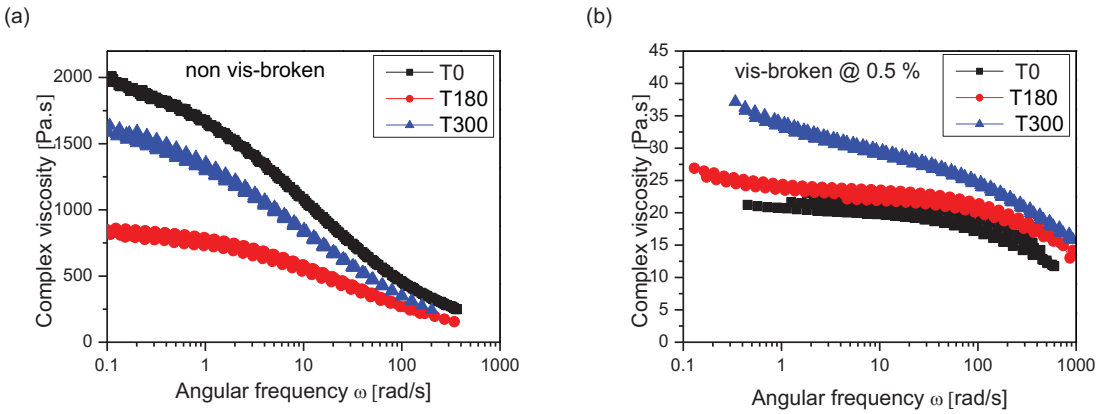

Figure 4.8 Complex viscosity curves of the (a) non vis-broken and (b) vis-broken HEPCs obtained from the frequency sweep experiments

4.2.6 Conclusions

At this stage, it was clear that the effects of the vis-breaking were more visible at the 0.5 wt % vis-breaking step. According to HT-SEC, the decrease in molar mass increased with increasing ethylene content. This was due to the "soft" copolymer phase acting as an aid in the mixing/dispersion of the peroxide within the HEPCs resulting in a more efficient vis-breaking process. It was also noted that the vis-breaking caused a phase separation between the ethylene-propylene copolymers and PP sequences. Lastly, from the complex viscosity curves, it appeared as though the effect of the vis-breaking on samples with a low ethylene content was more than the one with a high ethylene content.

4.3 References

1. Swart, M., *The effect of controlled degradation with an organic peroxide on the molecular characteristics and properties of heterophasic propylene-ethylene copolymers (HECO)*. 2013, PhD Thesis, University of Stellenbosch.

2. De Goede, E., *The development of analytical techniques for studying degradation in impact polypropylene copolymers*. 2009, University of Stellenbosch.

3. Gulmine, J., Janissek, P. R., Heise, H. M., Akcelrud, L., *Degradation profile of polyethylene after artificial accelerated weathering*. Polymer Degradation and stability, 2003. **79**(3): p. 385-397.

4. Edge, M., *Infrared spectroscopy in analysis of polymer degradation.* Encyclopedia of Analytical Chemistry, 2006.

5. Gugumus, F., *Thermooxidative degradation of polyolefins in the solid state: part 5. Kinetics of functional group formation in PE-HD and PE-LLD.* Polymer degradation and Stability, 1997. **55**(1): p. 21-43.

6. Nekhoroshev, V., Turov, Y. P., Nekhorosheva, A. V., Ogorodnikov, V. D., Gaevoi, K. N., *Composition and structure of low-molecular-weight products of thermal oxidative degradation of atactic polypropylene.* Russian Journal of Applied Chemistry, 2006. **79**(5): p. 833-840.

7. Costa, L., Luda, M., Trossarelli, L., *Ultra high molecular weight polyethylene—II. Thermal-and photo-oxidation.* Polymer Degradation and Stability, 1997. **58**(1-2): p. 41-54.

8. Rabello, M., White, J., *Crystallization and melting behaviour of photodegraded polypropylene—I. Chemi-crystallization.* Polymer, 1997. **38**(26): p. 6379-6387.

9. Botha, L., *The effect of in-process ethylene incorporation on the evolution of particle morphology and molecular characteristics of commercial heterophasic ethylene propylene copolymers (HEPCs)*. 2014, PhD Thesis. Stellenbosch University.

10. TAinstruments, Rheology Theory and applications, viewed 29 March 2019, https://people.clarkson.edu/~skrishna/DHR_Rheology_Theory.pdf.

11. Doshev, P., Lohse, G., Henning, S., Krumova, M., Heuvelsland, A., Michler, G., Radusch, H.-J., *Phase interactions and structure evolution of heterophasic ethylene–propylene copolymers as a function of system composition.* Journal of Applied Polymer Science, 2006. **101**(5): p. 2825-2837.

Chapter 5

Analysis of solvent gradient elution fractionation fractions and preparative temperature rising elution fractionation fractions

This chapter gives a detailed report on the fractions of the non vis-broken and vis-broken HEPCs obtained from solvent gradient elution fractionation and preparative temperature rising elution fractionation.

5.1 Introduction

Preparative temperature rising elution fractionation (p-TREF) fractionates polymer chains based on the differences in chain microstructure affecting their crystallizability from dilute solution [1]. Therefore, p-TREF can be used to monitor the chemical changes of HEPCs before and after vis-breaking. In contrast, solvent gradient elution fractionation (SGEF) fractionates HEPCs according to molar mass. Therefore, fractions with narrow molar mass distributions (MMDs) and low dispersity can be obtained. HEPCs usually have broad MMDs. Therefore, for a comprehensive understanding of the structure-property relationship for these materials, fractions with narrow MMDs were prepared [2]. This chapter gives us information on the CCD of the HEPCs from two different perspectives: crystallizability and molar mass.

5.2 Preparative TREF

Figures 5.1 (a) and (b) show a comparison of the p-TREF profiles of non vis-broken and vis-broken HEPCs. Both Figures 5.1 (a) and (b) showed that about 65 wt. % of the bulk material in the HEPCs eluted at 110 °C. p-TREF fractionates polymer chains according crystallizability. For example, the amorphous material elutes at 30 °C, then the semi-crystalline material at 60 – 90 °C and the highly crystalline material elutes at 100 – 130 °C. In Figure 5.1 (a), the non vis-broken HEPCs show an increase in the amount of material eluting at 30 °C and a decrease of the material eluting at 120 °C with increasing ethylene content. This was an indication that the incorporation of ethylene resulted in an increase of the amorphous portion and a decrease of the crystalline portion of the polymers. Non vis-broken T180 showed a decrease of the material eluting at 100 °C and an increase of the material eluting at 90 °C. However, the amount of material eluting at 90 and 100 °C were fairly similar for the T0 and T300 samples. These results show that the decrease in the amount of the crystalline portion, caused by the ethylene incorporation did not only cause an increase in the amount of amorphous material but a significant increase of the semi-crystalline material eluting at 90 °C for the T180 sample.

The p-TREF profiles obtained after vis-breaking (see Figure 5.1 b) are a result of the vis-broken polymer being fractionated. After vis-breaking, a slight increase of the material eluting at 30 °C was observed for the T180 sample. The T180 sample also showed a decrease of the material eluting at 90 °C and an increase of the material eluting at 100 °C after vis-breaking. A slight decrease of the material eluting at 120 °C was also observed for the T0 and T180 samples after vis-breaking. All these results were indicative of the changes in CCDs caused by vis-breaking the HEPCs which then resulted in different CCDs reflected on a particular fraction.

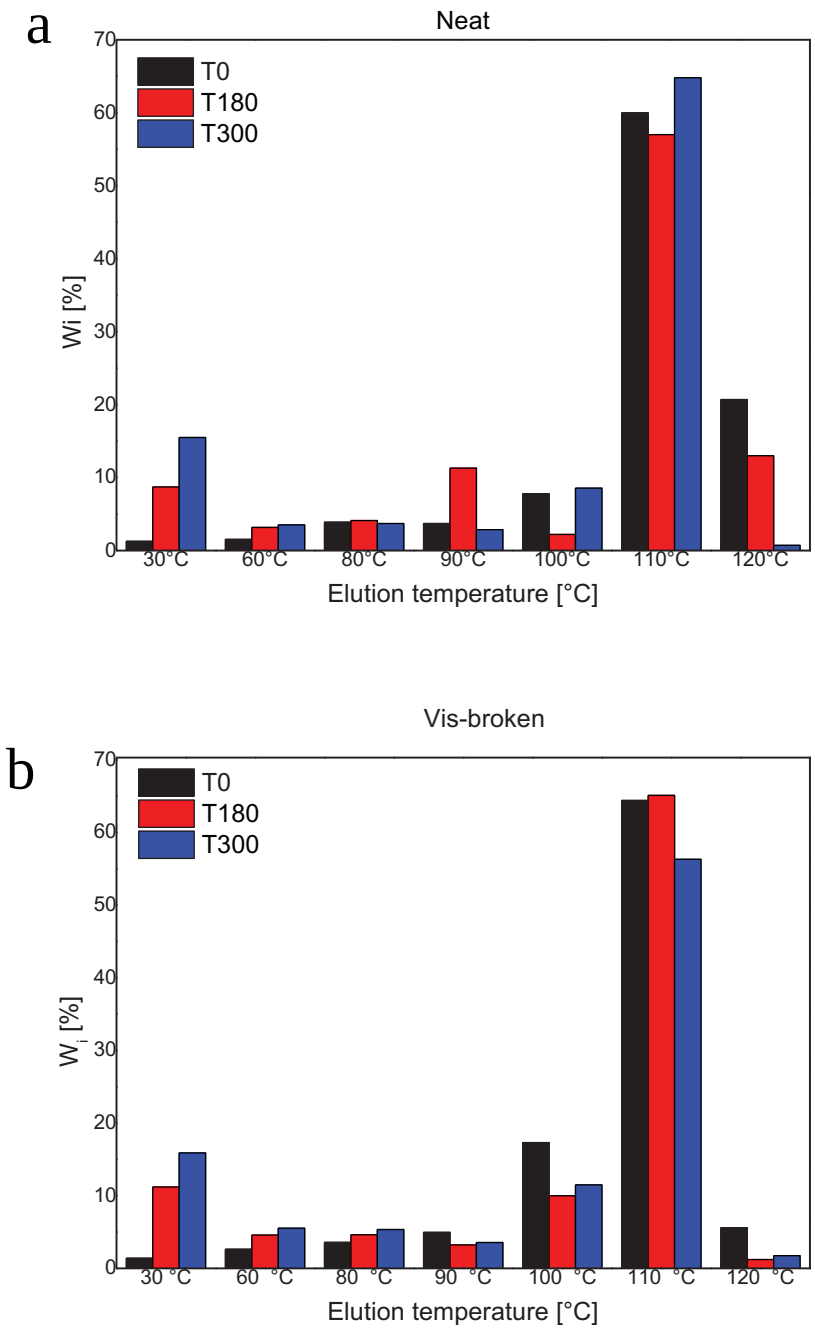

Figure 5.1 p-TREF profiles of (a) non vis-broken and (b) vis-broken HEPCs.

5.2.1 High temperature size exclusion chromatography (HT-SEC)

p-TREF profiles only provide information on the changes in crystallizability incurred by the vis-breaking. Therefore, changes in MM and MMD were investigated using HT-SEC. Figures 5.2 (a) – (f) below compare the MMD curves of fractions in the neat and vis-broken HEPCs. In both the neat and vis-broken HEPCs, the 30, 60, 80 and 90 °C fractions exhibited broad bimodal MMD curves, indicating compositional heterogeneity. The compositional

heterogeneity is due to the co-elution of non-identical products and it often occurs in the mid-temperature fractions of HEPCs [3, 4].

Noticeable changes were observed in the bimodal MMD curves of the 30, 60, 80 and 90 °C T0 fractions after vis-breaking. The changes were most obvious in the 80 and 90 °C fractions. However, the changes were less noticeable and almost absent in the T180 sample, and only partially visible in the T300 sample. In the T300 sample, the changes in MMD were only visible in the 60 and 80 °C fractions. From these results, it is clear that the composition of the fractions was altered by the vis-breaking. Most of the changes in MMD were most visible in the T0 sample. This could be due to the fact that the T0 sample consist of only isotactic PP. In the case of the T180 and T300 samples, both iPP and copolymer chains could be affected by the vis-breaking, and the MMD of a specific p-TREF fraction is influenced by products of both these materials after vis-breaking.

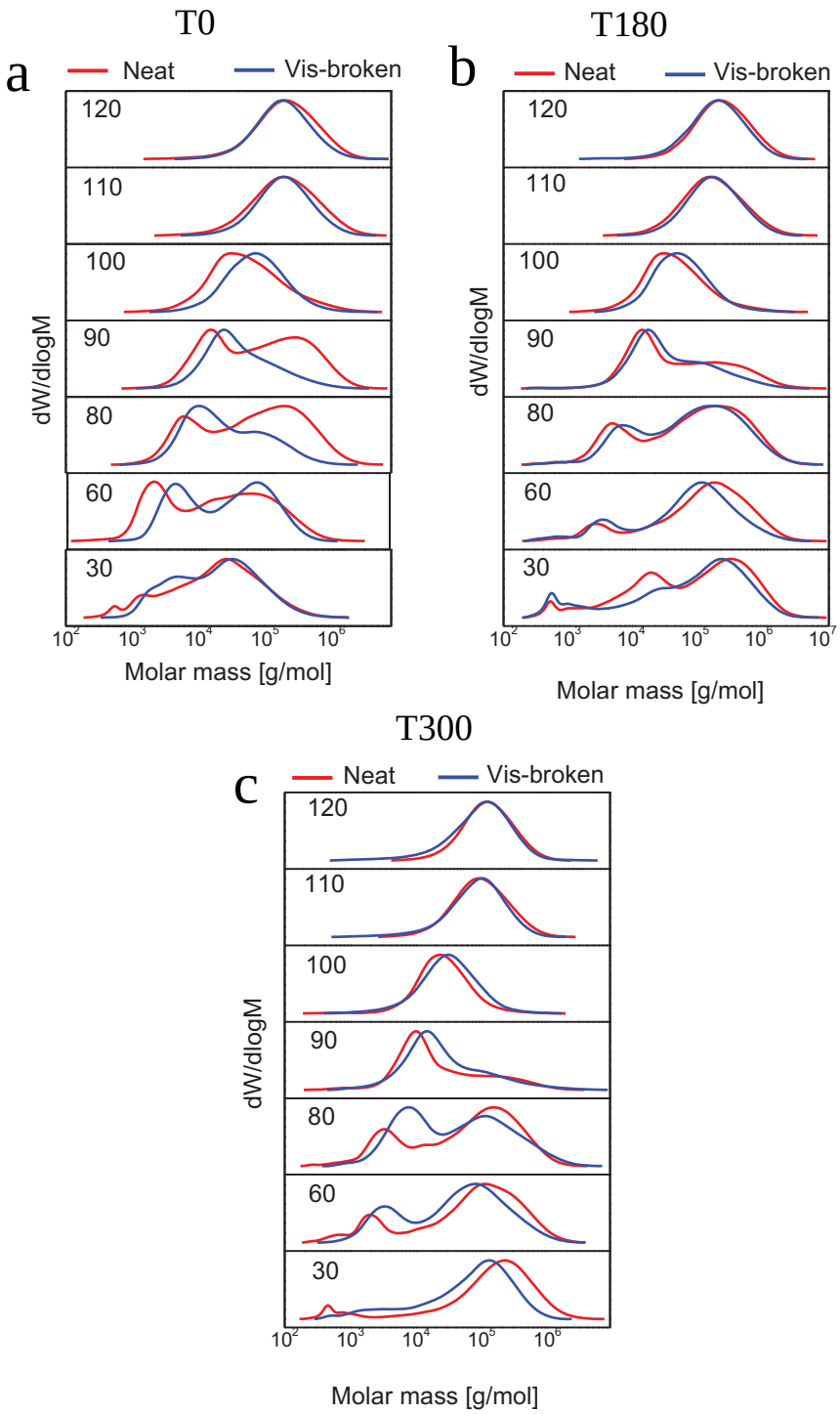

Figure 5.2 Molar mass distribution curves of fractions of neat and vis-broken (a) T0, (b) T180 and (c) T300 samples.

From the MMD curves in Figure 5.2 above, we can infer that there were changes in molar mass composition after vis-breaking. SEC data of the neat and vis-broken HEPC fractions is shown in Tables A.1 – A.6 in the appendix. In order to investigate the dispersity of polymer chain sizes in each fraction before and after vis-breaking, the Đ of each fraction was measured. Figures 5.3 (a) and (b) below compare the Đs of the fractions in the neat and vis-broken HEPCs.

From the plots in Figure 5.3, a decrease in Đ was observed with increasing elution temperature. The dispersity (Đ) of the 30, 60, 80 and 90 °C fractions were higher than the Đs of the 100, 110 and 120 °C fractions before and after vis-breaking. Furthermore, the Đs of the high temperature fractions appeared to be almost similar in all the samples, except the 100 °C fraction of the non vis-broken T180 sample. The 100 °C fraction of the non vis-broken T180 sample seemed to have a higher Đ as compared to the Đs of the 100 °C fractions in the non vis-broken T0 and T300 samples.

After vis-breaking, the Đ of the T180 100 °C decreased, indicating that the molar mass of the polymer chains eluting in this fraction were affected by the vis-breaking. Moreover, the T180 sample also showed a decrease of the Đs of the 60 and 80 °C fractions and an increase of the Đ of the 30 °C fraction after vis-breaking. T300 only showed an increase in the Đs of the 60, 80 and 90 °C fractions after vis-breaking. In T0, a significant decrease in Đ was observed for the 30, 60, 80 and 90 °C T0 fractions after vis-breaking. The increase in Đs could be as a result of the vis-breaking affecting certain parts of the sample and therefore causing a release of polymer chains of different molar masses. It is known that vis-breaking affects longer chains more significantly. If this were the only factor, one would expect an overall decrease in Đ, however, this is plainly not the case for the T180 and T300 samples. It can be concluded, therefore, that the copolymer chains are cleaved at specific points, based on the chemical composition distribution (CCD).

After vis-breaking, it was also observed that the 30, 60, 80 and 90 °C T0 fractions had the lowest Đs when compared to Đs of similar T180 and T300 fractions. These differences could be directly linked to chemical composition of the chains eluting in these fractions for each sample

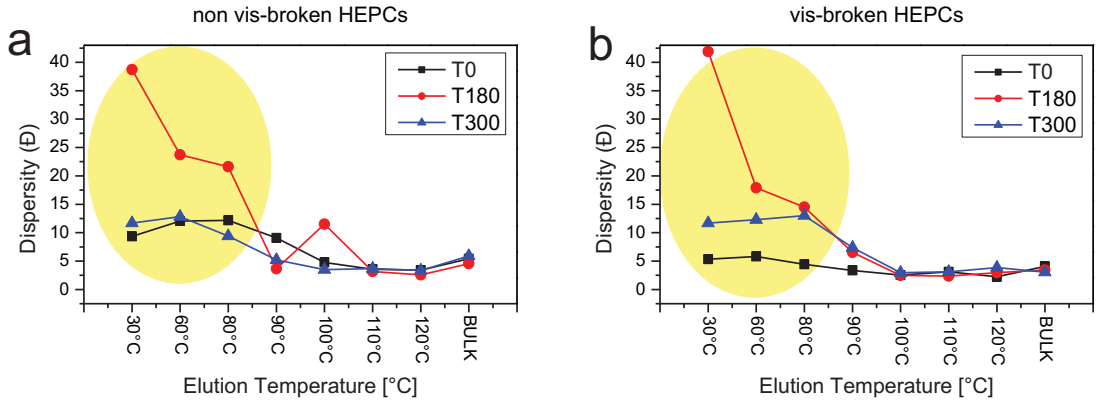

Figure 5.3 Illustration of dispersity across the p-TREF fractions of (a) non vis-broken and (b) vis-broken HEPCs

5.2.2 Differential scanning calorimetry (DSC)

From the HT-SEC results, it was observed that the compositional heterogeneity of the 30, 60, 80 and 90 °C was altered by the vis-breaking. DSC was then used to investigate the thermal behaviour of the fractions after vis-breaking. Figures 5.4 (a) – (f) compare the crystallization curves of p-TREF fractions in the neat and vis-broken HEPCs, while Figures 5.5 (a) – (f) compare the melting curves of the same fractions in the neat and vis-broken samples. A shift of the crystallization and melting curves towards higher temperatures with increasing elution temperature was observed. The increase in crystallization and melting peak temperatures was indicative of an increase in lamellae thickness [5]. Furthermore, a broadening of the crystallization and melting curves in the 60 °C fraction with increasing ethylene content was also observed indicating compositional heterogeneity within this fraction. The splitting of the melting and crystallization curves in the 60 °C fraction of the vis-broken T0 sample, as shown by Figures 5.4 (b) and 5.5 (b), might be due to different polymeric forms co-eluting at this fraction.

The 30 °C fractions showed no melting and crystallization peaks in all the samples except in the vis-broken T0 sample. The 30 °C fraction of the vis-broken T0 sample exhibited a broad low peak (indicated by the blue circle). The appearance of this peak could tentatively be assigned to syndiotactic PP or stereo irregular chains cleaved off during vis-breaking. The mid-elution temperature fractions (60, 80 and 90 °C) showed multiple melting peaks as shown by Figures 5.5 (a) – (f). This was indicative of the presence of both PE and PP segments. The peaks appearing around 120 °C were attributed to the presence of PE sequences and those around 160 °C were attributed to PP sequences [5]. Comparing only the melting curves of the neat HEPCs, a single peak around 160 °C in the 120 °C fractions was observed for all the samples, as shown by Figure 5.5 (a), (c) and (e). This was confirmation that these fractions consisted predominantly of isotactic PP [5]. However, splitting of the 160 °C melting peak was observed in the vis-broken samples indicating the co-melting of different polymeric crystallite forms, as shown by Figure 5.5 (b), (d) and (f). The polymeric forms might be due to the segregation together of low and high molar mass material resulting from the chain scission of long crystallisable PP sequences.

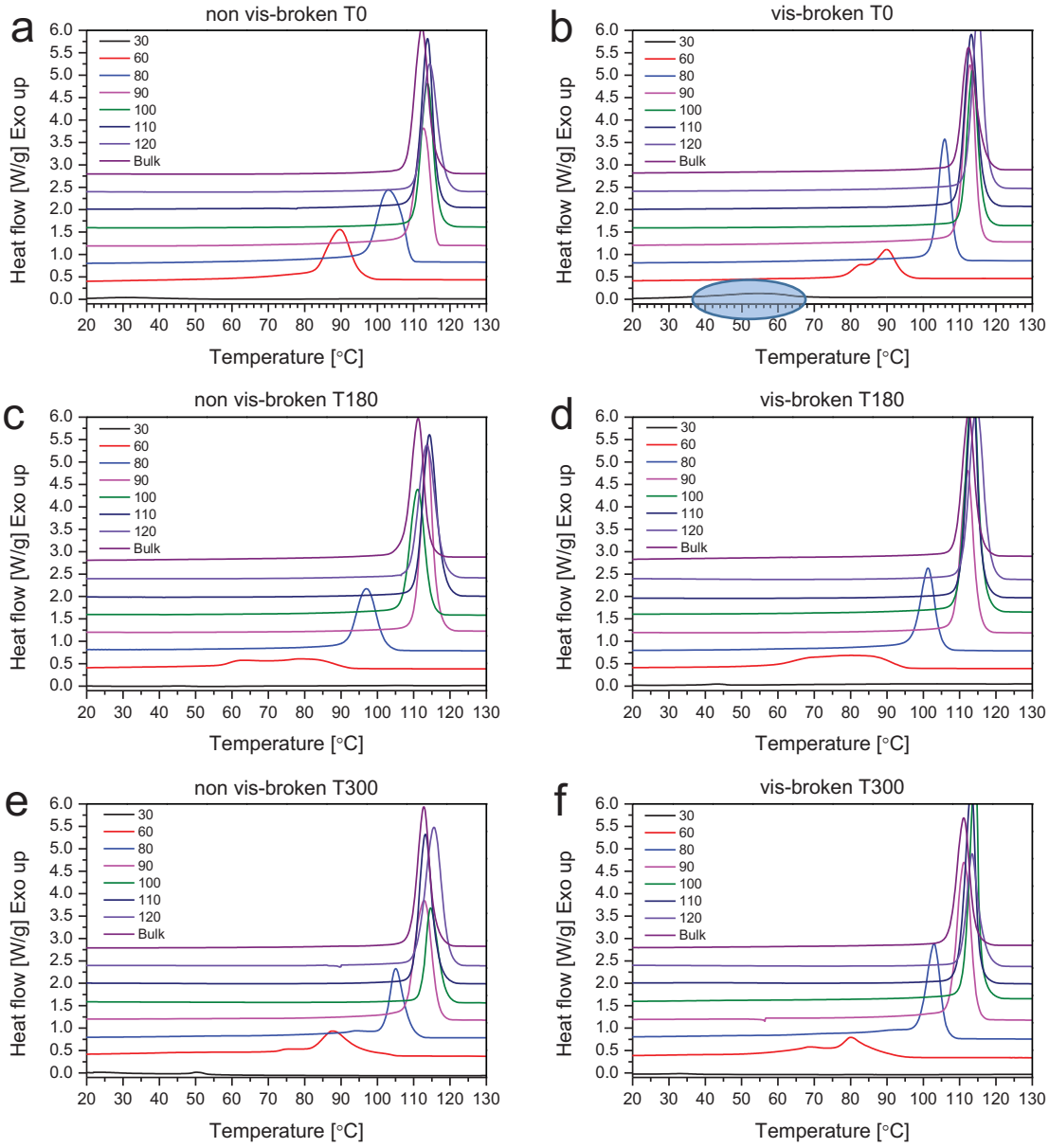

Figure 5.4 DSC crystallization curves of (a) non vis-broken T0, (b) vis-broken T0, (c) non vis-broken T180, (d) vis-broken T180, (e) non vis-broken T300 and (f) vis-broken T300

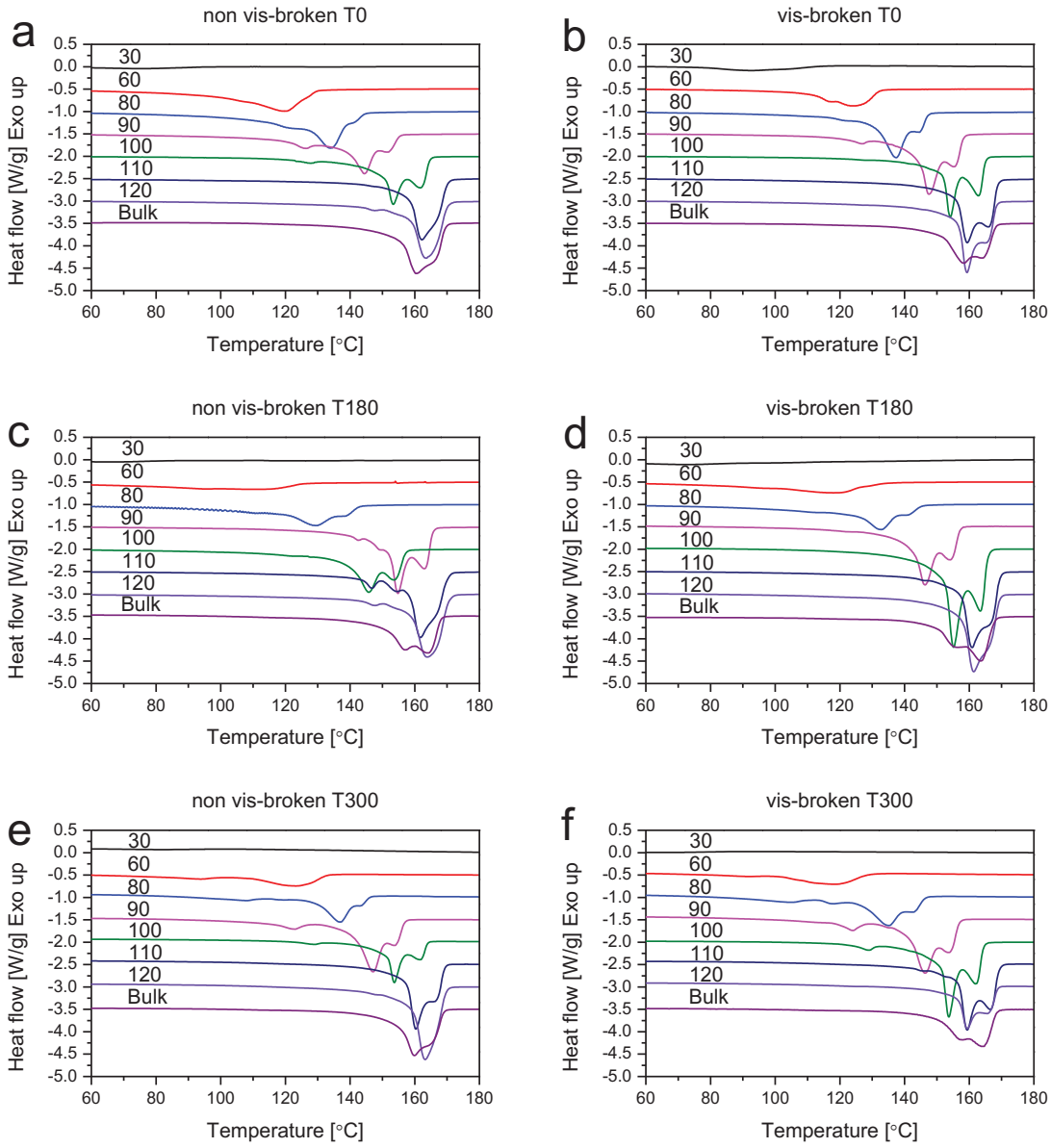

Figure 5.5 DSC 2nd melting curves of (a) non vis-broken T0, (b) vis-broken T0, (c) non vis-broken T180, (d) vis-broken T180, (e) non vis-broken T300 and (f) vis-broken T300

Figures 5.6 (a) and (b) below compare the crystallization peak temperatures of the p-TREF fractions in neat and vis-broken HEPCs. An increase of the crystallization peak temperatures with increasing elution temperature up to the 90 °C fraction was observed for all the samples. From the 90 to the 120 °C fraction, the crystallization temperatures remained constant and similar for all the samples except the 100 °C fraction of the non vis-broken T180 sample. The 100 °C fraction of the non vis-broken T180 sample indicated a decrease in crystallization temperature as compared to the 100 °C fractions of the T180 and T300 samples. In conclusion, the crystallization temperature was constant and similar for all the samples in the higher temperature fractions because most of the material eluting at these temperatures is

predominantly iPP. Furthermore, the decrease in crystallization temperature of the 100 °C in the non vis-broken T180 sample could be as a result of the chemical composition of the material eluting at this fraction being different from the composition of the materials eluting from the other samples.

Major differences in crystallization peak temperatures for all samples were observed in the 60 and 80 °C fractions, as highlighted by the yellow circle. This could be due to the compositional heterogeneity of these fractions caused by the random distribution of ethylene sequences. The 60 and 80 °C fractions of the non vis-brokenT180 sample had the lowest crystallization peak temperatures. Interestingly, the crystallization temperatures of the 60 and 80 °C fractions in the non vis-broken T0 and T300 samples were close to each other. This correlated well with the Đs of the non vis-broken T0 and T300 samples being close to one another and lower than the Đ of the non vis-broken T180 sample in the 60 and 80 °C fractions (see Figure 5.3 a).

After vis-breaking, it was observed that the crystallization temperature of the T0 sample was higher than the crystallization temperatures of the T180 and T300 samples. This again correlated well with the low Đ of the 60 and 80 °C fractions in the vis-broken T0 sample as compared to the high Đs of the T180 and T300 60 and 80 °C fractions. From the results, it was observed that a higher crystallization temperature is indicative of a lower Đ (more homogenous chain size distribution) and a lower crystallization temperature is indicative of a higher Đ (less homogenous chain distribution). So while these samples were all obtained by crystallization from dilute solution at similar conditions, the bulk crystallization temperature seems to be affected by both CCD and dispersity.

At this point, it seemed as though the vis-breaking created more compositional heterogeneity in the T180 and T300 samples as compared to the T0 sample (comparing samples before and after vis-breaking).

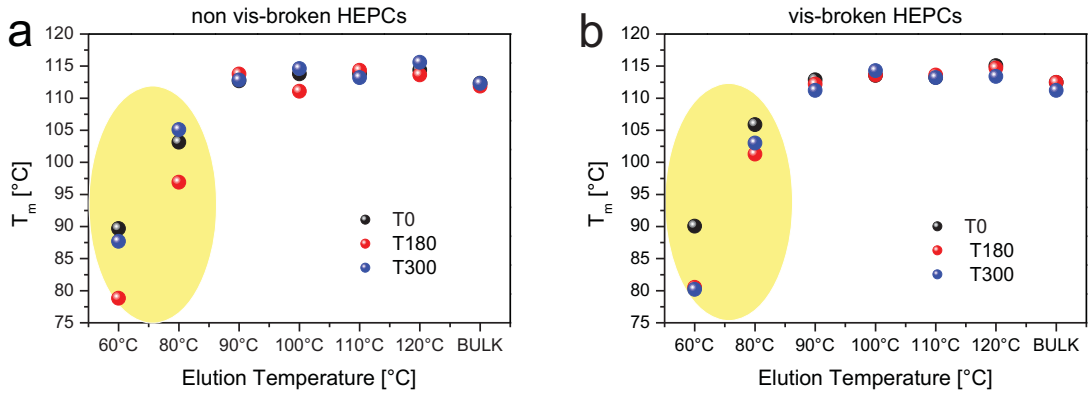

Figure 5.6 Comparison of crystallization peak temperatures, T_m [°C] of p-TREF fractions in (a) non vis-broken and (b) vis-broken HEPCs. The yellow circle highlights differences in T_c observed in the 60 and 80 °C fractions.

5.2.3 Fourier transform infrared spectroscopy (FTIR)

Since the structural composition of the samples before and after vis-breaking could not be monitored via DSC, FTIR was used. Figures 5.7 (a) – (f) compares the FTIR spectra (between 2600 cm^{-1} and 3100 cm^{-1}) of fractions in the neat and vis-broken HEPCs. In all the HEPCs, the high temperature eluting fractions (100, 110 and 120 °C) exhibited a single peak around 2840 cm^{-1}. As proven by the melting point in DSC (Figure 5.5), these fractions constitute mainly of isotactic PP. Therefore the 2840 cm^{-1} peak might be due to the C-H stretches present in the methylenes of long crystallisable propylene sequences. Interestingly, splitting of the 2840 cm^{-1} peak resulting in the appearance of a new peak around 2849 cm^{-1} was observed in the 60 °C fractions of the T180 samples (before and after vis-breaking), as shown by Figure 5.7 (c) and (d). This indicated the presence of two C-H stretches in different chemical environments. Interestingly, the 2849 cm^{-1} peak was the only peak appearing in the 30 °C fractions of the T180 and T300 samples (both neat and vis-broken), indicating the presence of ethylene sequences in essentially soluble EP copolymers and the absence of long crystallisable propylene sequences.

Comparing the neat and vis-broken samples, a decrease of the 2849 cm^{-1} peak was observed in the vis-broken T180 and T300 samples, shown by Figure 5.7 (d) and (f). However, the decrease was more pronounced in the 80 °C fraction of the vis-broken T300 sample, as shown in Figure 5.7 (f). Moreover, the 30 °C fractions of vis-broken T180 and T300 showed pronounced C=O peaks, confirming that the vis-breaking was more significant in these samples.

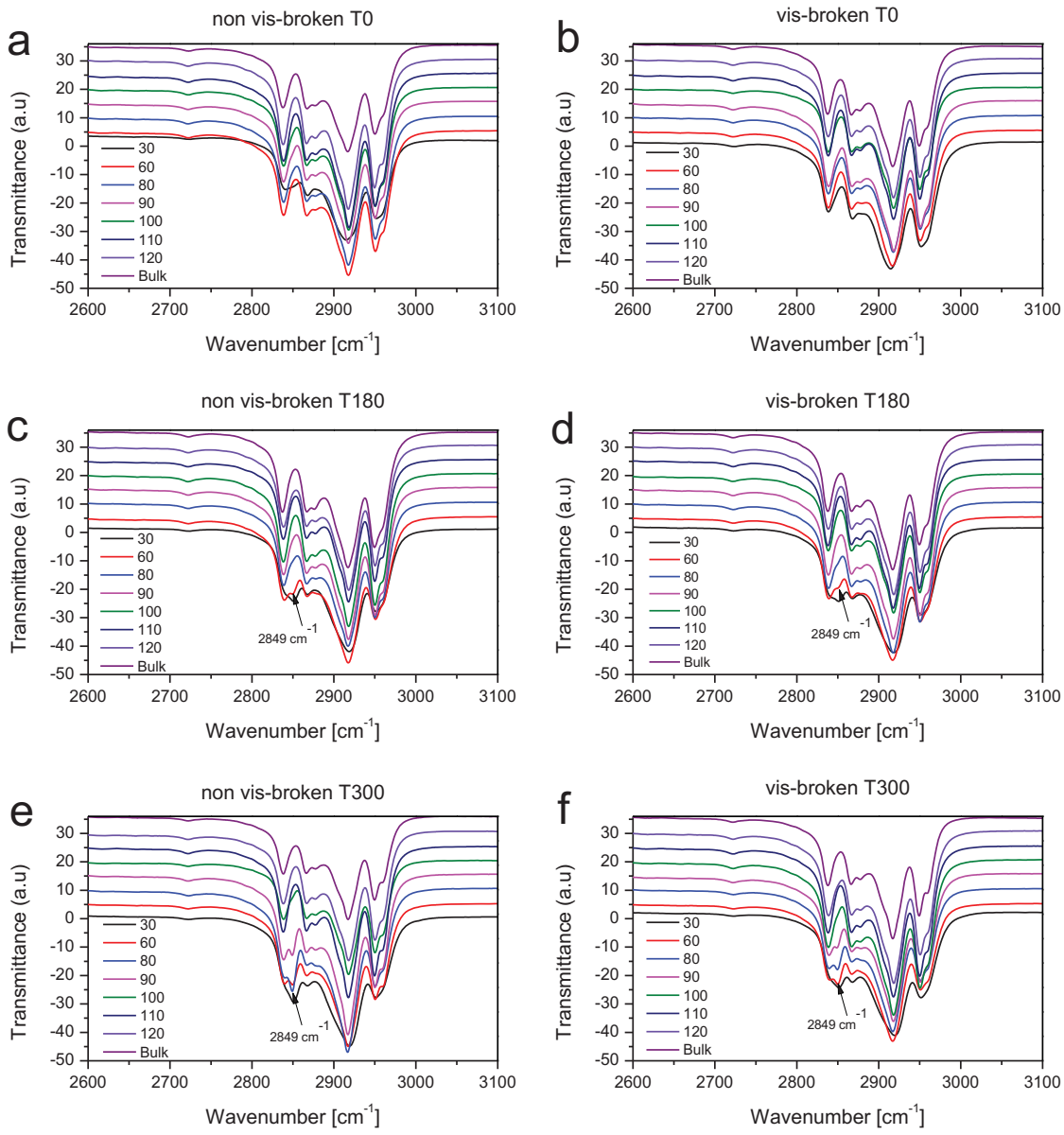

Figure 5.7 ATR-FTIR (between 2600 – 3100 cm^{-1}) spectra of (a) non vis-broken T0, (b) vis-broken T0, (c) non vis-broken T180, (d) vis-broken T180, (e) non vis-broken T300 and (f) vis-broken T300

Figures 5.8 (a) – (f) compares the fingerprint region of the fractions in the neat and vis-broken HEPCs. The IR peaks around 998 and 841 cm^{-1} are characteristic of CH_3 rocking vibrations in a threefold helix of isotactic PP [6, 7]. They appear for helix segments with at least ~ 11 to ~ 14 repeat units. The peak at 972 cm^{-1} is associated with CH_3 rocking vibrations of shorter helix segments. The peak at 720 cm^{-1} is due to CH_2 rocking vibrations of $(CH_2)_n$ where $n \geq 5$. Therefore, this peak is indicative of the presence long ethylene sequences. The presence of a doublet around 720 – 740 cm^{-1} is indicative of the presence of crystalline PE. When the crystallinity of PE is low, the 730 cm^{-1} peak reduces to a shoulder next to the 720 cm^{-1} peak [7].

Figures 5.8 (c) and (d) showed a distinct peak at 720 cm^{-1} in the 60 °C fraction as compared to the other fractions. This indicated that this fraction contains material with long ethylene sequences which was also confirmed by the appearance of the peak around 2849 cm^{-1} in Figures 5.7 (c) and (d). The 720 cm^{-1} peak was also observed to be more pronounced in the 60, 80 and 90 °C fractions of the T300 samples (both neat and vis-broken) as shown in Figures 5.8 (e) and (f). This was complemented by the appearance of the 2849 cm^{-1} peak in Figures 5.7 (e) and (f), indicative of the presence of long ethylene sequences. The 720 cm^{-1} peak was also observed in the 30 °C fractions of T180 and T300 (both neat and vis-broken) confirming the presence of l PE sequences. However, the peaks at 998 and 841 cm^{-1} were absent in the 30 °C fractions, confirming the absence of long PP sequences. Moreover, the 30 °C fractions of all the samples (both neat and vis-broken) showed a peak around 972 cm^{-1}, indicating the presence of shorter PP sequences.

Comparing the neat and vis-broken HEPCs, a new peak around 868 cm^{-1} was observed in the 60 °C fractions of all the vis-broken HEPCs. Therefore this peak could be assigned to the presence of propylene sequences that were cleaved off from long propylene sequences during vis-breaking. It appears the vis-breaking induced chain scission on long propylene sequences and a release of short propylene sequences in all the samples.

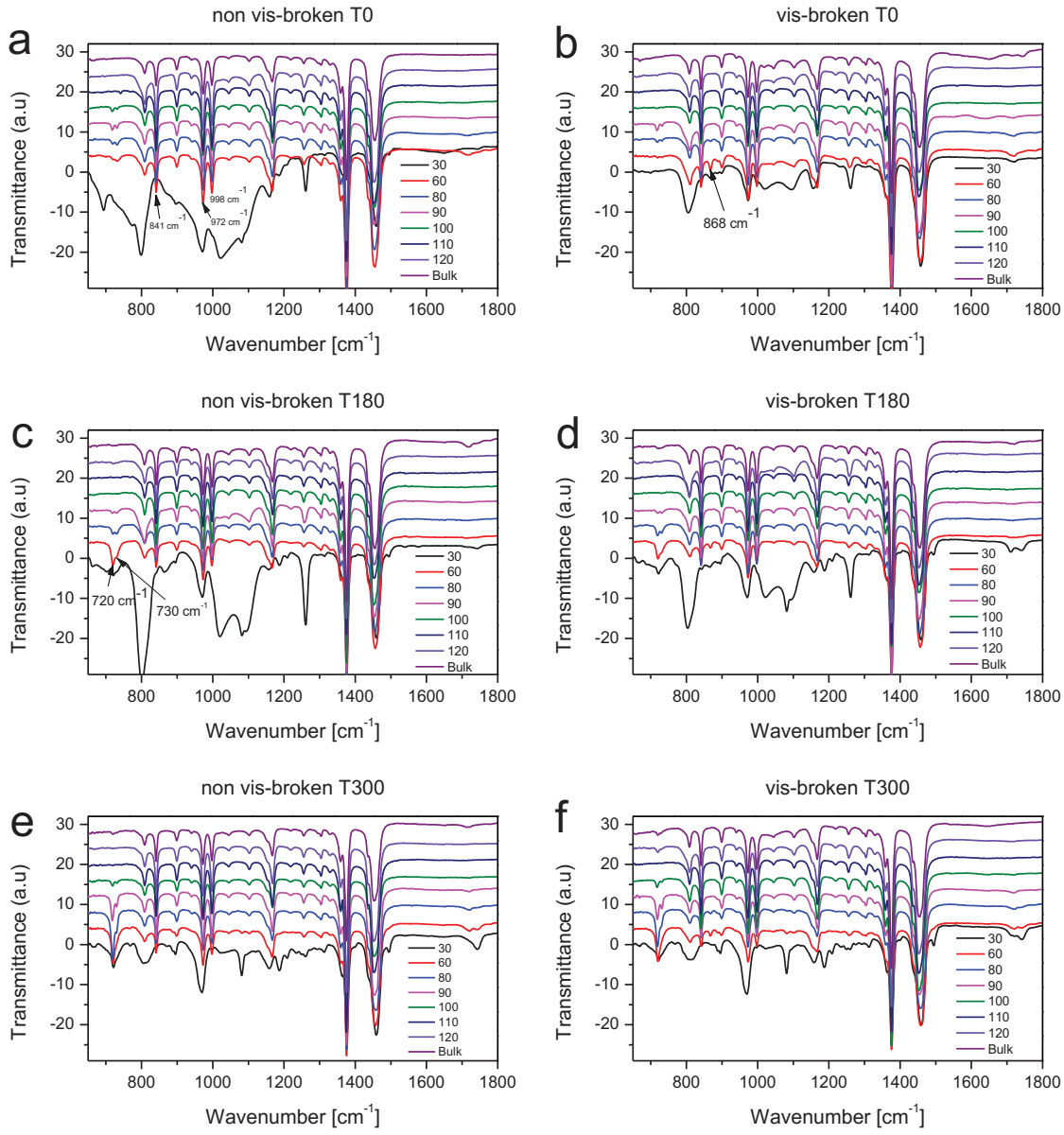

Figure 5.8 ATR-FTIR (between 650 – 1800 cm^{-1}) spectra of (a) non vis-broken T0, (b) vis-broken T0, (c) non vis-broken T180, (d) vis-broken T180, (e) non vis-broken T300 and (f) vis-broken T300

5.2.4 Gradient high temperature high performance liquid chromatography (HT-HPLC)

HT-HPLC has been applied with great success in separating heterogeneous entities within a HEPC matrix. One obvious advantage of HT-HPLC over the other analytical techniques is its sensitivity towards differences in chemical composition. Figures 5.9 (a) – (f) compares the HT-HPLC elugrams of the 30, 60, 80 and 90 °C fractions in the neat and vis-broken HEPCs. During the HPLC separation, PP chains in the 1-decanol phase are partially retained by the column and then desorbed during the gradient from 1-decanol to TCB [8]. In HT-HPLC, previous studies have shown that iPP in 1-decanol is partially retained on the porous graphite carbon (PGC) stationary phase. Coupling of HPLC to SEC has shown that the peak eluting between

1.0 – 1.4 ml has a lower molar mass eluting to that eluting at 3.0 ml [8]. Moreover, ethylene-propylene (EP) copolymers (referred to as the "rubbery" part of HEPCs) and PE homopolymers are fully retained due to selective adsorption on the column packing and tend to elute from 3.3 ml to higher elution volumes according to their methylene sequence lengths. EP copolymers with longer methylene sequences tend to interact more with the stationary phase as compared to EP copolymers with short methylene sequences [8].

HT-HPLC profiles indicated a decrease of the retained peak volumes with increasing elution temperature. Obviously, except in the T0 sample, this was an indication of a decrease in methylene sequence lengths with increasing elution temperature. Furthermore, the 60 °C fractions of the neat T180 and T300 samples exhibited a peak around 5.5 ml, indicating the presence of long ethylene sequences.

After vis-breaking, a decrease in the peak area of the retained component in the 60, 80 and 90 °C fractions and an appearance of a new small peak at 3.6 – 4.2 ml in the 60 °C fraction was observed for all fractions. It was interesting to note the appearance of the new peak at 3.6 – 4.2 ml was also observed in the 60 °C fraction of T0 sample after vis-breaking. Since T0 does not have any ethylene sequences, it could be speculated that the 3.6 ml peak was due to syndiotactic PP sequences.

Based on the appearance of the new peaks around 3.6 – 4.2 ml, it appears as though the effect of the peroxide causes a release of new sequences that elute at higher elution volumes.

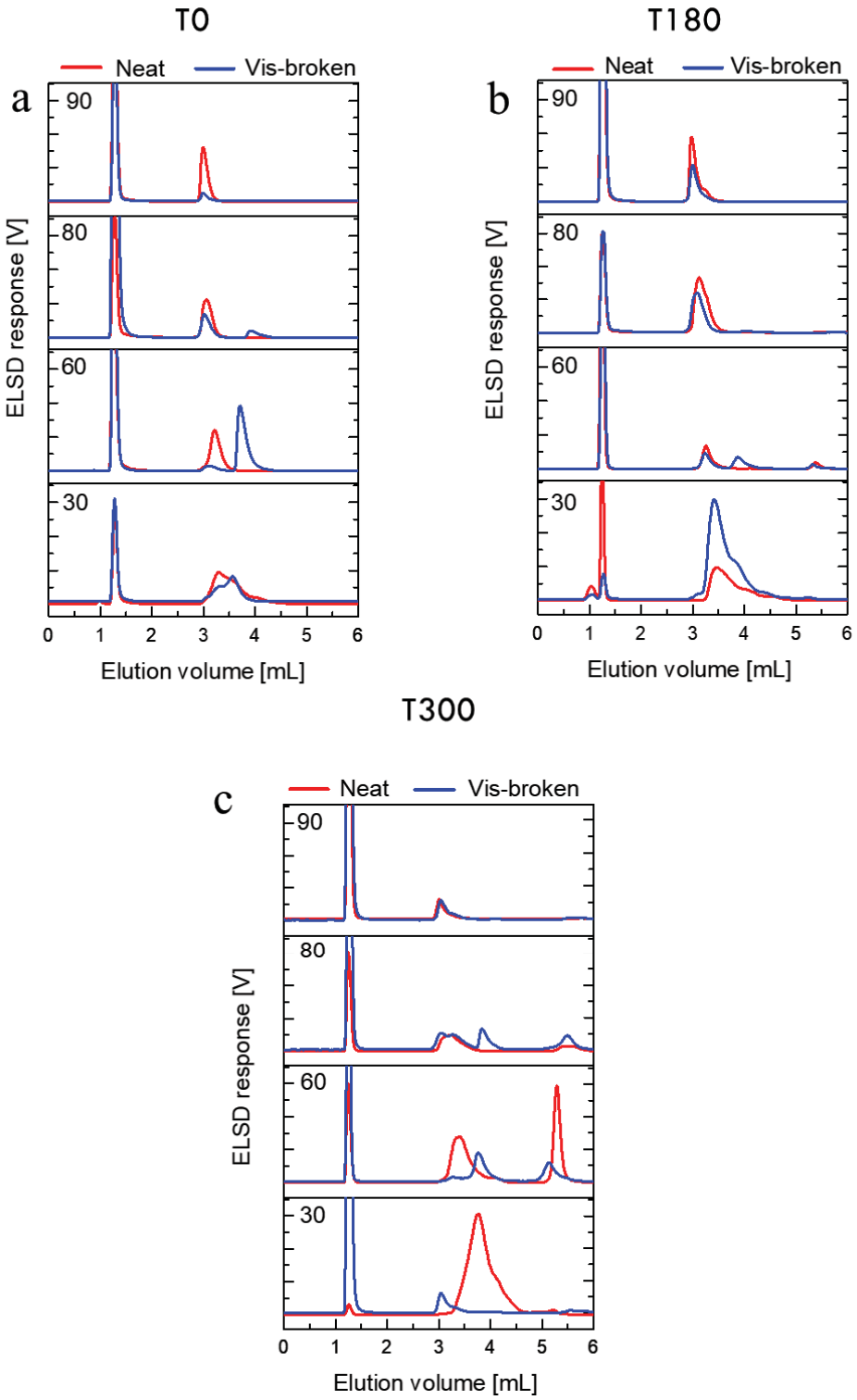

Figure 5.9 HT-HPLC elugrams of the 30, 60, 80, 90 °C fractions for (a) non vis-broken T0, (b) vis-broken T0, (c) non vis-broken T180, (d) vis-broken T180, (e) non vis-broken T300 and (f) vis-broken T300

5.3 Solvent gradient elution fractionation (SGEF)

The chemical composition distribution (CCD) of HEPCs is quite complex and mostly dominated by the iPP homopolymer phase. Therefore, it is quite challenging to detect any

subtle challenges in CCD and MMD in the various components of the bulk samples. As opposed to preparative TREF, SGEF produces fractions with narrow MMDs regardless of CCD (in theory).

During SGEF, bulk samples (non vis-broken and vis-broken) were fractionated using two solvents, a poor and a good solvent. The ratio of the good solvent was increased in aliquots, then preheated and pumped into the column containing the precipitated polymer and a support. A similar technique was reported by Xue *et al.* [2]. The recovered fractions of non vis-broken and vis-broken samples at each solvent/non-solvent ratio are shown in Figure 5.10 (a) – (b).

Upon comparing the non vis-broken HEPCs, a decrease in wt. % of fraction 10 and a simultaneous increase in wt. % of fractions 5, 6, 7, 8 and 9 with ethylene incorporation was observed. This merely indicates that the ethylene-propylene copolymers that were formed were of a lower molar mass than the iPP material that elutes in fraction 10 of the material without any ethylene incorporated. Moreover, when the non vis-broken and vis-broken HEPCs were compared, a shift towards lower fractions in the vis-broken samples was observed. This was as a result of the peroxide inducing chain scission on the longer (PP) chains, thus reducing their molar mass and thus causing them to elute at low molar mass fractions. All of this is supported by the general decrease in molar mass upon vis-breaking as observed in the HT-SEC results. Furthermore, the peak molar masses (M_p) and weighted average molar masses (M_w) seemed to have a general trend, an increasing molar mass with increasing fraction number. The molar mass values of the fractions are shown in Tables A.7 – A.12 of the appendix. The fractions appeared to have narrow dispersities ($Đ<3.0$) relative to their respective bulk samples, although some discontinuities were observed especially as the ethylene content increased. For example, the molar masses of fractions in the T0 sample (Figure 5.10 a) increased with increasing fraction number. However, in the T180 and T300 samples, fractions 5, 6 and 7 showed discontinuities which pointed to broad MMDs and higher than expected M_w.

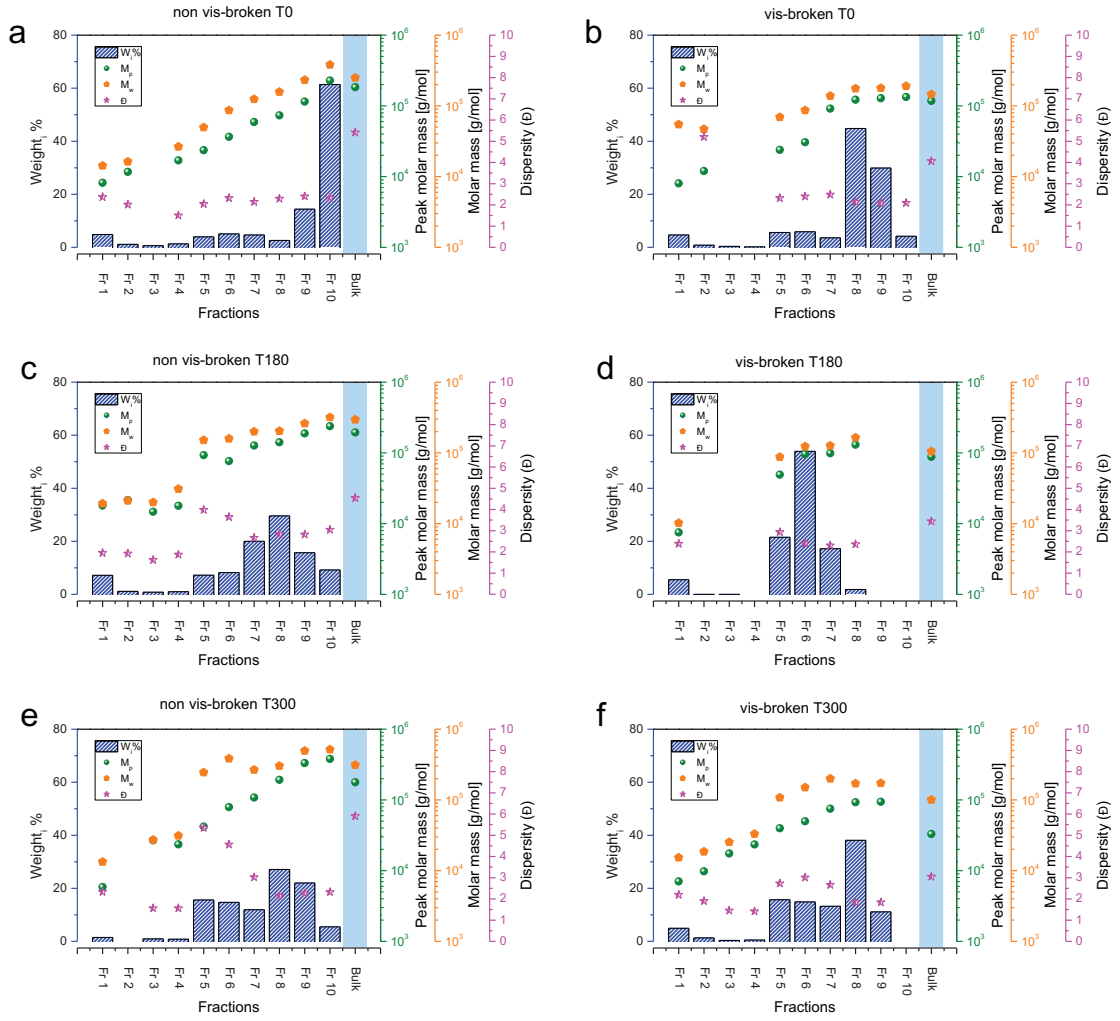

Figure 5.10 Plots showing the recovered fraction weight, peak and weight average molar masses (M_p and M_w) as well as the dispersities of (a) non vis-broken T0, (b) vis-broken T0, (c) non vis-broken T180, (d) vis-broken T180, (e) non vis-broken T300 and (f) vis-broken T300

5.3.1 High temperature size exclusion chromatography (HT-SEC)

The discontinuities in molar masses and dispersities in fractions 5, 6 and 7 of the T180 and T300 samples were apparent, as shown in Figure 5.10. It was suspected that the complex molar mass compositions were influenced by the presence of copolymers with different CCDs within these fractions. The molar mass distribution (MMD) curves of the respective SGEF fractions are shown in Figures 5.11 (a) – (f) below. Some of the samples were not analysed due to lack of material and this is denoted by the n.m abbreviation.

Upon comparison of the non vis-broken HEPCs, fractions 5, 6 and 7 of the T0 sample showed narrow MMD curves. However, fractions 5, 6 and 7 of the T180 and T300 samples showed broad MMD curves. HT-SEC separates according to hydrodynamic volume (V_h) which is then related to molar mass via a calibration. We suspect that due to the complex chemical composition makeup of the fractions, their respective V_h will be different in TCB solution,

giving rise to the broad MMDs. The differences in MMDs observed in fractions 5, 6 and 7 of the HEPCs seemed to follow the increase in bulk sample ethylene content, which correlated well with the dispersities and differences in molar masses from the expected trend shown by Figure 5.12 (a) and (c). The differences in MMDs could also be due to changes in solubility of the complex copolymers caused by changes in CCD.

When the non vis-broken and vis-broken HEPCs were compared, a narrowing of the MMDs was observed in fractions 5, 6 and 7 of the T180 and T300 samples, which correlated well with the decrease in discontinuities of molar mass and dispersities shown by Figures 5.12 (b) and (d). From these results, it was clear that the copolymer chains eluting in fractions 5, 6 and 7 were affected by the vis-breaking.

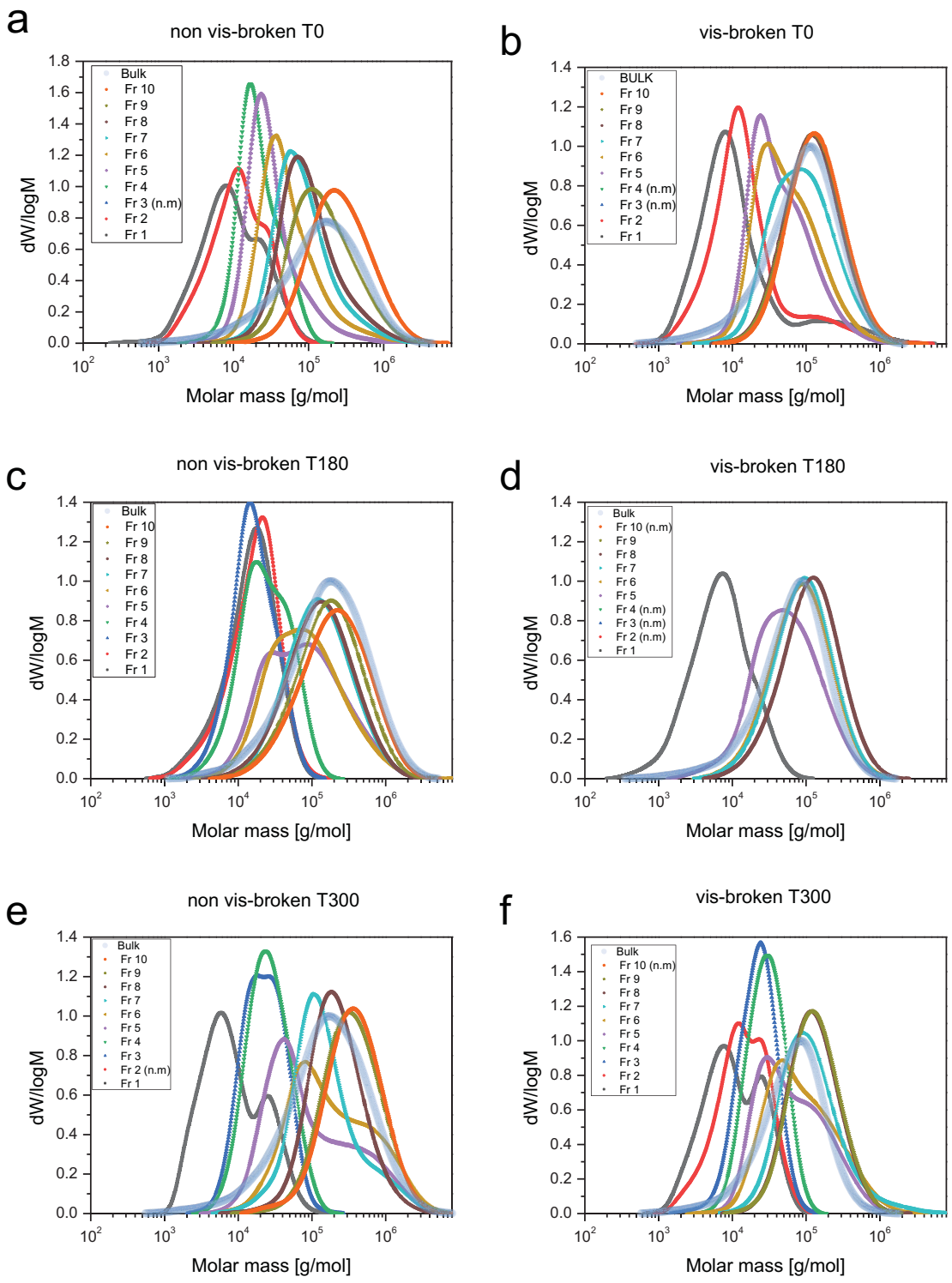

Figure 5.11 Molar mass distribution curves of SGEF fractions for (a) non vis-broken T0, (b) vis-broken T0, (c) non vis-broken T180, (d) vis-broken T180, (e) non vis-broken T300 and (f) vis-broken T300. (n.m means no material was available for analysis).

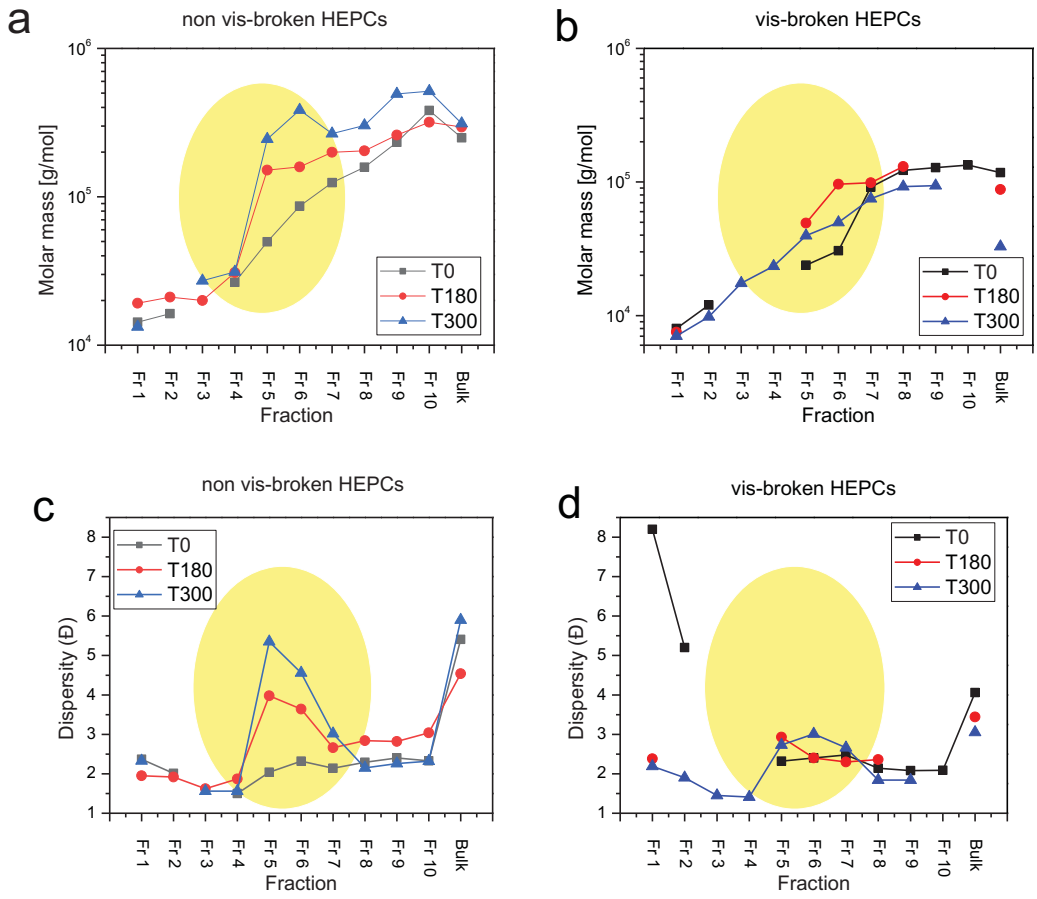

Figure 5.12 Overlays of molar masses for (a) non-vis-broken HEPCs and (b) vis-broken HEPCs together with polydispersities of (c) non-vis-broken HEPCs and (d) vis-broken HEPCs with increasing ethylene content. The yellow circles indicate regions of notable discontinuity.

5.3.2 Differential scanning calorimetry (DSC)

At this point, it was clear that the increase in bulk ethylene content contributed to the complex molar mass compositions of the fractions. Therefore, the crystallization and melting behaviour of the fractions in the respective samples was investigated using DSC. The crystallization and melting curves of the fractions are shown in Figures 5.13 (a) –(f) and Figures 5.14 (a) – (f). Some of the samples were not analysed due to lack of material and these samples were given the n.m abbreviation.

Upon comparison of the non vis-broken HEPCs (Figures 5.13 a, c and e), a slight shift towards lower crystallization temperatures of the peaks appearing above 120 °C (shown by the dotted lines) in the T0 sample was observed in the T180 and T300 samples. However, the shift was less pronounced in the T300 sample. The shift seemed to follow the increase in the bulk ethylene content. What we are seeing here may be due to changing solubility caused by changes in CCD. Thus the fractions that are obtained are not solely due to molar mass differences.

When comparing the vis-broken samples (Figures 5.13 b, d and f), the opposite of what was observed for the non vis-broken samples was observed. A shift of the crystallization peaks appearing above 120 °C (shown by the dotted lines) in the T0 sample towards higher temperatures was observed in the T180 and T300 samples. Again, the shift was less pronounced in the T300 sample. The less significant shift observed in the T300 sample could be due to the presence of more crystallisable ethylene sequences as opposed to PP rich sequences in this sample.

As a result of the complex chemical composition of fractions with increasing ethylene content, their respective DSC melting curves showed multimodal profiles as illustrated in Figures 5.14 (a) – (f). The high melting temperatures (above 140 °C) are indicative of PP being the predominant component with propylene rich chains forming the bulk of the EP chains. The influence of CCD on SGEF is a topic still to be investigated since the available literature targets only homopolymers such as LDPE. After vis-breaking, the high melting temperature peaks appearing above 160 °C in the non vis-broken samples, were shifted to lower melting temperatures. During vis-breaking, the peroxide radicals abstract a hydrogen atom from the tertiary carbon in the PP chains. Therefore, this action of the peroxide radicals induces beta scission on the PP chains, resulting in a decrease in molar mass and melting temperatures.

From the results obtained so far, it appears as though vis-breaking causes a cleaving of the PP rich sequences.

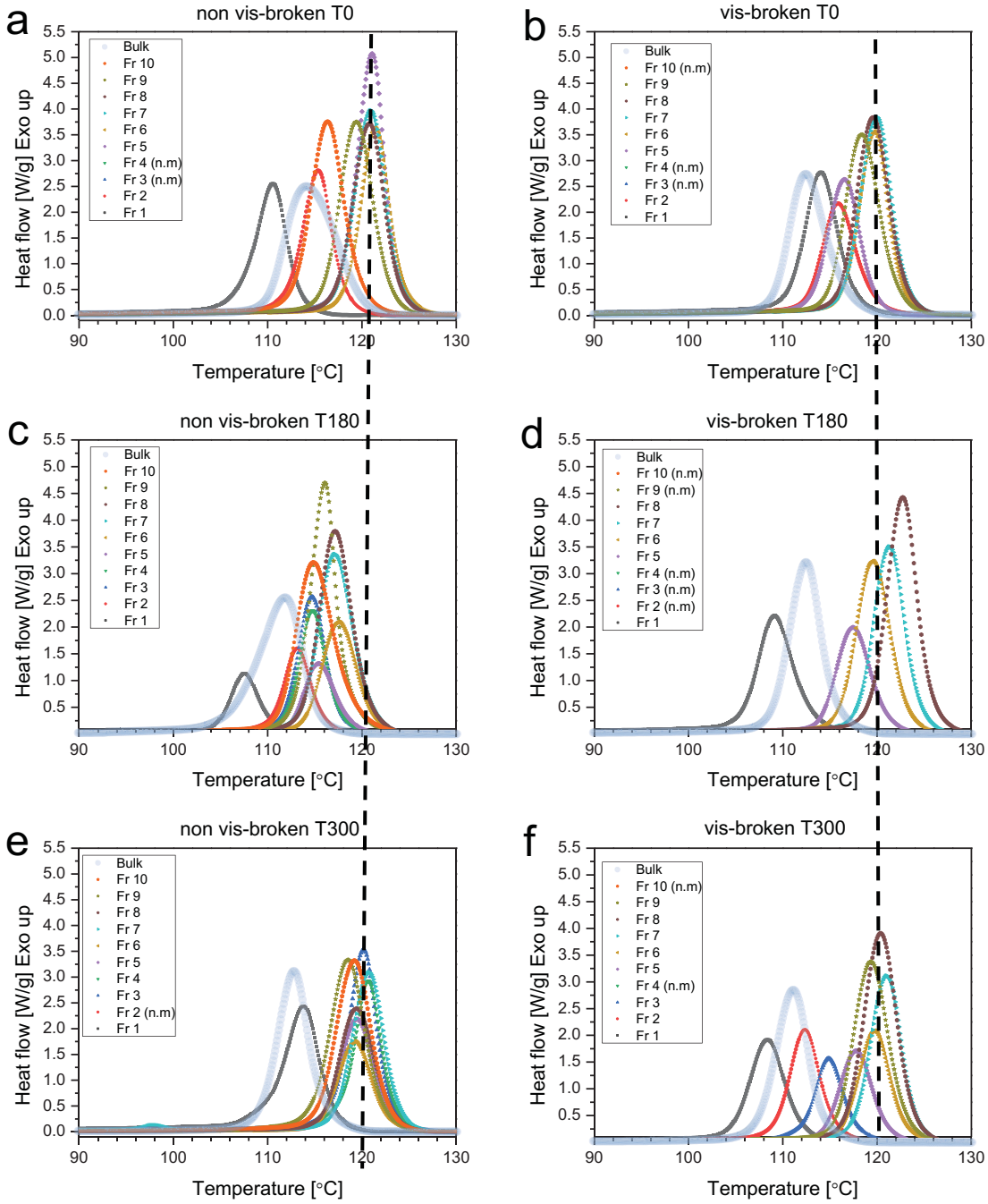

Figure 5.13 Crystallization curves of SGEF fractions for (a) non vis-broken T0, (b) vis-broken T0, (c) non vis-broken T180, (d) vis-broken T180, (e) non vis-broken T300 and (f) vis-broken T300. The dotted lines indicate the shift of the crystallization temperatures above 120 °C.

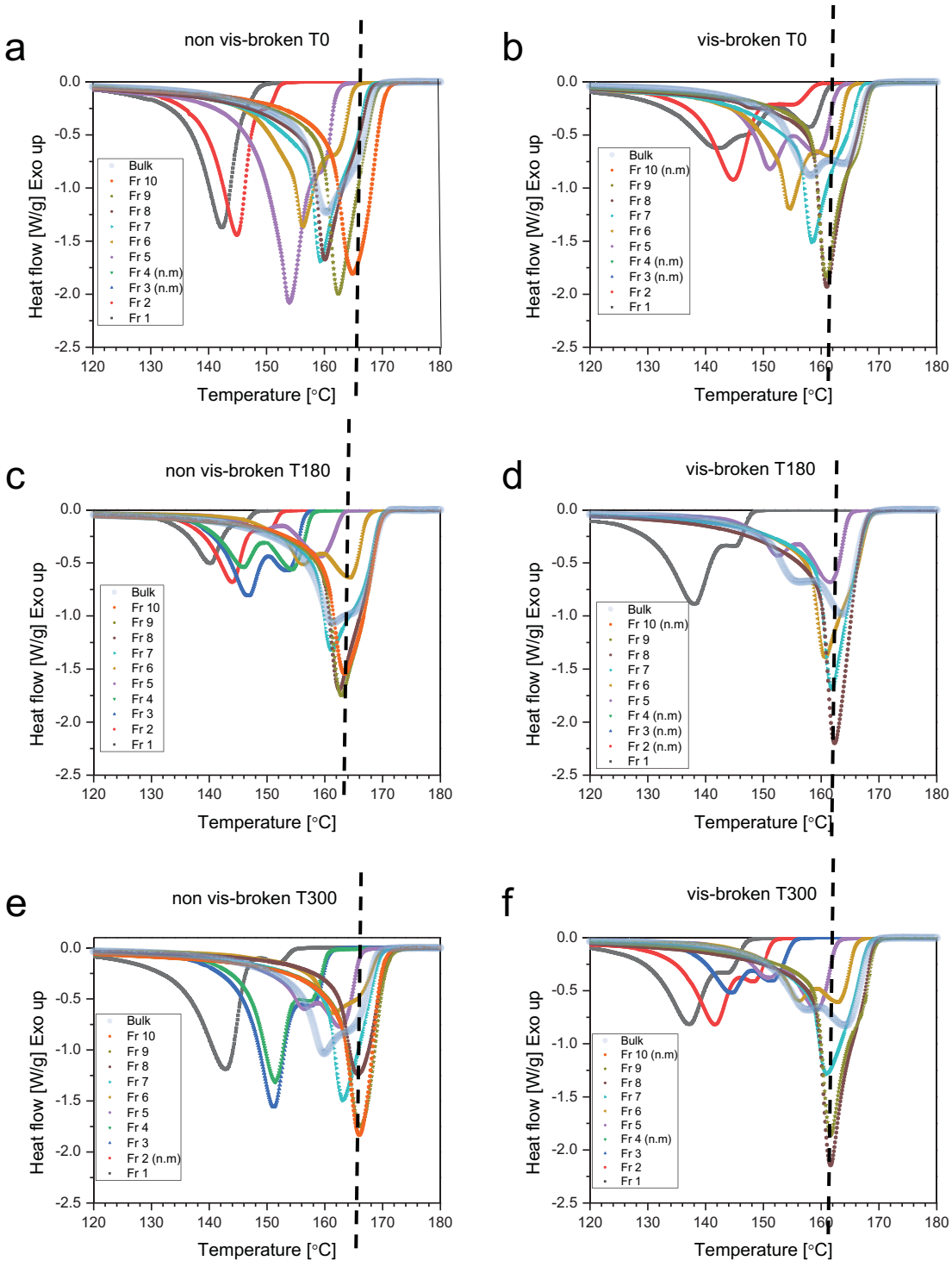

Figure 5.14 Melting curves of SGEF fractions for (a) non vis-broken T0, (b) vis-broken T0, (c) non vis-broken T180, (d) vis-broken T180, (e) non vis-broken T300 and (f) vis-broken T300.

5.3.3 Fourier transform infrared spectroscopy (FTIR)

From the results gathered so far, the chemical composition of the fractions proved complex. Therefore, FTIR was used to investigate the chemical structure of these fractions before and after vis-breaking. Two spectral regions of the FTIR spectra were shown for comprehensive

structural analyses. The first region is shown in Figures 5.15 (a) – (f) and the second region is shown in Figures 5.16 (a) – (f).

Upon comparison of the vis-broken HEPCs in Figure 5.15, the appearance of a shoulder peak was observed at 2849 cm^{-1} (indicated by the dotted arrow) in fraction 6 of the T180 and T300 samples. This peak was also observed in fraction 7 of the T300 sample. In addition, it was also noted that this 2849 cm^{-1} shoulder peak was more pronounced in fraction 6 of the T300 sample as opposed to the same fraction of the T180 sample. Furthermore, the appearance and build-up of the shoulder peak seemed to follow the increase in bulk ethylene content. Therefore, it was suspected that this shoulder peak could be due to CH_2 stretches coming from ethylene sequences.

After vis-breaking, Figure 5.15 (d) showed no shoulder at 2849 cm^{-1} in fraction 6 of the T180 sample. This correlated well with the disappearance of the 720 cm^{-1} peak (indicated by the red circle) in fraction 6 of the vis-broken T180 sample as shown in Figure 5.16 (d). Furthermore, a slight decrease of the 2849 cm^{-1} shoulder peak was observed in fraction 6 of T300 sample after vis-breaking. The disappearance of the 2849 cm^{-1} and 720 cm^{-1} peaks could be an indication that the vis-breaking the vis-breaking led to a separation between PP sequences and ethylene sequences. However, since PP forms the predominant phase, the ethylene sequences were not detected because they were overshadowed by the PP sequences.

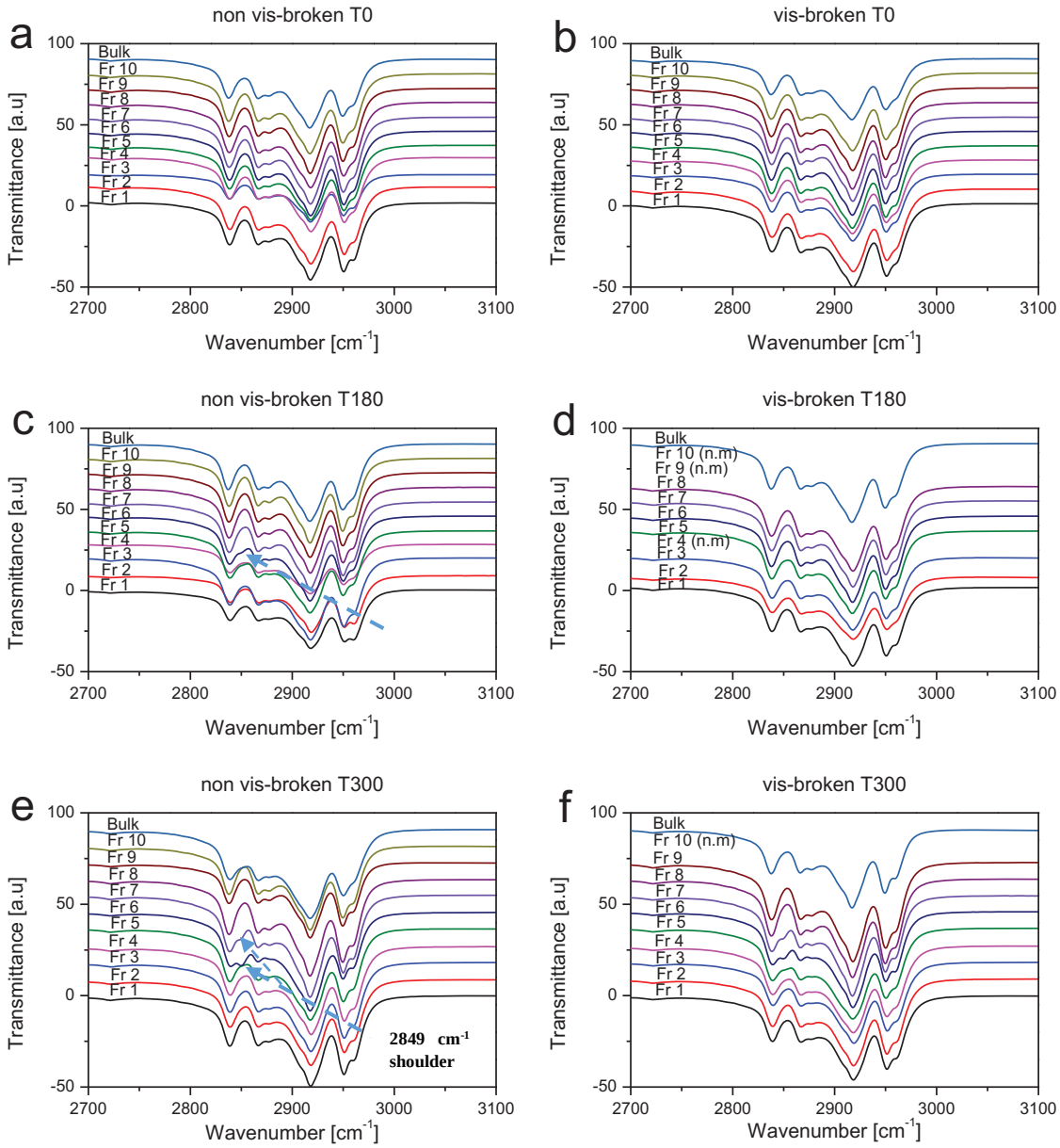

Figure 5.15 ATR-FTIR (2600 – 3100 cm^{-1}) spectra of SGEF fractions for (a) non vis-broken T0, (b) vis-broken T0, (c) non vis-broken T180, (d) vis-broken T180, (e) non vis-broken T300 and (f) vis-broken T300 (n.m stands for no material). The dotted arrows indicate the appearance of the shoulder at 2849 cm^{-1}.

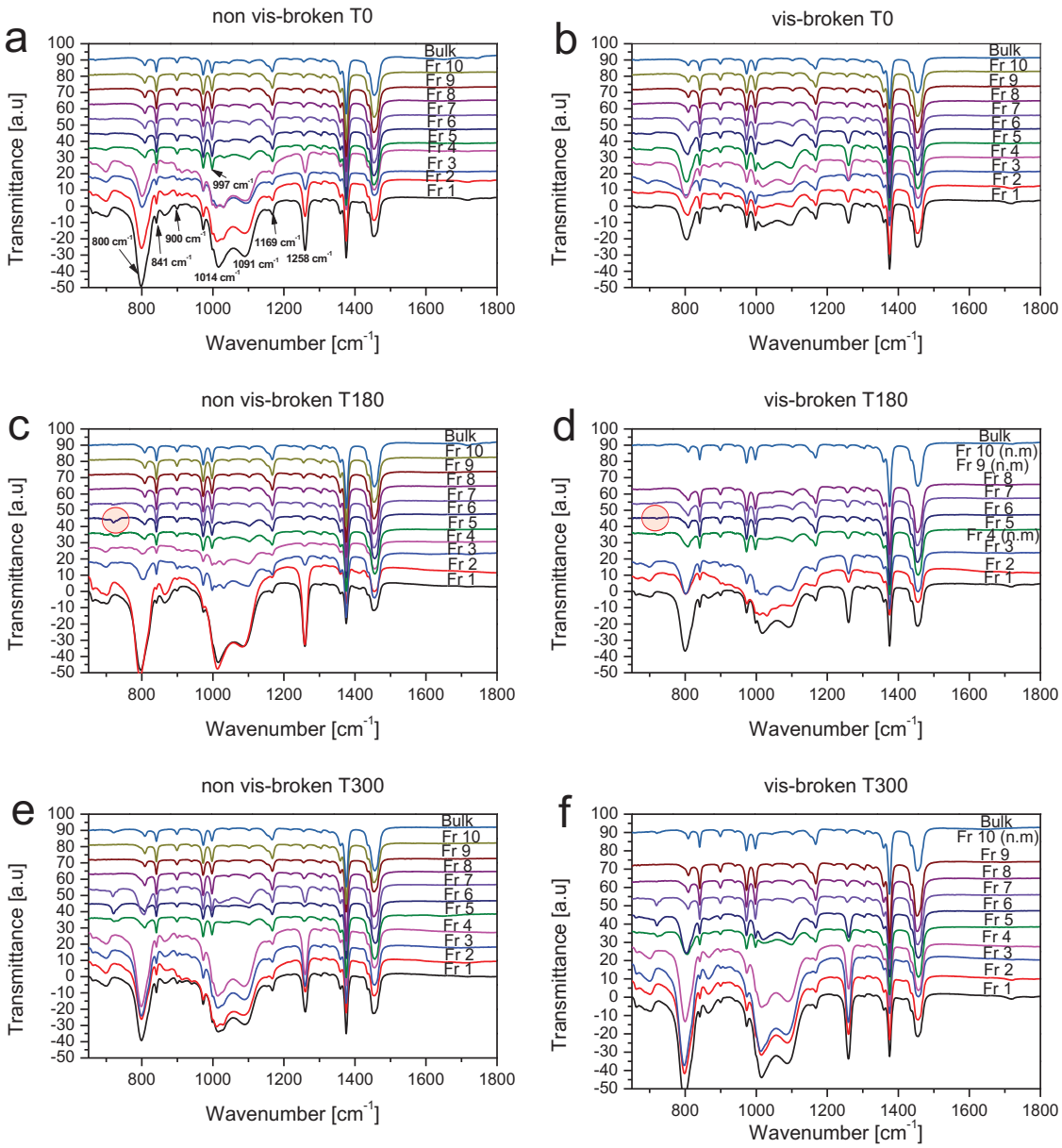

Figure 5.16 ATR-FTIR (between 650 – 1800 cm^{-1}) spectra of SGEF fractions for (a) non vis-broken T0, (b) vis-broken T0, (c) non vis-broken T180, (d) vis-broken T180, (e) non vis-broken T300 and (f) vis-broken T300. The red circle shows the disappearance of the 720 cm^{-1} PE peak after vis-breaking.

5.3.4 Gradient high temperature high performance liquid chromatography (HT-HPLC)

Unlike all the analytical techniques used thus far, HT-HPLC is sensitive to the presence of long ethylene segments in the copolymer chains and these chains usually elute separate to the iPP homopolymer. Therefore, HT-HPLC was employed to separate the components within the SGEF fractions using a 1-decanol → $TCB_{10\ min}$ gradient. Figures 5.17 (a) – (f) show elugrams of the fractions obtained from non vis-broken and vis-broken samples.

In HT-HPLC, iPP elutes in two peaks under a 1-decanol → $TCB_{10\ min}$ gradient. The first peak elutes in SEC mode between 1.0 – 1.6 ml. This peak is usually assigned to the low molar mass component of the iPP sample which is not retained in 1-decanol. The second peak appears just after the start of the gradient, which implies very weak interactions with the PGC stationary phase.

The elution behaviour of the fractions in sample T0 (which is iPP) is illustrated in Figure 5.17 (a). The second peak was observed to increase in size with increasing fraction number, which agrees with the increase in M_w observed in HT-SEC analysis. When the T0 sample was vis-broken, fractions 3, 5 and 6 showed extra peaks (shown in the insert in Figure 5.17 b) at ~ 3.8 ml. Since no ethylene sequences were detected via FTIR or ^{13}C-NMR in the T0 sample, the peaks around 3.8 ml were speculated to be due to stereo irregular chains cleaved off during vis-breaking. However, this elution behaviour is yet to be understood as more studies are still being conducted on the elution behaviour PP in HT-HPLC.

The introduction of ethylene co-monomers results in the formation of EP copolymer chains with different blocks. Depending on the monomer feed rate as well as reaction time, a specific co-monomer content can be targeted. After the fractionation of sample T180, it was evident from the elugrams that fractions 1 – 7 contained some EP chains eluting from ~ 3.2 ml. In both the non vis-broken and vis-broken samples, fraction 5 showed the presence of more EP chains. Fractions 7 – 10 did not show the presence of EP copolymer fractions, implying that the predominant component is iPP. After vis-breaking, the elution profile of fraction 5 was altered (Figure 5.17 d). After vis-breaking, the fraction contained groups of components with close to descrete CCD and could be isolated on the PGC column. A 1-decanol → $TCB_{10\ min}$ gradient was used to allow for better detection of the smaller components. Longer gradients usually result in the spreading of material over a large elution volume resulting in a poor detection.

Similar trends were observed with the non vis-broken and vis-broken fractions of the T300 sample. Here, the EP copolymer component eluting between 3.2 – 4.0 ml in the non vis-broken fraction was monomodal and close to symmetrical. After vis-breaking, components that eluted in this region (3.2 – 4.0 ml) for the vis-broken T300 sample showed multimodal behaviour, indicating increased complexity of the EP copolymer composition. In addition, the peak maxima of the components shifted towards higher elution volumes, indicating some sort of isolation of chains with long ethylene sequences from the propylene rich ones. Fractions 6 and 7 of the non vis-broken and vis-broken T300 sample showed peaks eluting between 5.0 -6.0

ml. To properly visualize these peaks, inserts were put in Figures 5.17 (e) and (f). These peaks indicate the presence of components that are rich in ethylene and have long ethylene sequences.

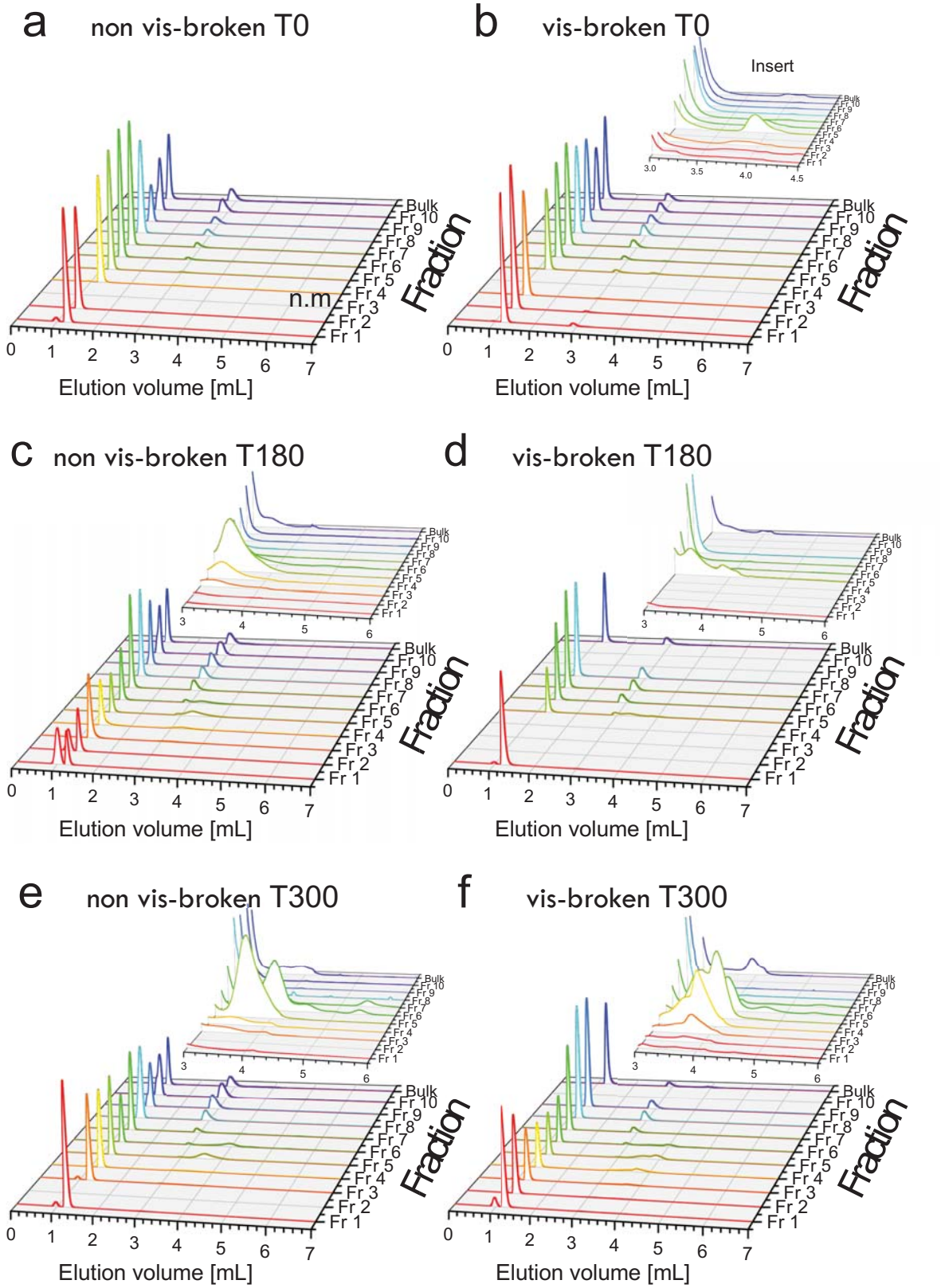

Figure 5.17 HT-HPLC elugrams of SGEF fractions for (a) non vis-broken T0, (b) vis-broken T0, (c) non vis-broken T180, (d) vis-broken T180, (e) non vis-broken T300 and (f) vis-broken T300. (n.m stands for no material). The inserts zoom in on the peaks eluting between 3 – 6 ml.

5.3.5 Two dimensional HPLC

To monitor the interdependence of chemical composition and molar mass of the various alloy components in the HEPCs, HT-HPLC was coupled to HT-SEC online to obtain comprehensive two dimensional plots as illustrated in Figures 5.18 – 5.21 below. From the contour plots below, it was clear that the unretained iPP homopolymer constitutes the majority of the sample, while the later eluting components were quite small. It was also evident that the PP homopolymer greatly influences what is observed in the SEC dimension, masking the smaller but crucial copolymer components. Furthermore, it must be noted that the detector responses of PP and EP copolymers are affected by their respective chemical composition. PP is generally known to give higher ELSD responses as compared to PE and ethylene-1-olefin copolymers.

When the elution behaviours of the non vis-broken and vis-broken T300 bulk samples in Figures 5.18 (a) and (b) were compared, a shift towards higher SEC elution volumes was observed in the vis-broken T300 bulk samples. This shift was indicative of a decrease in molar mass. However, the components were affected differently, the iPP homopolymer and PP rich fractions appeared to have a greater change in elution volume.

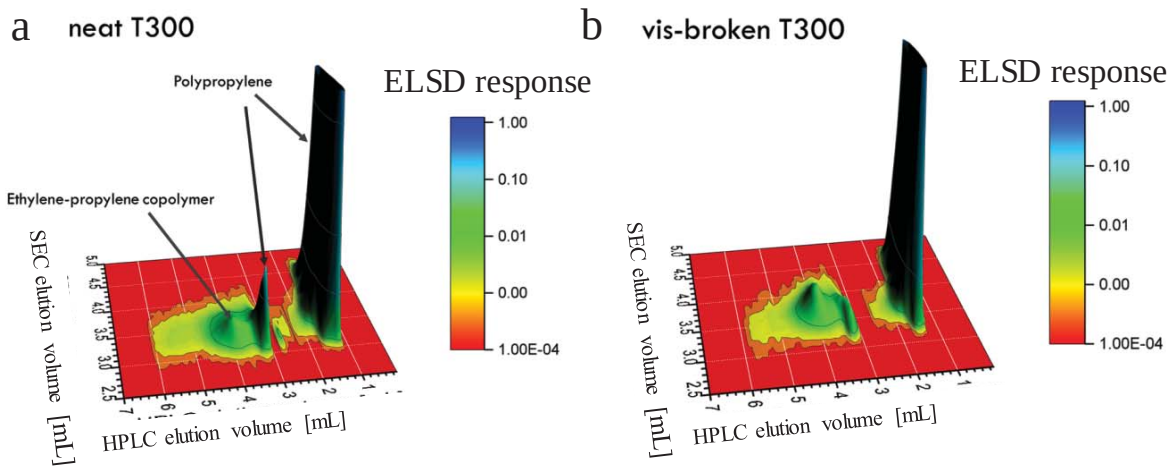

Figure 5.18 HT-2D-LC contour plots comparing the elution behaviour of the (a) non vis-broken T300 and (b) vis-broken T300 bulk samples.

To better illustrate the differences observed in the contour plots shown in Figures 5.18 (a) and (b), Figure 5.18 (b) was subtracted from Figure 5.18 (a) in order to obtain Figure 5.19. The observed mismatch in the two samples was due to differences in molar mass. Furthermore, the differences appeared to be less pronounced at higher HPLC elution volumes (indicated by the red dotted circle), implying that the vis-breaking affected more of the polyolefin chains with more PP segments and less those with more ethylene co-monomer.

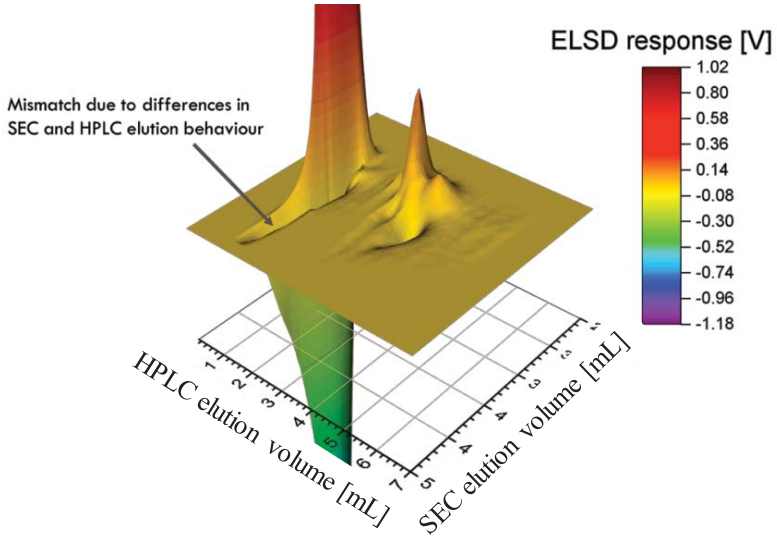

Figure 5.19 A contour plot obtained from subtracting the contour plot of the vis-broken T300 bulk sample form that of the non vis-broken T300 bulk sample.

HT-2D-LC was also used to analyse fractions 5 and 6 of the non vis-broken T300 sample, as illustrated in Figures 5.20 (a) and (b). The elution behaviour of the late eluting component in fraction 5 correlated well with the elution behaviour of the ethylene-propylene copolymers with low ethylene contents. As such, a small component of fraction 5 extended up to 5.5 ml (see Figure 5.20 a). On the other hand, it was clear that fraction 6 had more ethylene and a larger component was retained after 5.0 ml (see Figure 5.20 b).

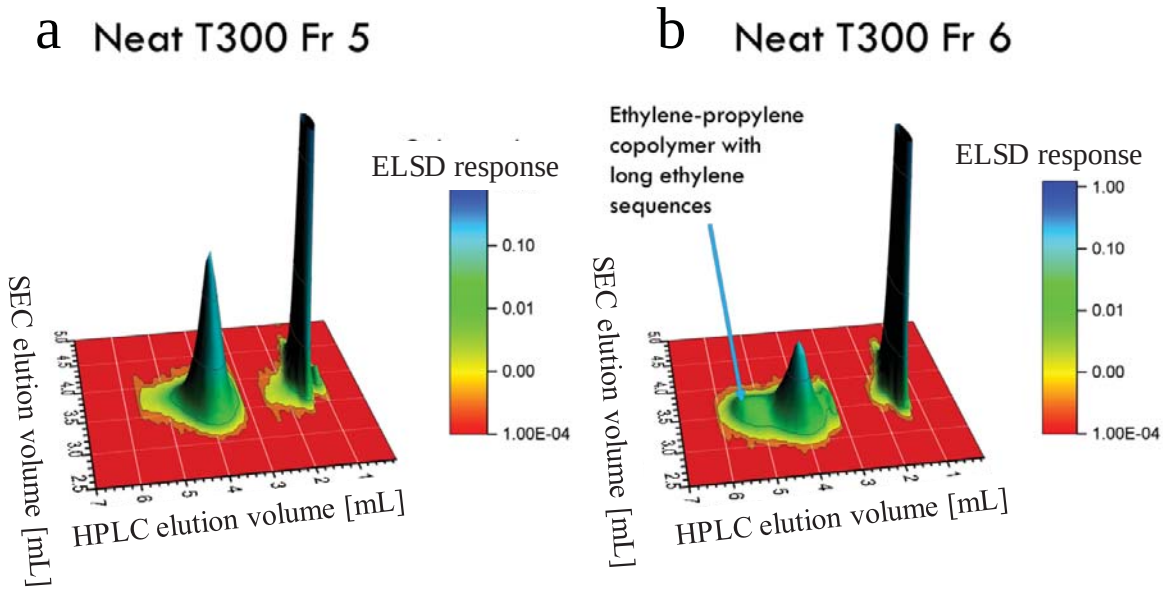

Figure 5.20 HT-2D-LC contour plots of (a) non vis-broken T300 Fr 5 and (b) non vis-broken T300 Fr 6.

Fraction 6 of the non vis-broken and vis-broken T300 samples was compared in Figures 5.21 (a) and (b). This fraction was collected at a similar solvent/non solvent ratio in both samples and comparable recoveries were obtained. From the 2D contour plots, differences in molar mass were observed for the eluting components, the iPP components had different molar masses. After vis-breaking, the iPP component shifted towards higher SEC elution volumes indicating a decrease in molar mass. This was as a result of the low molar mass PP material that shifted towards fraction 6 during vis-breaking. Apart from the iPP homopolymer, the propylene-rich copolymers appeared to be more susceptible to attack by the peroxide as compared to the ethylene-rich components. The molar mass of the ethylene-rich copolymers appeared to remain unchanged, mirroring what was observed with the bulk samples in Figures 5.18 and 5.19. This is what gave the contour plots their skewed appearance as highlighted by the yellow arrows.

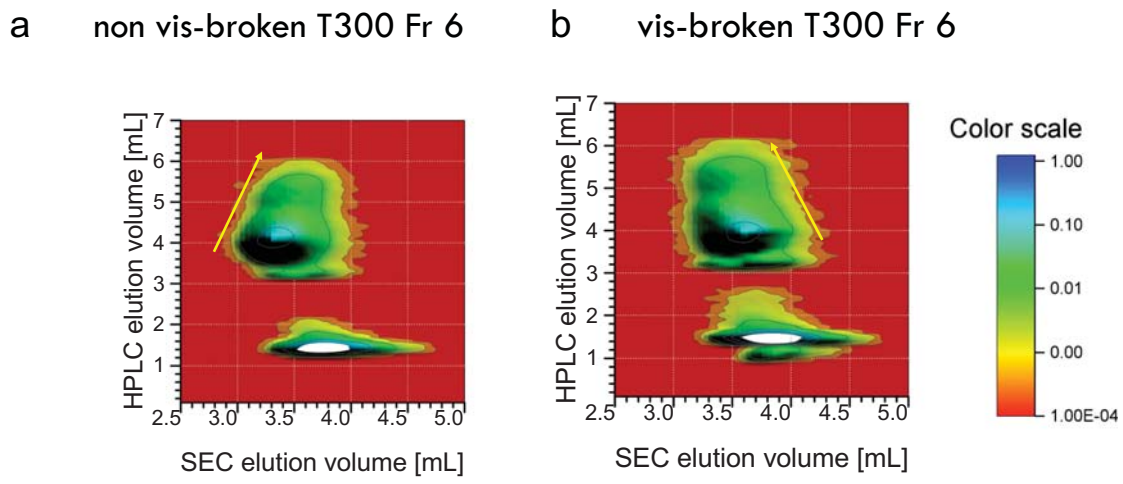

Figure 5.21 HT-2D-LC contour plots of (a) non vis-broken T300 Fr 6 and (b) vis-broken T300 Fr 6.

5.3.6 HPLC-FTIR

HT-HPLC was coupled to FTIR in order to confirm the presence of the ethylene co-monomer within the separated HT-HPLC peaks. HT-HPLC-FTIR plots of selected bulk samples are shown in Figures 5.22 (a) – (d). The Gram-Schmidt is a result of the separation obtained via HT-HPLC and the propylene content is calculated from the CH_3/CH_2, A(1405-1320 cm^{-1})/A(1500-1405 cm^{-1}) ratio obtained from FTIR. The elution profiles were changed after vis-breaking e.g. the change in the peak at 3.0 – 3.8 ml. The shift in elution volume from what was observed in HT-HPLC (see Figure 5.17) was due to the addition of a longer transfer line between the column and the LC transform interface.

From the HPLC-FTIR results shown in Figure 5.22 (a) and (b), it is clear that the T0 sample contained no ethylene sequences but was purely PP.

For the non vis-broken and vis-broken T300 samples, there was evidence of ethylene co-monomer containing chains at high elution volumes as observed in Figures 5.22 (c) and (d). The ratio of methyl groups to the consecutive methylene sequences [CH_3/CH_2, A (1405 1320 cm^{-1}) / A (1500 – 1405 cm^{-1})] was observed to decrease at high elution volumes indicating a decrease in the propylene content and an increase in the ethylene content. While the resolution of close eluting peaks is poor in HT-HPLC-FTIR due to unavoidable sample mixing during sample deposition on the germanium disc, there were clear differences between the non vis-broken and vis-broken bulk samples. A clear segregation of ethylene rich copolymer chains was observed in the vis-broken sample. The later eluting peak in Figure 5.22 (d) (3.7 – 5.0 ml) showed a lower CH_3/CH_2 ratio or higher ethylene content.

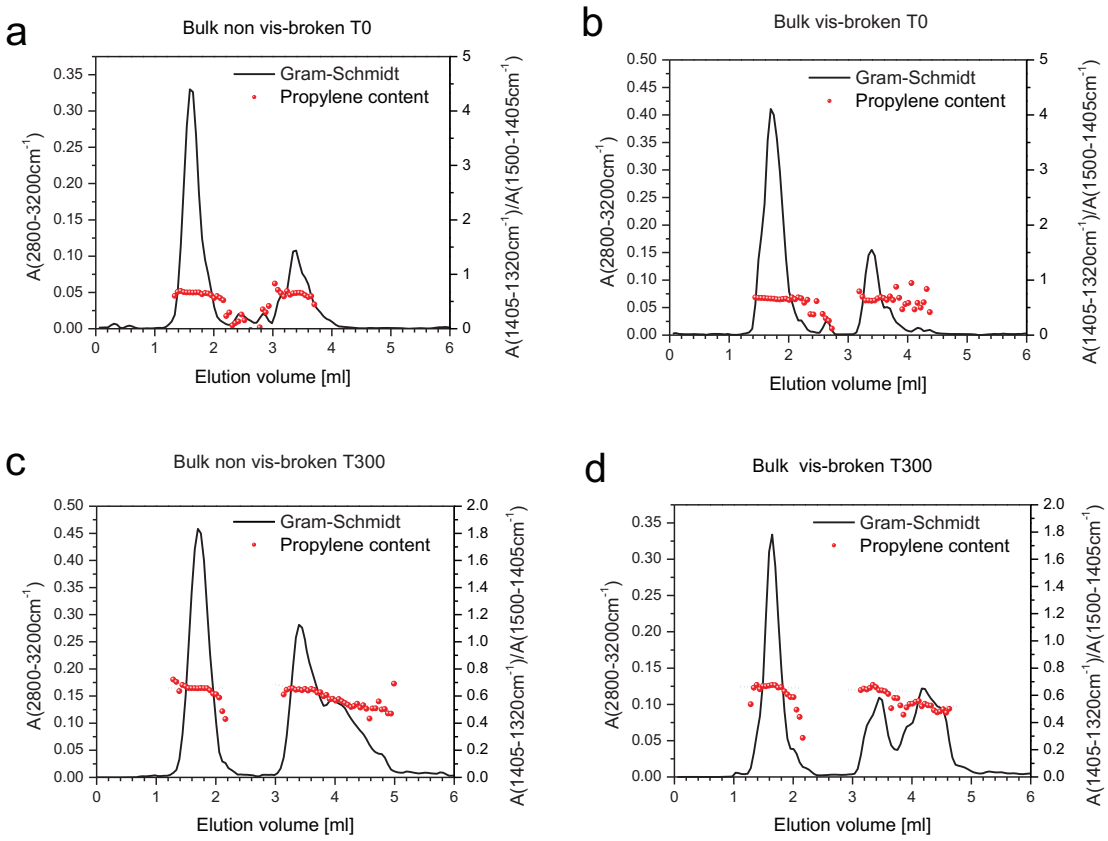

Figure 5.22 HPLC-FTIR plots showing propylene content as a function of elution volume for bulk samples of (a) non vis-broken T0, (b) vis-broken T0, (c) non vis-broken T300 and (d) vis-broken T300.

Fraction 5 of the non vis-broken T300 sample and fraction 6 of the non vis-broken and vis-broken T300 samples were compared in Figures 5.23 (a) –(c). Upon comparing the elution behaviour of fraction 5 and 6 of the non vis-broken T300 sample, a decrease in the CH_3/CH_2

ratio or increase in ethylene content was observed with increasing elution volume in fraction 6 of the non vis-broken T300 sample. This was confirmation that fraction 6 contained more of the ethylene co-monomer chains as compared to fraction 5. After vis-breaking, it was interesting to note that the CH_3/CH_2 ratio in the non vis-broken T300 sample followed the same trend as observed in fraction 6 of the non vis-broken T300 sample, indicating that the longer ethylene sequences were still present in fraction 6 even after vis-breaking.

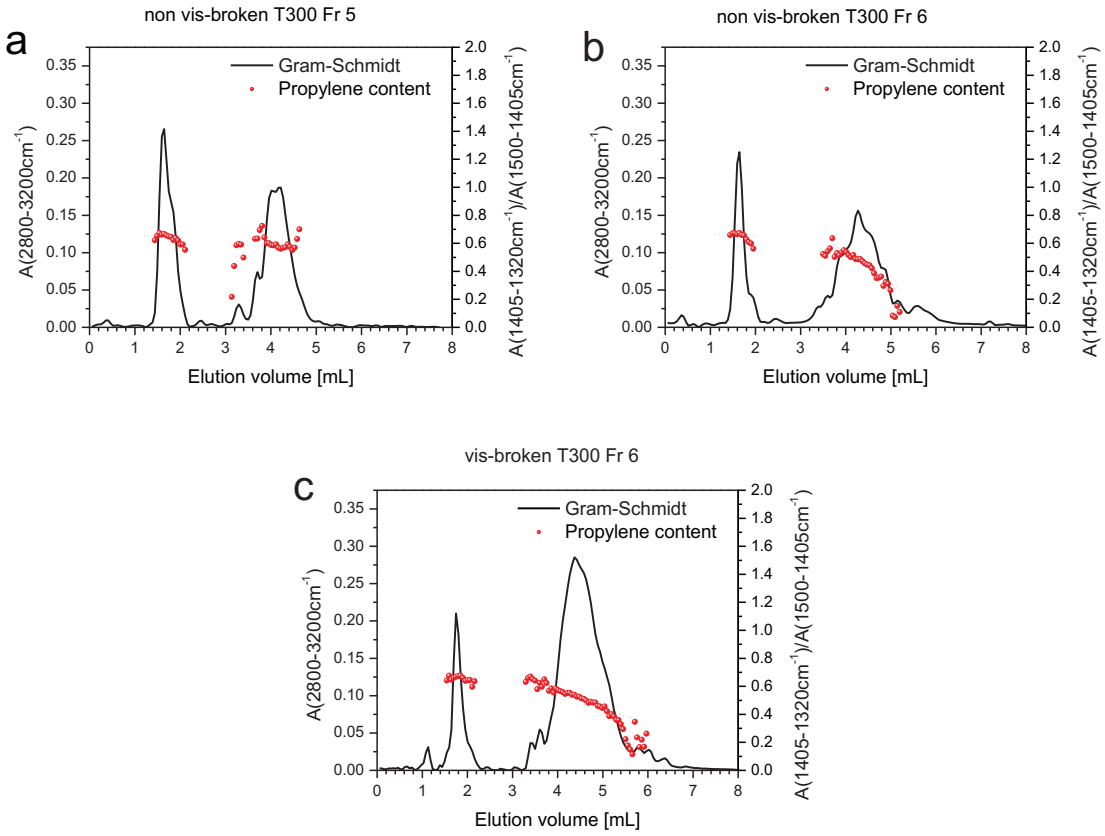

Figure 5.23 HT-HPLC-FTIR plots showing propylene content as a function of elution volume of (a) non vis-broken T300 fraction 5, (b) non vis-broken T300 fraction 6 and (c) vis-broken T300 fraction 6.

5.3.7 Solution-state carbon 13 nuclear magnetic resonance spectroscopy (^{13}C-NMR)

^{13}C-NMR was used to determine the chemical composition of the SGEF fractions. Figures 5.24 and 5.25 below show the ^{13}C-NMR spectrum of an ethylene-propylene copolymer with a low ethylene content and an illustration of the nomenclature used for the different carbons identified by the ^{13}C-NMR spectrum. According to terminology described by Carman and Wilkes [9], the letters S, P and T stand for secondary, primary and tertiary carbon atoms, respectively. The two Greek letters shown by Figures 5.24 and 5.25 refer to the distance, on both sides, of any given carbon from the nearest neighbouring tertiary carbon. For example, the notation $S_{\alpha\alpha}$

refers to a secondary carbon with two tertiary carbons on both sides. $S_{\alpha\beta}$ on the other hand refers to a secondary carbon with one tertiary carbon on one side and another tertiary carbon found one carbon away. $S_{\delta\delta}$ stands for a secondary carbon with two tertiary carbons found four carbons away on both sides. Lastly, $S_{\alpha\gamma}$ refers to a secondary carbon with a tertiary carbon on one side and another tertiary carbon found two carbons away. Moreover, when the distance to the nearest tertiary carbon exceeds four, the notation δ^+ is used.

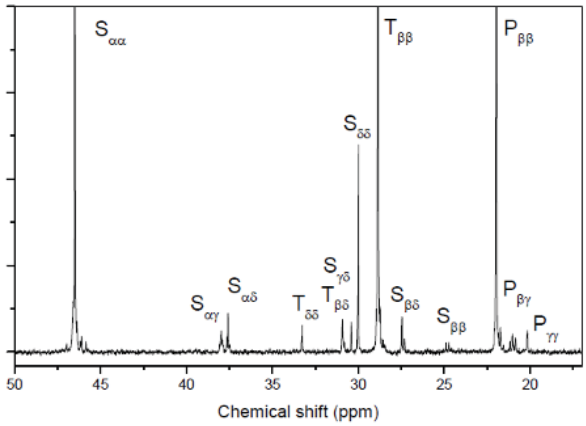

Figure 5.24 ^{13}C-NMR spectrum of an ethylene-propylene copolymer showing assignments of each peak [5]

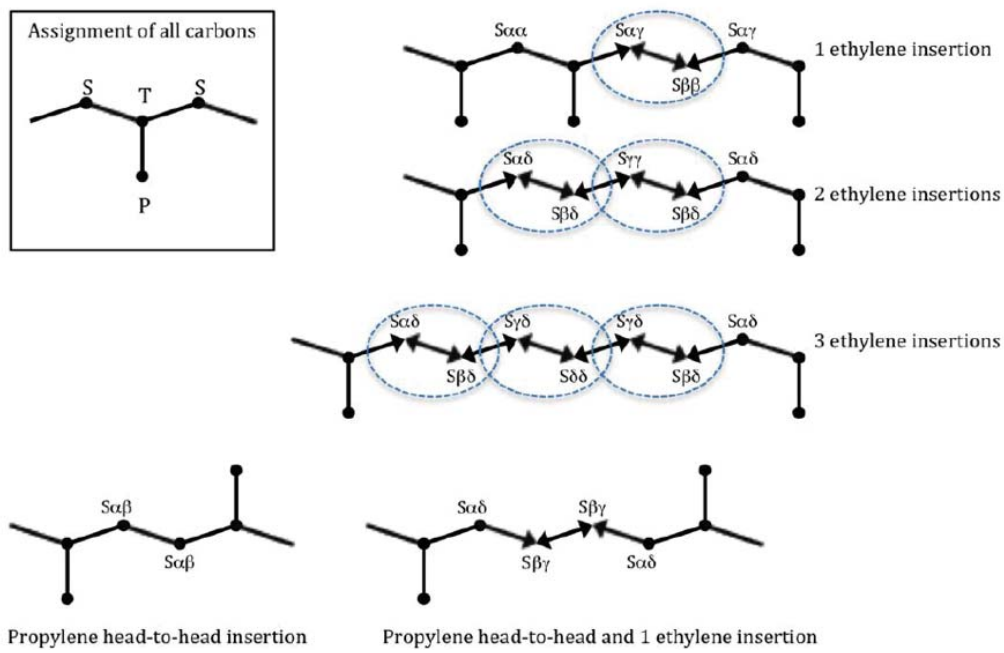

Figure 5.25 A diagram showing notations for the different carbons in ethylene-propylene copolymers as proposed by Carmen and Wilkes [9] as well as Ray *et al* [10].

Figures 5.26 (a) – (f) compares ^{13}C-NMR spectra of fractions 5, 6 and 7 for the neat and vis-broken HEPCs. All the spectra exhibited three distinct peaks, $S_{\alpha\alpha}$, $T_{\beta\beta}$ and $P_{\beta\beta}$, indicating the presence of CH_2, CH and CH_3's, which are part of the constitutional base unit of the PP

homopolymer [5]. Moreover, minor peaks ($S_{\alpha\gamma}$, $S_{\alpha\delta}$, $T_{\delta\delta}$, $T_{\beta\delta}$, $S_{\gamma\delta}$, $S_{\delta\delta}$, $S_{\beta\delta}$, $S_{\beta\beta}$) were also observed in the T180 and T300 samples, indicating the presence of PPE, EPE, PEP, EPP, PEE, EEP and EEE sequences [5]. However, the $S_{\delta\delta}$ peak was more significant in the T300 sample as compared to the T180 sample, indicating the development of EEE sequences as a result of the high ethylene content in this sample. The T180 and T300 samples also exhibited a decrease in intensity of the minor peaks from fraction 5 to 7, indicating a decrease in ethylene-propylene sequences with increasing molar mass fractionation. All the fraction 5s of the vis-broken samples exhibited a new peak around 47 ppm close to the $S_{\alpha\alpha}$ peak, as shown by Figures 5.26 (b), (d) and (f). This new peak was more distinct in the fraction 5 of the vis-broken T0 sample as compared to the other vis-broken samples. Therefore, the 47 ppm peak might be due to the presence of new CH_2's associated with new propylene sequences released during vis-breaking. Furthermore, fractions 5 and 6 of vis-broken T0 exhibited distinct $P_{\beta\gamma}$ and $P_{\gamma\gamma}$ peaks as compared to the neat T0 sample, as shown by Figure 5.23 (a) and (b). This might be due to the development of new CH_3's as a result of vis-breaking.

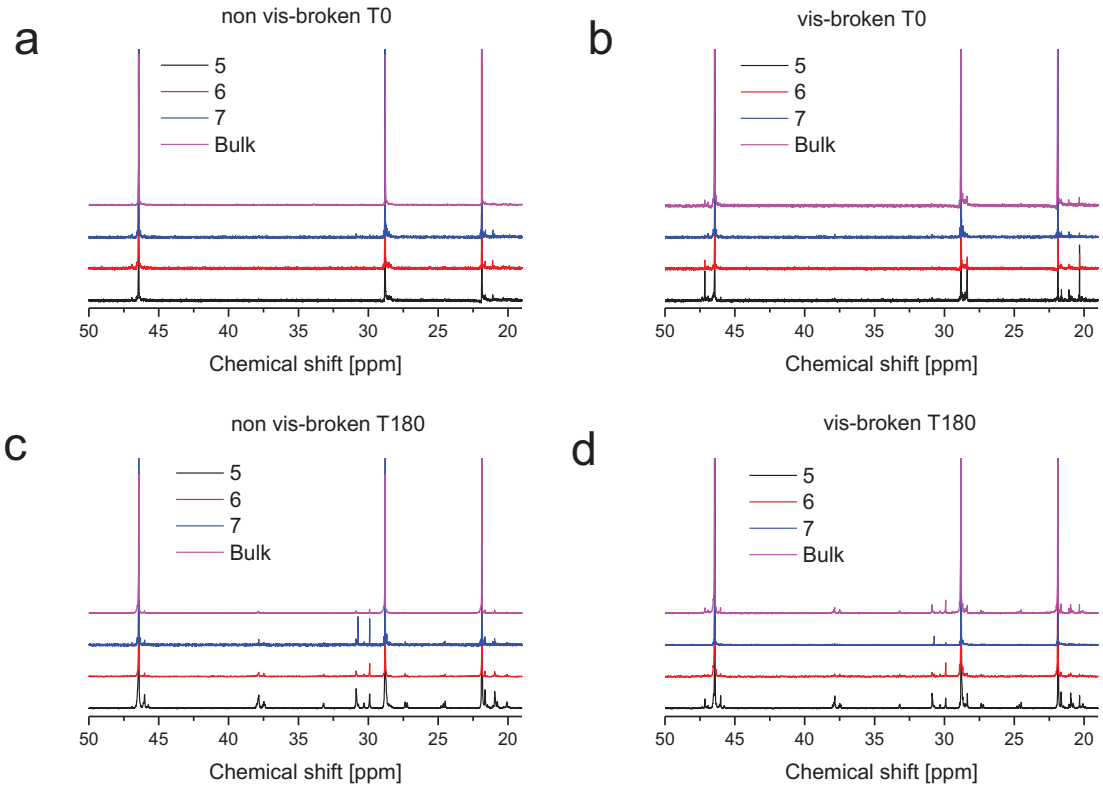

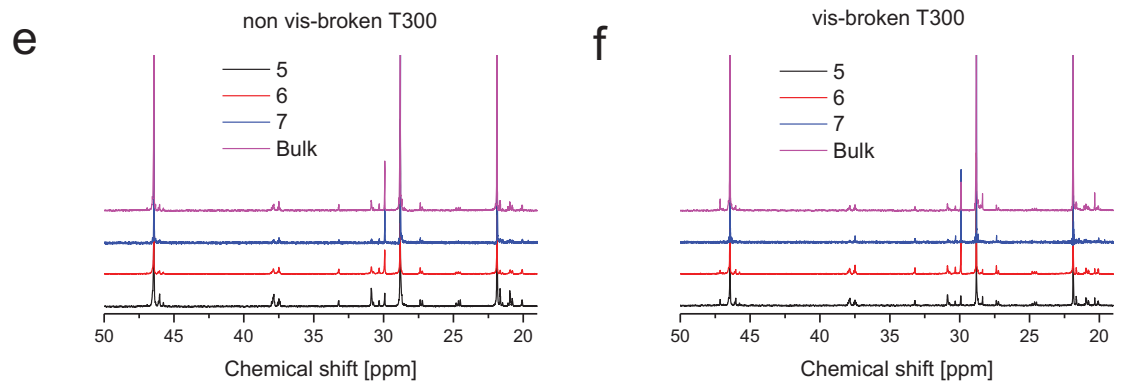

Figure 5.26 ^{13}C-NMR stack plots of fractions 5, 6 and 7 in (a) non vis-broken T0, (b) vis-broken T0, (c) non vis-broken T180, (d) vis-broken T180, (e) non vis-broken T300 and (f) vis-broken T300.

Tables 5.1 – 5.6 show the sequence analysis data of the non vis-broken and vis-broken HEPCs. Some of the fractions were not analysed because there was not enough material to analyse them. T180 and T300 samples exhibited a decrease of PP and PPP sequences at fractions 5 and 6 and increase of these sequences from fraction 7 to 10, as shown by Tables 5.3 – 5.6. The decrease PP and PPP sequences at fractions 5 and 6 were because most of ethylene sequences eluted in these fractions. Samples T180 and T300 also exhibited a decrease of the propylene and an increase of the ethylene content at fractions 5 and 6, confirming the presence of more ethylene sequences in these fractions. Moreover, the EE and EEE sequences were higher in fraction 6 as compared to fraction 5 in all the neat samples. This was an indication that most of the ethylene sequences eluted in fraction 6. Furthermore, a decrease of the EPE, EPP and PEE sequences was observed in the T180 and T300 samples with increasing molar mass fraction, indicating a decrease of ethylene-propylene sequences with increasing molar mass. This correlated well with the decrease of the minor peaks observed in Figure 5.23.

It was interesting to note the appearance of the PE/EP and PPE/EPP sequences in fractions 8 and 9 of the neat T180 sample, as shown by Table 5.3. This could be due to regio- and stereo errors. During polypropylene polymerization using a Ziegler-Natta catalyst, the propylene monomers can undergo either a 1,2- or a 3,1-insertion or both due to the heterogenous nature of the catalyst. Therefore, these 1,2- and 3,1- insertions can be interpreted as PE junctions by NMR.

Tables 5.3 – 5.4 show a decrease in E (mol %) after vis-breaking for the bulk samples. As indicated by preparative molar mass fractionation, the quantities of fractions 5,6 and 7 increase, therefore diluting the ethylene content due the increase in polypropylene content. The vis-breaking causes a change in molar mass which consequently shifts pMMF elution behaviour.

As a result, the determined ethylene content appears less in the degraded fractions which explains what we see in the bulk as well.

Table 5.1 ^{13}C-NMR sequence analysis of non vis-broken T0

	1	2	3	4	5	6	7	8	9	10	Bulk
P (mol %)	100	n.a	n.a	n.a	100	100	100	100	100	100	100
E (mol %)	0	n.a	n.a	n.a	0	0	0	0	0	0	0
PP	100	n.a	n.a	n.a	100	100	100	100	100	100	100
PE / EP	0	n.a	n.a	n.a	0	0	0	0	0	0	0
EE	0	n.a	n.a	n.a	0	0	0	0	0	0	0
PPP	100	n.a	n.a	n.a	100	100	100	100	100	100	100
EPP / PPE	0	n.a	n.a	n.a	0	0	0	0	0	0	0
EPE	0	n.a	n.a	n.a	0	0	0	0	0	0	0
EEE	0	n.a	n.a	n.a	0	0	0	0	0	0	0
EEP / PEE	0	n.a	n.a	n.a	0	0	0	0	0	0	0
PEP	0	n.a	n.a	n.a	0	0	0	0	0	0	0

n.a stands for not analysed

Table 5.2 ^{13}C-NMR sequence analysis of vis-broken T0

	1	2	3	4	5	6	7	8	9	10	Bulk
P (mol %)	100	n.a	n.a	n.a	100	100	100	100	100	100	100
E (mol %)	0	n.a	n.a	n.a	0	0	0	0	0	0	0
PP	100	n.a	n.a	n.a	100	100	100	100	100	100	100
PE / EP	0	n.a	n.a	n.a	0	0	0	0	0	0	0
EE	0	n.a	n.a	n.a	0	0	0	0	0	0	0
PPP	100	n.a	n.a	n.a	100	100	100	100	100	100	100
EPP / PPE	0	n.a	n.a	n.a	0	0	0	0	0	0	0
EPE	0	n.a	n.a	n.a	0	0	0	0	0	0	0
EEE	0	n.a	n.a	n.a	0	0	0	0	0	0	0
EEP / PEE	0	n.a	n.a	n.a	0	0	0	0	0	0	0
PEP	0	n.a	n.a	n.a	0	0	0	0	0	0	0

n.a stands for not analysed

Table 5.3 ^{13}C-NMR sequence analysis of non vis-broken T180

	1	2	3	4	5	6	7	8	9	10	Bulk
P (mol %)	99.6	n.a	n.a	n.a	85.3	82.3	95.7	100	100	100	93.7
E (mol %)	0.4	n.a	n.a	n.a	14.7	17.7	4.3	0	0	0	6.3
PP	92.2	n.a	n.a	n.a	78.6	73.1	93.2	97.6	98.5	100	92
PE / EP	7.4	n.a	n.a	n.a	16.9	16.8	4.2	2.4	1.5	0	5.1
EE	0.5	n.a	n.a	n.a	4.5	10.1	2.6	0	0	0	3
PPP	87.1	n.a	n.a	n.a	72.4	69	90.4	95.2	97.2	100	89.4
EPP / PPE	12.5	n.a	n.a	n.a	12.3	10	5.4	4.8	2.8	0	3.5
EPE	0	n.a	n.a	n.a	0.6	3.3	0	0	0	0	0.9
EEE	0.4	n.a	n.a	n.a	2.4	6.8	2	0	0	0	2
EEP / PEE	0	n.a	n.a	n.a	6.8	6.6	1.3	0	0	0	2.6
PEP	0	n.a	n.a	n.a	5.5	4.3	0.9	0	0	0	1.7

n.a stands for not analysed

Table 5.4 ^{13}C-NMR sequence analysis of vis-broken T180

	1	2	3	4	5	6	7	8	9	10	Bulk
P (mol %)	97.2	n.a	n.a	n.a	88.7	97	99.8	n.a	n.a	n.a	95.1
E (mol %)	2.8	n.a	n.a	n.a	11.3	3	0.2	n.a	n.a	n.a	4.9
PP	88.5	n.a	n.a	n.a	81.3	95.5	98.3	n.a	n.a	n.a	92.4
PE / EP	10.6	n.a	n.a	n.a	14.2	2.4	1.5	n.a	n.a	n.a	5.1
EE	0.9	n.a	n.a	n.a	4.5	2.1	0.2	n.a	n.a	n.a	2.5
PPP	84.4	n.a	n.a	n.a	77.8	94.3	96.9	n.a	n.a	n.a	90.9
EPP / PPE	12.1	n.a	n.a	n.a	8.9	2.7	2.9	n.a	n.a	n.a	3.4
EPE	0.7	n.a	n.a	n.a	2	0	0	n.a	n.a	n.a	0.8
EEE	0.7	n.a	n.a	n.a	2	1.6	0.2	n.a	n.a	n.a	1.5
EEP / PEE	1.1	n.a	n.a	n.a	5.5	0.9	0	n.a	n.a	n.a	2.1
PEP	1.1	n.a	n.a	n.a	3.8	0.5	0	n.a	n.a	n.a	1.3

n.a stands for not analysed

Table 5.5 ^{13}C-NMR sequence analysis of non vis-broken T300

	1	2	3	4	5	6	7	8	9	10	Bulk
P (mol %)	n.a	n.a	n.a	n.a	82.2	70.4	90.4	99.3	100	100	88.7
E (mol %)	n.a	n.a	n.a	n.a	17.8	29.6	9.6	0.7	0	0	11.3
PP	n.a	n.a	n.a	n.a	71.3	53.8	87.9	99.3	100	100	84.6
PE / EP	n.a	n.a	n.a	n.a	20.7	25.8	4	0	0	0	8.5
EE	n.a	n.a	n.a	n.a	8	20.3	8.1	0.7	0	0	7
PPP	n.a	n.a	n.a	n.a	66.4	51.3	87.8	99.3	100	100	82.4
EPP / PPE	n.a	n.a	n.a	n.a	12.8	13.4	1.7	0	0	0	4.8
EPE	n.a	n.a	n.a	n.a	3	5.7	0.9	0	0	0	1.6
EEE	n.a	n.a	n.a	n.a	3.8	13.3	6.6	0.7	0	0	5
EEP / PEE	n.a	n.a	n.a	n.a	8.5	10.5	2.1	0	0	0	4
PEP	n.a	n.a	n.a	n.a	5.5	5.7	0.9	0	0	0	2.4

n.a stands for not analysed

Table 5.6 ^{13}C-NMR sequence analysis of vis-broken T300

	1	2	3	4	5	6	7	8	9	10	Bulk
P (mol %)	100	n.a	n.a	n.a	83.5	75.8	86.1	99.5	100	n.a	91.8
E (mol %)	0	n.a	n.a	n.a	16.5	24.2	13.9	0.5	0	n.a	8.2
PP	100	n.a	n.a	n.a	72.3	61.3	82.1	99.5	100	n.a	86.6
PE / EP	0	n.a	n.a	n.a	20.6	21.4	5.3	0	0	n.a	7.8
EE	0	n.a	n.a	n.a	7.1	17.3	12.5	0.5	0	n.a	5.6
PPP	100	n.a	n.a	n.a	69.1	60.3	82.1	99.5	100	n.a	85.6
EPP / PPE	0	n.a	n.a	n.a	12.1	10.7	2.4	0	0	n.a	4.7
EPE	0	n.a	n.a	n.a	2.3	4.8	1.6	0	0	n.a	1.6
EEE	0	n.a	n.a	n.a	3	11.1	10.7	0.5	0	n.a	3.5
EEP / PEE	0	n.a	n.a	n.a	8.1	8.5	2.4	0	0	n.a	3.1
PEP	0	n.a	n.a	n.a	5.5	4.5	0.8	0	0	n.a	1.6

n.a stands for not analysed

Figures 5.27 (a) and (b) show the average ethylene content of the fractions plotted as a function of fraction number. Fractions with sufficient material were analysed and their monomer values as well as diad and triad sequences were reported in Tables 5.1 – 5.6.

For sample T180 (see Figure 5.27 a), the ethylene content was highest in fraction 6 and then decreased afterwards. This correlated well with what was observed in HT-HPLC where the presence of long ethylene sequences was observed at late eluting fractions. Fractions 8-10 did not show any ethylene sequences as determined by ^{13}C-NMR. After vis-breaking, the quantities of fractions 5, 6 and 7 were observed to increase, hence diluting the ethylene content as a result of the increase in propylene content. The vis-breaking caused a change in molar mass which consequently shifted the SGEF elution behaviour. As a result, the determined ethylene content appeared to be less in the degraded fractions. Vis-broken T180 showed highest ethylene content and ethylene sequences at fraction 5. This was an indication of the release of ethylene sequences that started to elute at fraction 5.

When sample T300 was vis-broken, significant changes in fraction quantities were only observed between fractions 8-10 where iPP is the main component, see Figures 5.10 (e) and (f). Fractions 5 – 7 did not change significantly in their quantities most probably due to the stabilising effect of the longer ethylene sequences which were more immune to peroxide attack. From Figure 5.27 (b), it was evident that after vis-breaking the ethylene copolymer was spread to fraction 7 in the vis-broken T300 sample. From the ^{13}C-NMR and HT-HPLC results, it appeared as though the peroxide action is targeting propylene rich segments leading to the isolation of chains with long and short ethylene sequences.

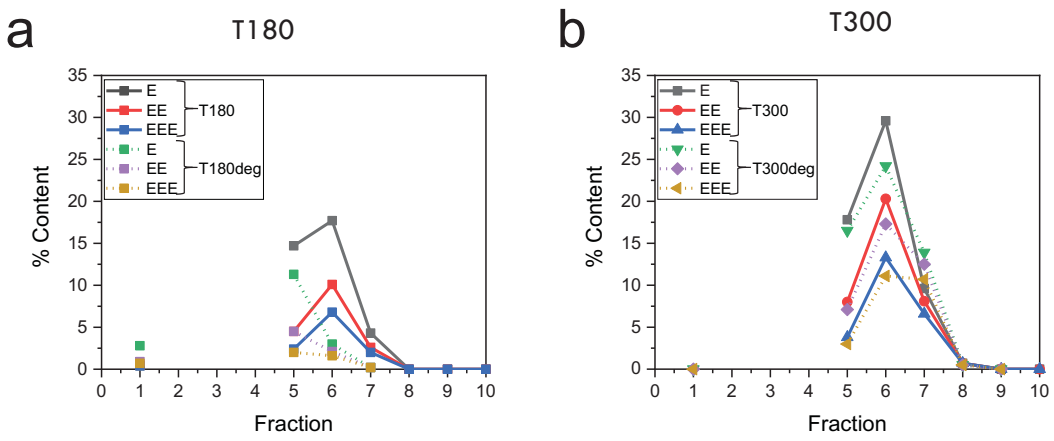

Figure 5.27 Plot of determined percentage ethylene content for the non vis-broken and vis-broken (a) T180 and (b) T300 SGEF fractions.

5.4 Conclusions

Heterophasic ethylene-propylene copolymers were successfully fractionated according to crystallizability using p-TREF and molar mass using SGEF. Three copolymers with ethylene contents of 0, 5.2 and 10.8 mol % were treated with 0.5 wt. % peroxide before comparing the changes in molecular structure.

SGEF was implemented for reducing the complexity of the molar mass dimension in the HEPCs. Ten fractions were targeted for the non vis-broken and vis-broken samples. Molar mass analysis using HT-SEC revealed that the fractions containing more ethylene co-monomer or ethylene-propylene copolymer have broader MMDs while the fractions iPP as the major component had narrow MMDs. Therefore, this was proof that SGEF is less desirable as a preparative fractionation tool for mixtures of homopolymers and copolymers since it was less effective at discriminating the polymer chains into narrow fractions. The different chemical compositions of the chains may affect solubility in solvent/non solvent mixtures giving rise to fractions with complex molar mass contributions. A shift in material towards low fractions was observed after vis-breaking as would be expected. Again, the analyses of the fractions with high ethylene contents revealed the stability of the ethylene rich copolymer against peroxide attack.

5.5 References

1. Anantawaraskul, S., Soares, J. B. P, Wood-Adams, P. M., *Fractionation of semicrystalline polymers by Crystallization Analysis Fractionationand Temperature Rising Elution Fractionation*, in *Polymer Analysis Polymer Theory*. 2005, Springer. p. 1-54.

2. Xue, Y., Bo, S., Ji, X., *Solvent gradient fractionation and chain microstructure of complex branched polyethylene resin.* Journal of Polymer Research, 2016. **23**(7): p. 131.

3. Zacur, R., Goizueta, G., Capiati, N., *Dispersed phase morphology of impact PP copolymers. Effects of blend composition as determined by TREF*. Polymer Engineering & Science, 2000. **40**(8): p. 1921-1930.

4. Zacur, R., Goizueta, G., Capiati, N., *Polypropylene reactor blends: Composition evaluation by analytical TREF*. Polymer Engineering & Science, 1999. **39**(5): p. 921-929.

5. Swart, M., *The effect of controlled degradation with an organic peroxide on the molecular characteristics and properties of heterophasic propylene-ethylene copolymers (HECO)*. 2013, PhD Thesis, University of Stellenbosch.

6. Fan, Z.-q., Zhang, Y.-t., Xu, J.-t., Wang, H.-t., Feng, L.-t., *Structure and properties of polypropylene/poly (ethylene-co-propylene) in-situ blends synthesized by spherical Ziegler–Natta catalyst.* Polymer, 2001. **42**(13): p. 5559-5566.

7. Xue, Y., Fan, Y., Bo, S., Ji, X., *Characterization of the microstructure of impact polypropylene alloys by preparative temperature rising elution fractionation.* European Polymer Journal, 2011. **47**(8): p. 1646-1653.

8. Cheruthazhekatt, S., Pijpers, T. F. J., Harding, G. W., Mathot, V. B. F., Pasch, H., *Multidimensional analysis of the complex composition of impact polypropylene copolymers: Combination of TREF, SEC-FTIR-HPer DSC, and high temperature 2D-LC.* Macromolecules, 2012. **45**(4): p. 2025-2034.

9. Carman, C., Wilkes, C., *Monomer sequence distribution in ethylene propylene elastomers. I. Measurement by carbon-13 nuclear magnetic resonance spectroscopy.* Rubber Chemistry and Technology, 1971. **44**(3): p. 781-804.

10. Ray, G. J., Johnson, P. E., Knox, J. R., *Carbon-13 nuclear magnetic resonance determination of monomer composition and sequence distribution in ethylene-propylene copolymers prepared with a stereoregular catalyst system.* Macromolecules, 1977. **10**(4): p. 773-778.

Chapter 6

Variable temperature and room temperature solid-state ^{13}C-NMR analyses

This chapter gives a detailed discussion on the development of a new methodology which uses variable temperature solid-state C-NMR to investigate the reaction of the peroxide with the HEPCs *in situ.*

6.1 Introduction

In this section of the study, the use of *in-situ* solid state ^{13}C NMR to determine the effect of peroxide treatment on the chemical structure of ethylene-propylene copolymers is discussed. The copolymers contained differing quantities of ethylene (0, 5.2 and 10.8 mol %), with the 0 mol % ethylene content corresponding to pure isotactic PP.

The results discussed in Chapters 4 and 5 were based on fractionation by either crystallizability or molar mass. It was, therefore, necessary to correlate these results with changes observed in the solid state. In order to achieve this, for the first time variable temperature solid state NMR was used to monitor vis-breaking *in-situ* and directly identify the affected components and morphological changes as a result thereof.

Solid-state ^{13}C NMR is a technique that enables the study of the actual chain conformation instead of the averaged microstructure obtained by solution state NMR. Solid state NMR can therefore be used to study polymers in the solid state and under conditions that are similar to their application environment [1]. Furthermore, with solid state NMR, one is able to selectively probe the different phases of HEPCs (amorphous, crystalline, ordered amorphous) based on molecular dynamics, for example cross-polarization dynamics or relaxation behaviour [2]. Variable temperature solid state NMR is sensitive to both rigid and more mobile components. Variable temperature solid state NMR has been proven to be useful in studying the temperature dependent development of segmental mobility in HEPCs with increasing ethylene content [3]. It has previously been shown that the incorporation of ethylene attenuates the crystallinity of bulk HEPCs [3, 4]. This ethylene incorporation also generates a range of molecules with different defect concentrations and distributions, which melt at different temperatures [3]. Vis-breaking has been reported to attenuate the crystallinity of bulk HEPCs, resulting in chain microstructures with different chemical composition distributions and chain lengths, which melt at different temperatures [5, 6]. The variable temperature solid state NMR experiments in this study were thus focused on the *in-situ* degradation of the bulk HEPCs using solid-state NMR in order to monitor the effect of vis-breaking in the solid state.

It has been reported that polymorphism, between α – and γ – allomorphs can co-exist in ethylene-propylene copolymers [7]. This tends to influence the “up” and “down” orientation of helices in the unit cell of the crystal. The chain packing in the neat HEPCs used in this study was reported to be influenced by the α – allomorph alone [4]. Therefore, XRD experiments in this study were used to investigate the crystal structure of the HEPCs before and after vis-

breaking. This crystal structure will help in identifying the allomorphs present in the HEPCs before and after vis-breaking.

6.2 Room temperature solid-state ^{13}C-NMR

The solid state NMR results in this section are based on the bulk samples vis-broken in the MFI instrument. The samples were vis-broken in the MFI instrument at 190 °C for 30 minutes using 0.5 wt. % Trigonox®301 peroxide. Furthermore, the fractions that are reported in this section were obtained before and after vis-breaking of the HEPCs at 190 °C for 30 minutes using 0.5 wt. % Trigonox®301 peroxide in the MFI instrument.

6.2.1 Solid state NMR of bulk samples

Figures 6.1 (a) and (b) compares the CPMAS solid-state NMR spectra at room temperature of the bulk HEPCs taken before and after vis-breaking at 0.5 wt. % peroxide concentration for 30 minutes in an MFI instrument. The CPMAS solid-state NMR spectra of both the non vis-broken and vis-broken HEPCs exhibited three distinct peaks representing the CH_2, CH and CH_3 groups of PP sequences. Since the CPMAS experiment in the solid state NMR is sensitive only to the rigid domains of a polymer sample, the three dinstict peaks were representative of PP rigid domains. Furthermore, two more peaks were also observed around 30 and 32 ppm in both the non vis-broken and vis-broken solid-state NMR profiles of T300 samples. According to literature, these peaks are indicative of the presence of ethylene sequences in crystalline and amorphous environments. For the CPMAS experiments of HEPCs, the sharpness of peaks in the spectra can be correlated to ordered domains in the polymer. When the non vis-broken and vis-broken solid-state NMR profiles were compared, a decrease of the three distinct PP peaks was observed in the vis-broken HEPCs, as shown by Figure 6.1 (b). This was indicative of the presence of disordered domains within the PP sequences of the polymer caused by chain scission.

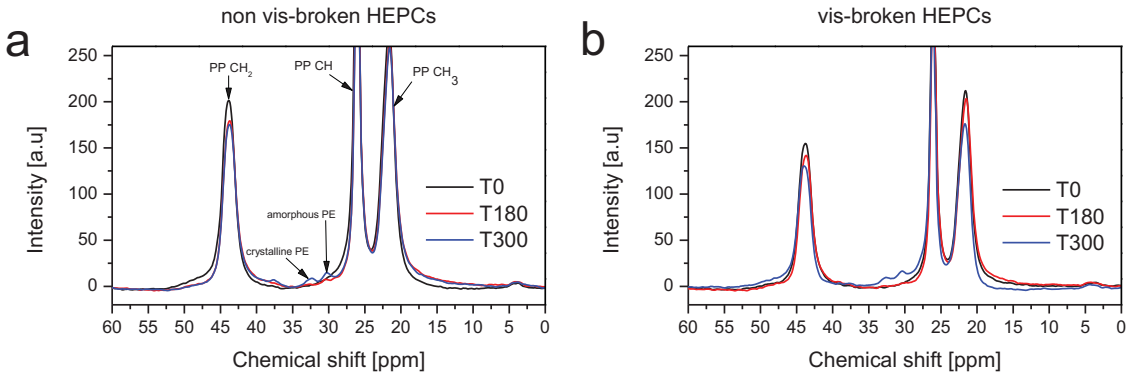

Figure 6.1 Solid-state ^{13}C NMR (CPMAS) profiles of (a) non vis-broken and (b) vis-broken HEPCs

6.2.2 Solid state NMR of p-TREF fractions

Figure 6.2 (a) – (f) shows solid-state NMR spectra at room temperature of the 60, 80, 90 and 110 °C p-TREF obtained before and after the vis-breaking of HEPCs. p-TREF fractions of the non vis-broken HEPCs (Figure 6.2 a, c and e) all showed an increase of the amorphous and crystalline PE peaks (~ 30 and 32 ppm) with increasing ethylene content except the 110 °C fraction, which consist mainly of isotactic PP. The crystalline and amorphous PE peaks were more pronounced in the 60 °C fractions of the non vis-broken T180 and T300 samples. The crystalline PE peak in the 60 °C of the non vis-broken T300 sample was more pronounced than the amorphous PE peak. This crystalline PE peak was also observed in the 90 °C fraction of the non vi-broken T300 sample (Figure 6.2 e). However, this peak was not observed in the 90 °C fraction of the non vis-broken T180 sample (Figure 6.2 c). Therefore, no crystalline ethylene content was present. Furthermore, the 60 °C fractions of the non vis-broken T180 and T300 samples exhibited a peak at ~ 39 ppm (Figure 6.2 c and e). This peak was more distinct in the non vis-broken T300 sample and it appeared to increase with increasing ethylene content.

Figures 6.2 (b), (d) and (f) show solid state NMR spectra at room temperature of the p-TREF fractions obtained after vis-breaking the HEPCs. Interestingly, there was an appearance of the ~ 39 ppm peak in the 60 °C fraction of the vis-broken T0 sample (Figure 6.2 b). As reported before, non vis-broken T0 does not contain any ethylene sequences. Therefore, this peak was indicative a new CH_2 peak in a different chemical or morphological environment and thus indicating the presence of new rigid or ordered amorphous polymeric sequences induced by the vis-breaking. The 30 and 32 ppm peaks appear relatively less in the vis-broken sample due to the relative increase of the PP peaks. Furthermore, a new peak appeared at ~ 47 ppm in the 60 °C fractions of all vis-broken samples (Figures 6.2 b and f). The ~ 47 ppm peak appeared

to be more distinct in the 60 °C of the vis-broken T0 sample. This ~ 47 ppm peak was assigned to the CH_2 groups of amorphous PP sequences by Agarwal *et al*.[2].

The results show that the action of the peroxide introduced new CH_2 peaks around 47 ppm which indicated the presence of new polymer sequences.

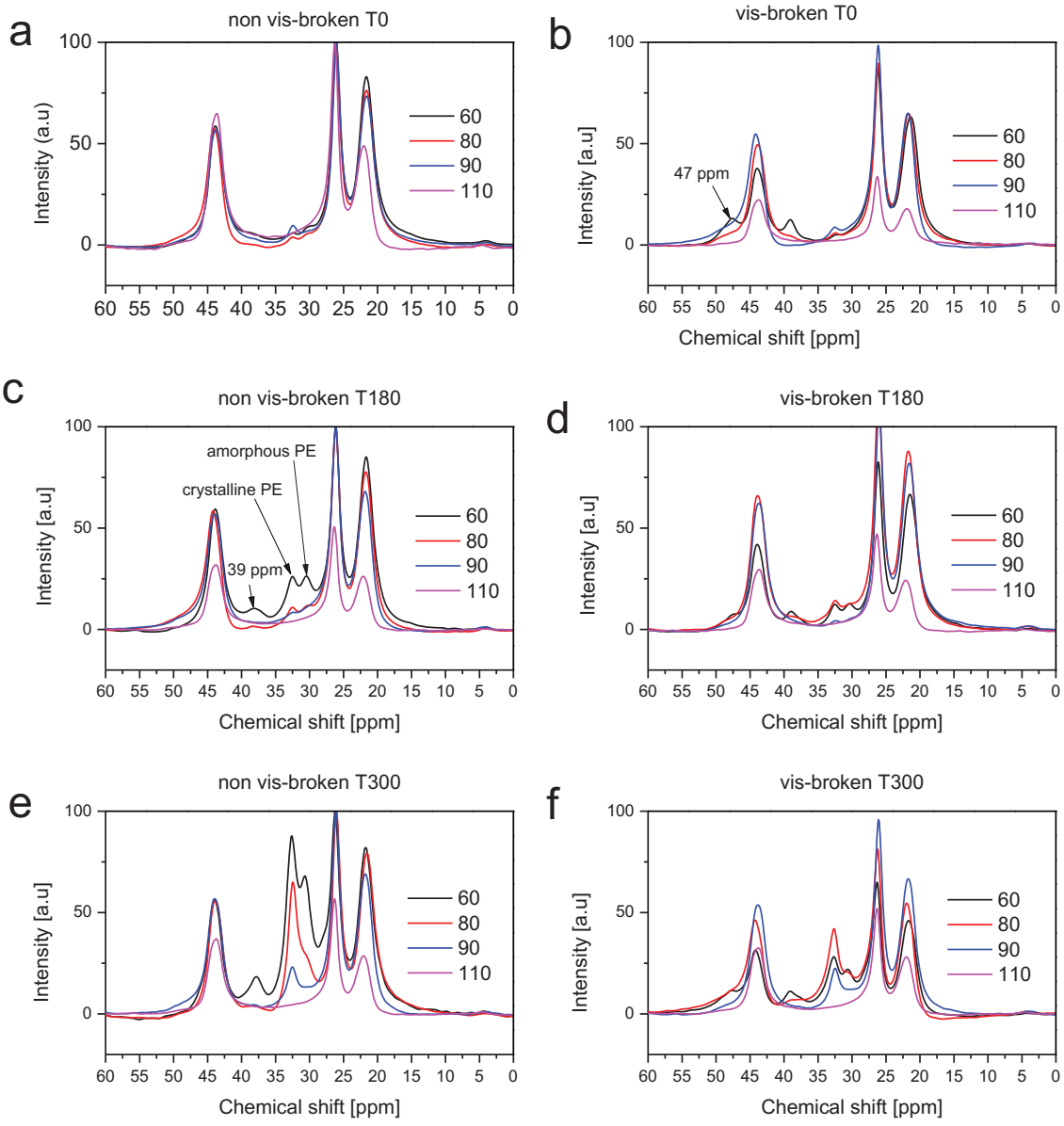

Figure 6.2 Solid-state ^{13}C NMR (CPMAS) profiles of the 60, 80, 90 and 110 °C p-TREF fractions obtained from (a) non vis-broken T0, (b) vis-broken T0, (c) non vis-broken T180, (d) vis-broken T180, (e) non vis-broken T300 and (f) vis-broken T300 HEPCs

6.2.3 Powder X-ray diffraction (XRD)

Powder XRD was used to investigate the crystal structures of the 60 °C fractions of the non vis-broken and vis-broken HEPCs.

Since most of the differences in solid state NMR spectra were observed in the 60 °C fraction, powder XRD was performed to study the crystal structure in the 60 °C fractions. Figure 6.3 compares powder XRD patterns of the 60 °C fractions in the non vis-broken and vis-broken samples. There was an increase of the amorphous halo with increasing ethylene content. The increase might be due to an increase in amorphous material with increasing the ethylene content. Furthermore, an increase of the peak at 2θ = 21.6 ° was observed with increasing ethylene content, indicating that the development of this peak was influenced by the ethylene content.

After vis-breaking, new peaks (indicated in red) were observed at 2θ = 12.2 ° and 2θ = 18.6 ° (Figure 6.4 b). The 2θ= 12.2 ° peak was previously reported to be due to syndiotactic PP [9]. The 2θ = 18.6 ° peak is characteristic of the α – allomorph. Furthermore, a decrease of the 2θ = 21.6 °C was also observed in the vis-broken samples, confirming that the crystal structure of the samples were altered by vis-breaking.

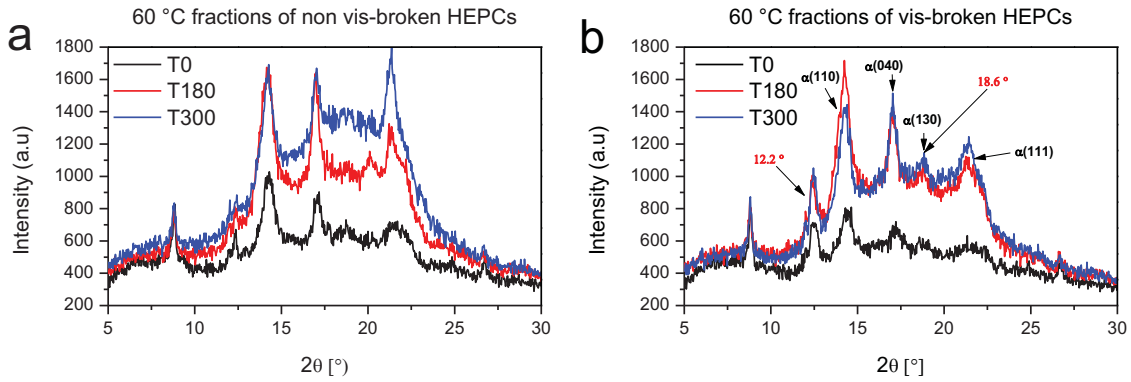

Figure 6.3 Powder X-Ray diffraction patterns of the 60 °C fractions in the (a) non vis-broken and (b) vis-broken HEPCs. The new peaks are indicated in red.

6.3 Variable temperature solid state ^{13}C-NMR

All the vis-broken bulk HEPCs reported in this section were heated together with 0.5 wt. % of Trigonox®301 peroxide in the NMR instrument. The non vis-broken HEPCs were also heated inside the NMR instrument under the same conditions as the vis-broken samples except that they were not peroxide treated.

6.3.1 *In situ* solid-state ^{13}C-NMR experiments

In order to monitor the structural changes induced by vis-breaking in the solid state, *in situ* experiments were done at different temperatures in the solid state NMR instrument. During the *in situ* experiments, the polymer was treated with 0.5 wt % peroxide and the treated polymer was heated in the instrument while spectra were taken at each predetermined temperature.

Figures 6.4 (a) – (f) below shows CP/MAS spectra of the treated and untreated copolymers taken at different temperatures. It is important to note that the HEPCs were heated with the peroxide in the NMR instrument. Additional methylene and methine carbon signals were observed with increasing temperature, particularly those at 46.5 – 47 ppm and at around 28.5 ppm (indicated by the arrows in Figure 4.6). The appearance of the additional methylene and methine carbon peaks was an indication of increased mobility caused by the presence of more disordered domains at higher temperatures. Furthermore, these resonances were assigned to methylene and methine carbons in amorphous PP by Agarwal *et al*. [2], and were also observed by Botha *et al*. [3, 8] who noted that these peaks appeared under heating of iPP homopolymer as well as in bulk and fractionatated HEPCs with notable amounts of ethylene incorporated. The increased localised mobility with increasing temperature can be ascribed to small amounts of amorphous PP that start being mobile as the temperature increases [3]. This was proved by Botha *et al*. by the use dipolar dephasing experiments which selectively robed the amorphous, mobile regions of the HEPCs (at room temperature)[3]. A decrease of the three main PP peaks was also observed with increasing temperature. This decrease was an indication of increasing mobility within the ordered PP domains. In the T300 sample, the PP peaks were almost disappearing at all temperatures, especially at 150 °C. This was due to the segmental mobility caused by both temperature and ethylene incorporation [3].

After vis-breaking, an increase in segmental mobility was observed in the T0 sample, especially at 120 and 150 °C. This is due to the fact that T0 contains only isotactic PP. The increased segmental mobility observed after vis-breaking was due to the peroxide radicals inducing β – scission of the PP sequences.

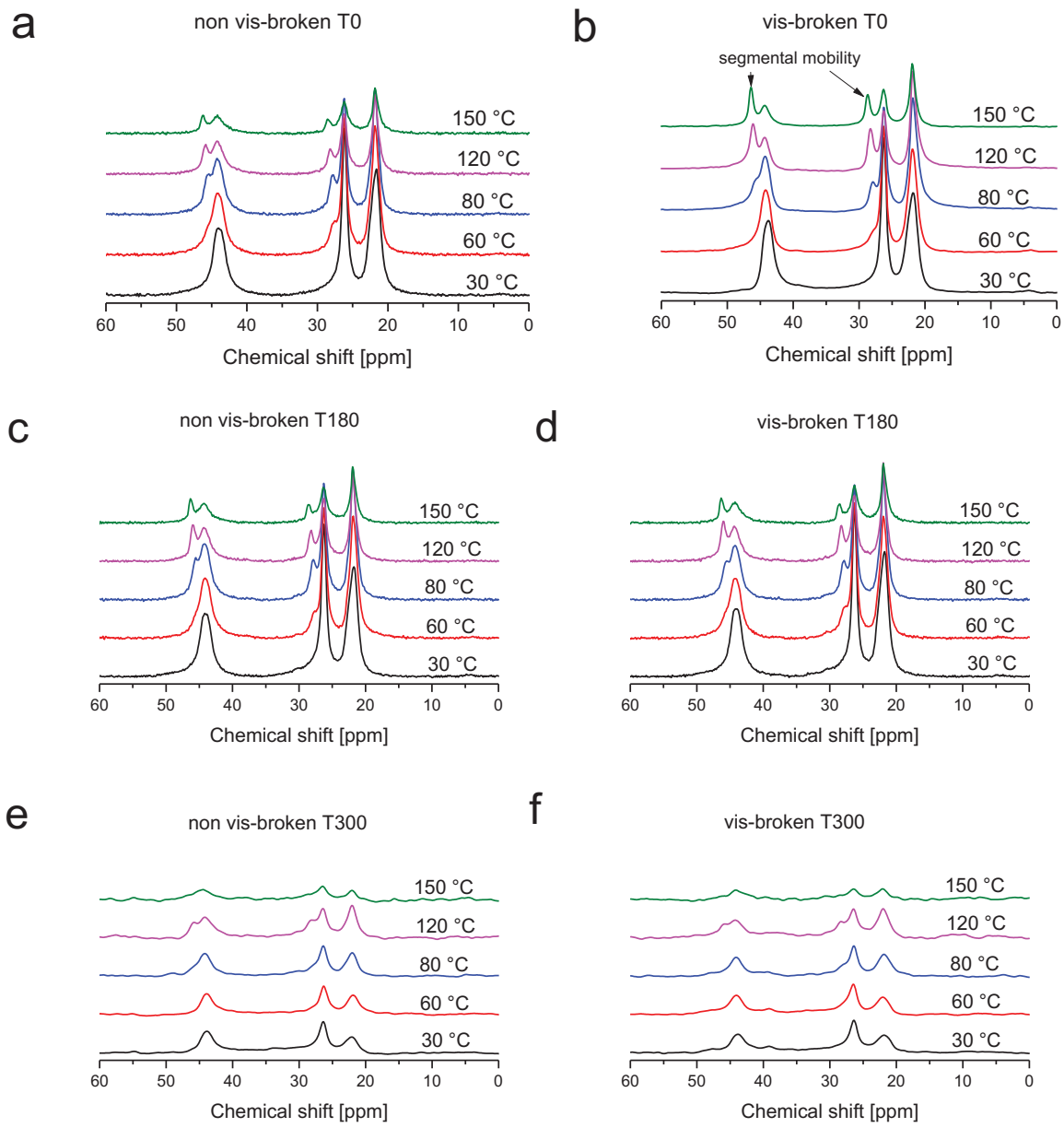

Figure 6.4 Variable temperature solid-state ^{13}C NMR (CP/MAS) profiles of (a) non vis-broken T0, (b) vis-broken T0, (c) non vis-broken T180, (d) vis-broken T180, (e) non vis-broken T300 and (f) vis-broken T300 taken at 30, 60, 80, 120 and 150 °C. These samples were heated with the peroxide in situ.

Figures 6.5 (a) – (f) displays the CP/MAS spectra recorded at room temperature with increasing annealing times at 150 °C for both untreated and peroxide treated HEPCs. It should be noted that upon reaching 150 °C (i.e 0 min spectrum) the CPMAS spectra showed a new CH_2 peak around 47 ppm indicating the presence of disordered domains. Figure 6.5 showed minimal differences of the CP/MAS spectra after vis-breaking. The T0 and T300 samples showed a higher intensity of the 47 ppm peak than the T180 sample indicating the presence of more disordered domains in the T0 and T300 samples than in the T180 sample.

Figures 6.5 (c) and (d) shows the CP/MAS spectra of the untreated and treated T180 samples. It was apparent that the spectra of the T180 sample were different from that of the T0 and T300 samples. For the T180 sample, the disordered contribution appeared to dominate even at 0 min annealing time for both untreated and peroxide treated samples. Furthermore, the presence of the ethylene domains at ~ 30 – 32 ppm could not be observed in the T300 sample as the melting temperature would be below that of the annealing temperature. The study of the effect of the *in situ* peroxide degradation on the ethylene domains was therefore inconclusive.

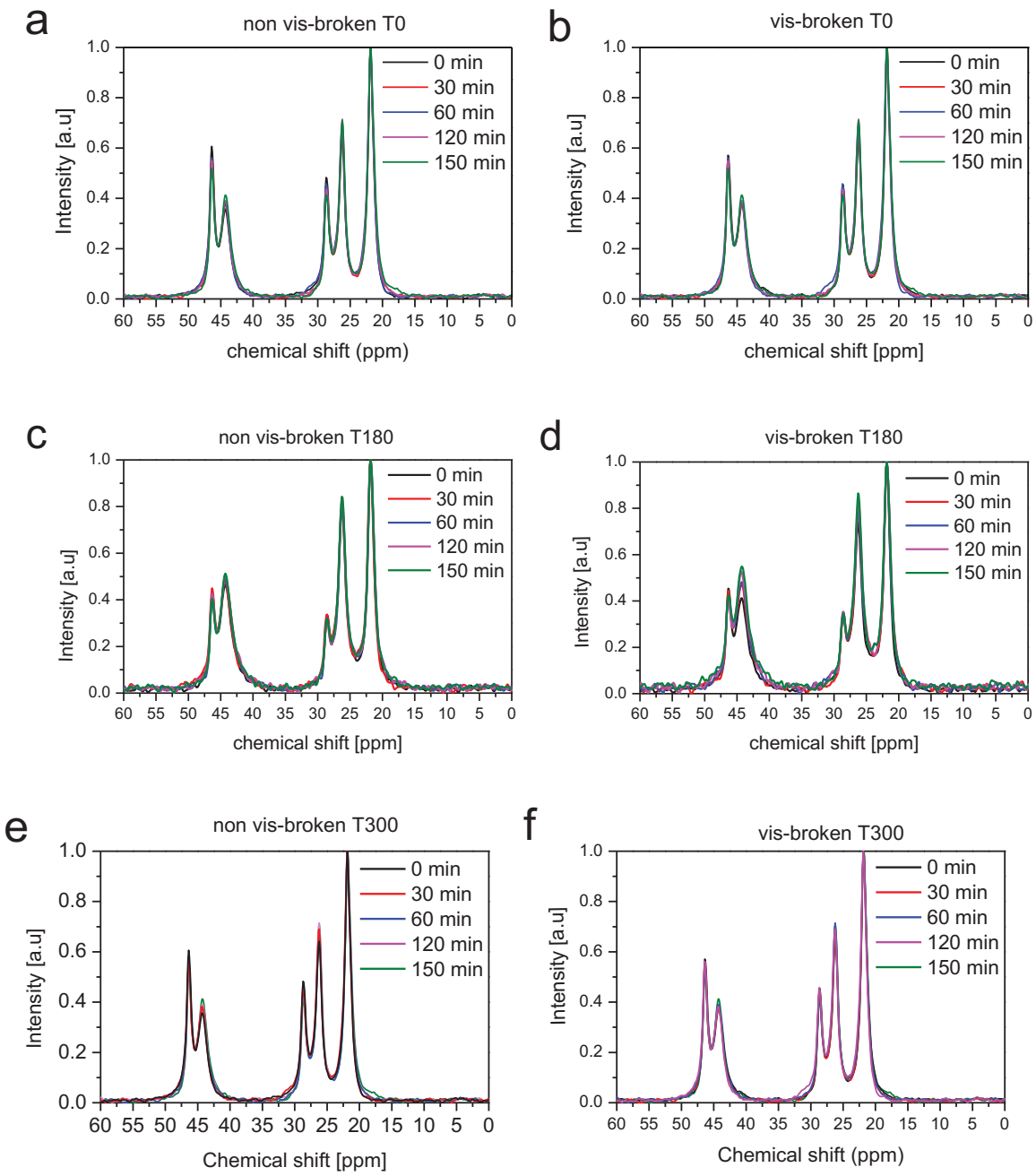

Figure 6.5 Solid state ^{13}C NMR (CP/MAS) profiles of (a) non vis-broken T0, (b) vis-broken T0, (c) non vis-broken T180, (d) vis-broken T180, (e) non vis-broken T300 and (f) vis-broken T300 during in situ vis-breaking. The treated and untreated polymers were heated to 150 °C and allowed to stay there for 150 mins before cooling them down. The spectra was recorded at room temperature after each annealing time.

Figure 6.6 (a) – (f) shows CP/MAS spectra of the HEPCs at room temperature before and after the *in situ* peroxide treatment at 150 °C for 150 minutes. The T180 sample displayed significant decreases of both the CH_2 and CH peaks, indicating the presence of disordered domains after vis-breaking. According to solution state NMR, the T180 sample contained shorter chain sequences while the T300 sample contained more of the long chain polyethylene-type sequences. While most polyolefins are vulnerable to oxidative degradation, polyethylene is less likely to undergo β scission than PP due to the instability of the primary radical formed when cleaving linear hydrocarbons [10]. It appeared that these polyethylene-type sequences yielded a similar resistance to degradation as would normally be seen for polyethylenes. When these ethylene sequences are not of sufficient length they simply act as a disruption for crystalline packing in the polypropylene, increasing the quantity of amorphous zones and making the PP more susceptible than usual to oxidative degradation. The room temperature CP/MAS spectra of the T0 sample before and after *in situ* vis-breaking displayed minimal chemical changes (Figures 6.7 a & b). This was in agreement with the observations from the solution state NMR spectra. Furthermore, a slight broadening of the peaks at the baseline could be observed which was most likely due to a slight increase in amorphous regions after peroxide treatment. While chain scission had occurred the molecular weight of the resultant chains remained high enough to not observe any end groups by NMR techniques.

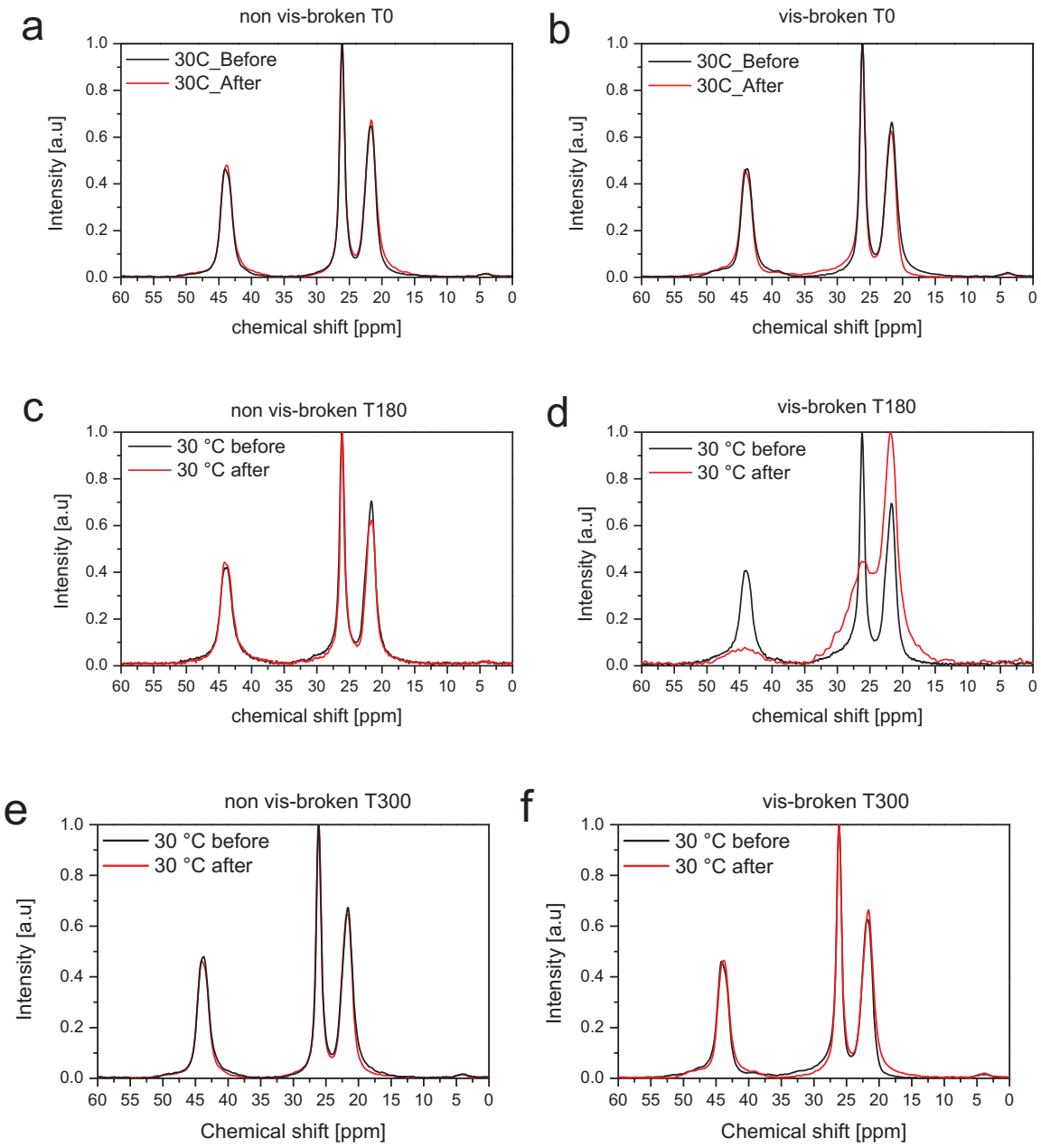

Figure 6.6 Solid-state ^{13}C NMR (CP/MAS) profiles of (a) non vis-broken T0, (b) vis-broken T0, (c) non vis-broken T180, (d) vis-broken T180, (e) non vis-broken T300 and (f) vis-broken T300 taken at 30 °C before and after in situ vis-breaking at 150 °C for 150 minutes.

The effect of *in situ* vis-breaking on the ethylene domains between ~ 30 – 32 ppm was not visible in the bulk samples. However, this effect was illustrated by Figures 6.8 (a) and (b) below. Here, the T180 and T300 60 °C fractions exhibited a distinct phase separation between the crystalline and amorphous ethylene domains after the *in situ* vis-breaking as shown by the peaks between ~ 30 – 32 ppm. This was indicative of the phase separation between chains containing long and short ethylene sequences. A narrowing of the PP peaks was also observed which was most likely due to the decrease in molar mass caused by the vis-breaking.

Furthermore, a decrease of the peaks was also observed which was indicative of increased mobility as a result of peroxide treatment.

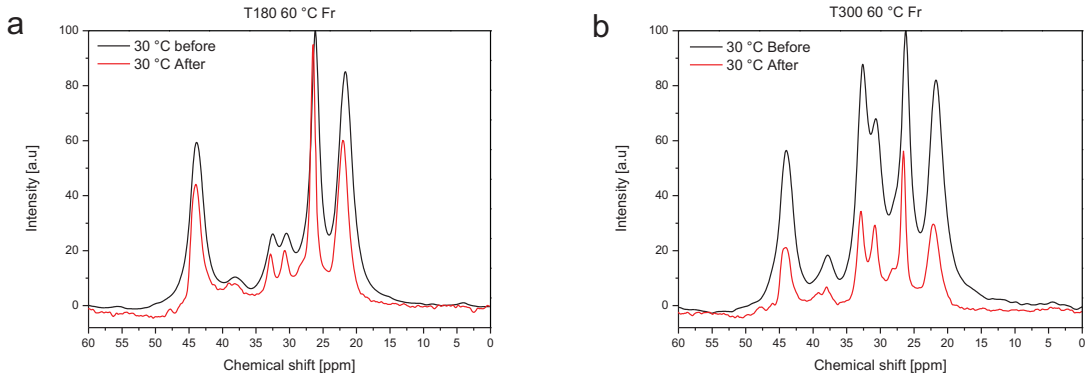

Figure 6.7 CP/MAS spectra of (a) T180 and (b) T300 60 °C fractions taken before and after in situ vis-breaking.

6.4 Conclusions

For the first time *in situ* NMR vis-breaking was used to monitor in the solid state structural changes induced by the vis-breaking of HEPCs. The T180 sample with lower ethylene content appeared to be more greatly affected by the peroxide than the T300 sample which contained greater quantities of ethylene. The difference in the responses of the two copolymers lies in the manner in which the ethylene sequences are distributed within them. For sample T180 the ethylene was incorporated as short ethylene sequences while for sample T300 the greater ethylene incorporation led to the formation of longer chain ethylene sequences which resemble the behaviour of polyethylenes. T0 displayed little to no change in chemical structure. While T0 still displayed changes in the molecular mass distributions, the focus of this section was on changes in chemical composition and susceptibility to degradation.

When significant amounts of ethylene were added to the structure, as in the case of the T300 sample, the long chain sequences lend protection by the enhanced resistance of the ethylene to radical degradation as compared to polypropylene. In contrast, in the case of the T180 sample the junction joints, or points where changes in ethylene-propylene sequences occur, played an important role. The T180 sample did not contain enough ethylene to grant the protection of long chain ethylene sequences but increased number of E-P transition points enhanced the susceptibility to a greater extent than was observed in isotactic PP.

The peroxide increased the phase separation between chains containing long and short ethylene sequences. This was most likely as a result of the peroxide attacking PP rich sequences and thus causing a release of sequences with long and short ethylene sequences.

6.5 References

1. Zhu, H., Graf, R. H., Guangjin, Z., Ying, W., Dujin, S., Hans W., *Solid-State NMR characterization of the multiphase structure of polypropylene in-reactor alloy.* Macromolecular Chemistry and Physics, 2010. **211**(10): p. 1157-1166.

2. Agarwal, V., van Erp, T. B.,Balzano, L., Gahleitner, M., Parkinson, Matthew, G., Leon, E., Litvinov, V., Kentgens, A. P. M., *The chemical structure of the amorphous phase of propylene–ethylene random copolymers in relation to their stress–strain properties.* Polymer, 2014. **55**(3): p. 896-905.

3. Botha Linda, S.P., Duveskog, H., Van Reenen, A. J., *The use of solid-state NMR to investigate the development of segmental mobility in commercial heterophasic ethylene propylene copolymers (HEPCs).* Macromolecular Reaction Engineering, 2015. **9**(4): p. 313-324.

4. Botha, L., *The effect of in-process ethylene incorporation on the evolution of particle morphology and molecular characteristics of commercial heterophasic ethylene propylene copolymers (HEPCs)*. 2014, PhD Thesis. Stellenbosch University.

5. Swart, M., Van Reenen, A. J, *The effect of controlled degradation on the molecular characteristics of heterophasic ethylene–propylene copolymers.* Journal of Applied Polymer Science, 2015. **132**(14).

6. Swart, M., *The effect of controlled degradation with an organic peroxide on the molecular characteristics and properties of heterophasic propylene-ethylene copolymers (HECO)*. 2013, PhD Thesis, University of Stellenbosch.

7. Guidetti, G., Busi, P., Giulianelli, I., Zanenetti, R., *Structure-properties relationships in some random copolymers of propylene.* European Polymer Journal, 1983. **19**(9): p. 757-759.

8. Botha, L., Sinha, P., Joubert, S., Duveskog, H., van Reenen, A. J., *Solution and solid-state NMR characterization of heterophasic propylene–ethylene copolymers (HEPC) with increasing ethylene content.* European Polymer Journal, 2014. **59**: p. 94-104.

9. Yave, W., Quijada, R., Ulbricht, M., Benavente, R., *Syndiotactic polypropylene as potential material for the preparation of porous membranes via thermally induced phase separation (TIPS) process.* Polymer, 2005. **46**(25): p. 11582-11590.

10. Hogt, A., Meijer, J., Jelenič, J., *Modification of polypropylene by organic peroxides*, in *Reactive modifiers for polymers*. 1997, Springer. p. 84-132.

Chapter 7

Conclusion

This chapter highlights and summarizes the main findings of this study. It also discusses possibilities for future work.

7.1 Synopsis, conclusions and recommendations for future work

7.2 Introduction

In 2013, Morne Swart conducted a PhD study on the effect of controlled rheology on the molecular characteristics of HEPCs. During this study, it was revealed that the use of chemically similar yet structurally different organic peroxides (Trigonox®101 and Trigonox®301) had different effects on the molecular make-up and properties of HEPCs [1]. In his recommendations, Dr. Swart stated that more work needs to be done in order to understand why specific organic peroxides influence/interact differently with the various phases of HEPCs and how the characteristics of the peroxides can be utilized to obtain a HEPC with optimal or desired properties. In response to Dr. Swart's recommendation, an MSc study was conducted by Sifiso Magagula. During the MSc study, it was revealed that the different organic peroxides prefer to associate with specific parts of the HEPCs more than others, hence the differences observed in the final macroscopic properties [2].

The studies mentioned above were focused on the effect of the type of peroxide on the molecular characteristics of the HEPCs. However, the current study is focused on the effect of changing chemical composition distribution on the action of the organic peroxides. During this study, for the first time, variable temperature solid state NMR was used to investigate the reaction of the organic peroxides with the HEPCs *in situ*.

7.3 Analysis of bulk samples

Analyses of the bulk samples revealed a decrease in molar mass and peak melting temperatures with increasing vis-breaking step. The most significant decrease was observed at 0.5 wt. %. The concentration of the peroxy radicals ($RO^{\cdot}$) increases with increasing with the vis-breaking step. The increase in the peroxy radicals therefore results in more chains being broken down during the vis-breaking. Furthermore, an increasing decrease in molar mass was observed with increasing ethylene content. This was due to the copolymer phase facilitating the mixing/dispersion of the peroxide resulting in a more efficient vis-breaking process. Tan δ curves revealed a phase separation between the ethylene-propylene copolymer phase and the PP homopolymer phase after vis-breaking. This was due to the peroxide "attacking" particular parts of the HEPCs resulting in the cleaving off of EP copolymers and PP homopolymer sequences.

In order to gain a comprehensive understanding on the molecular composition of the non vis-broken and vis-broken HEPCs, the HEPCs were fractionated according to crystallizability

using p-TREF and molar mass using SGEF. Three HEPCs were successfully fractionated according to p-TREF and SGEF. The three copolymers with ethylene contents 0, 5.2 and 10.8 mol % (with the least ethylene content similar to iPP) were treated with 0.5 wt. % peroxide before comparing the changes in molecular structure.

7.4 Analysis of p-TREF fractions

The non vis-broken and vis-broken HEPCs were successfully fractionated into eight fractions (30, 60, 80, 90, 100, 110, 120 and 130 °C). About 65 wt. % of the samples eluted at 110 °C. Therefore the 110 °C fraction constituted the bulk of the samples. Furthermore, p-TREF was not able to give us comprehensive information on the structural changes induced by the vis-breaking. However, the HPLC results revealed what appeared to be a separation between the ethylene rich copolymers and propylene rich copolymers after vis-breaking. This correlated well with what was observed in the bulk analyses. However, more information was required to give any conclusive information.

7.5 Analysis of SGEF fractions

Non vis-broken and vis-broken HEPCs were successfully fractionated according to molar mass into ten fractions. SGEF was implemented in order to reduce the molar mass complexity in HEPCs. However, molar mass analyses revealed broad MMDs for the fractions containing ethylene-propylene copolymers and narrow MMDs for the fractions consisting of mainly iPP. This was proof that SGEF was not an ideal preparative fractionation tool for mixtures of homopolymers and copolymers. Furthermore, a shift of the SGEF elution profile towards lower molar masses was observed after vis-breaking. This was due to the peroxide breaking down the long PP sequences. 2D HT-HPLC revealed a significant shift towards higher SEC elution volumes at lower HPLC elution volumes whilst the higher HPLC volumes indicated no shift after vis-breaking. This was due to the peroxide affecting the iPP and propylene rich copolymers and leaving the ethylene rich copolymers unaffected.

7.6 *In situ* Solid-state ^{13}C-NMR analysis

For the first time *in situ* solid state NMR vis-breaking was used to monitor structural changes induced by the reaction of the peroxides with HEPCs *in situ*. The T180 sample with lower ethylene content showed the most structural changes as compared to the T300 sample with a higher ethylene content. The differences in response of the two copolymers lies in the manner in which the ethylene sequences are distributed within them. In T180, the incorporation of the short ethylene sequences led to an increased number of E-P transition points whilst in the T300

sample, the greater ethylene incorporation led to the formation of longer chain ethylene sequences which resembled the behaviour of polyethylenes. Therefore, in the T300 sample, the long chain ethylene sequences lend protection by the enhanced resistance of the ethylene to radical degradation a. However, in the T180 sample, the protection of the long chain ethylene sequences was not available, instead the increased E-P transition points increased the susceptibility to a greater extent than was observed in isotactic PP.

In situ NMR vis-breaking of the T180 and T300 60 °C fractions revealed an increased phase separation between the crystalline and amorphous PE domains. This was due to the peroxide causing a separation between the ethylene rich and propylene rich EP copolymers.

The results obtained in this study revealed that the long chain ethylene sequences were resistant to vis-breaking whilst the long chain propylene sequences were susceptible. Therefore based on the results, it can be concluded that the release of the ethylene rich sequences was as a result of the peroxide attacking the propylene rich sequences

7.7 References

1. Swart, M., *The effect of controlled degradation with an organic peroxide on the molecular characteristics and properties of heterophasic propylene-ethylene copolymers (HECO)*. 2013, PhD Thesis, University of Stellenbosch.

2. Magagula, S.I., *The effect of organic peroxides on the molecular composition of heterophasic ethylene-propylene impact copolymers*. 2015, Masters Thesis, Stellenbosch University.

Appendix

This contains supporting data which could not be shown in the body of the thesis.

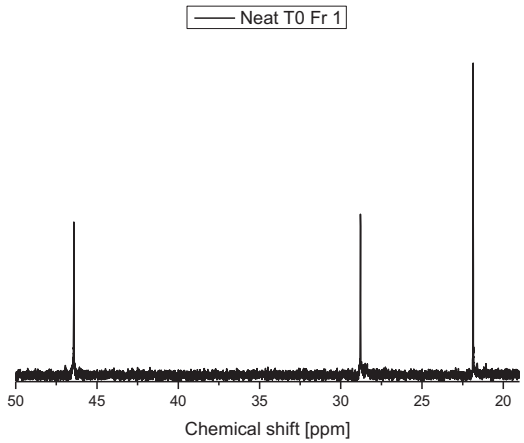

Figure A.1 Solution-state ^{13}C-NMR spectrum for fraction 1 of non vis-broken T0

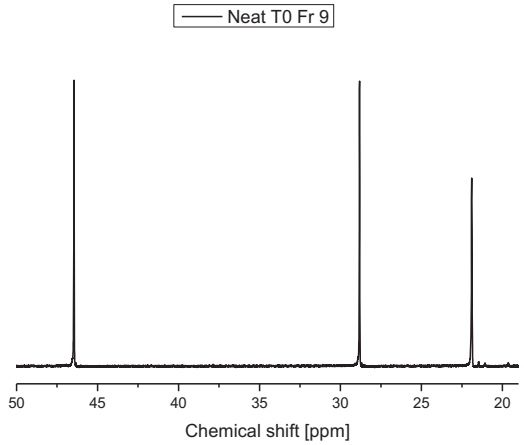

Figure A.2 Solution-state ^{13}C-NMR spectrum for fraction 9 of non vis-broken T0

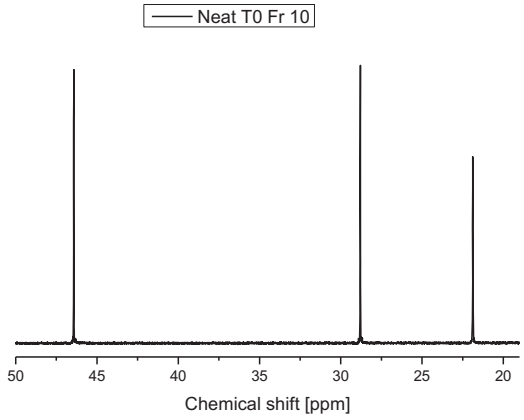

Figure A.3 Solution-state ^{13}C-NMR spectrum for fraction 10 of non vis-broken T0

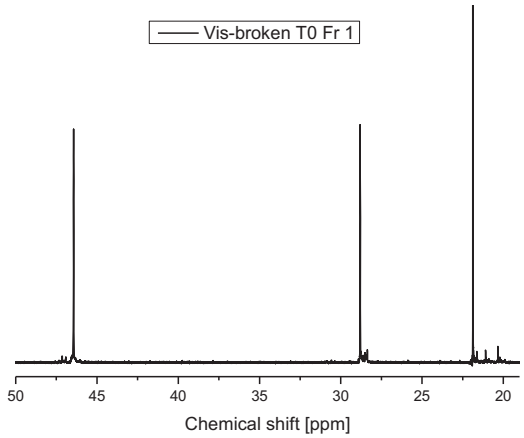

Figure A.4 Solution-state ^{13}C-NMR spectrum for fraction 1 of vis-broken T0

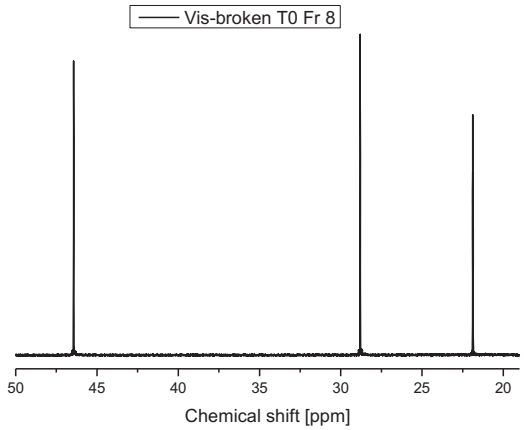

Figure A.5 Solution-state ^{13}C-NMR spectrum for fraction 8 of vis-broken T0

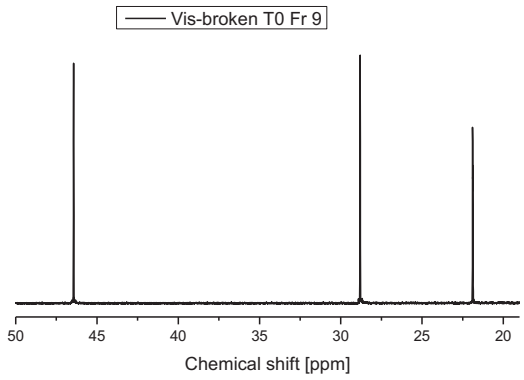

Figure A.6 Solution-state ^{13}C-NMR spectrum for fraction 9 of vis-broken T0

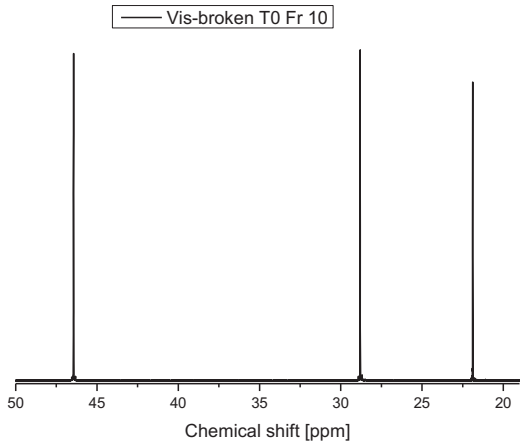

Figure A.7 Solution-state ^{13}C-NMR spectrum for fraction 10 of vis-broken T0

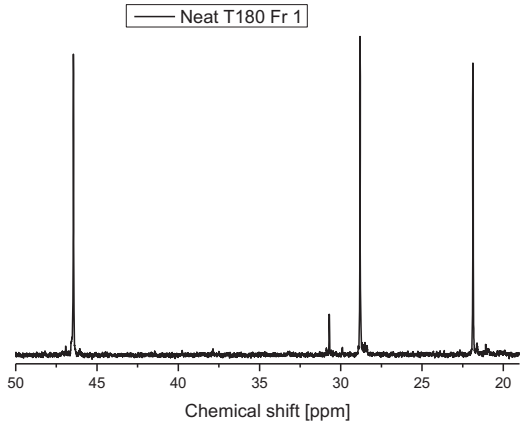

Figure A.8 Solution-state ^{13}C-NMR spectrum for fraction 1 of non vis-broken T180

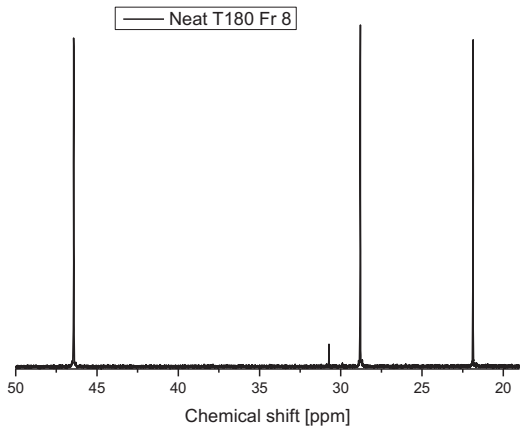

Figure A.9 Solution-state ^{13}C-NMR spectrum for fraction 8 of non vis-broken T180

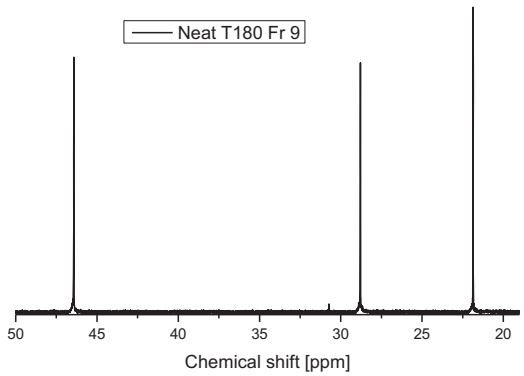

Figure A. 10 Solution-state ^{13}C-NMR spectrum for fraction 9 of non vis-broken T180

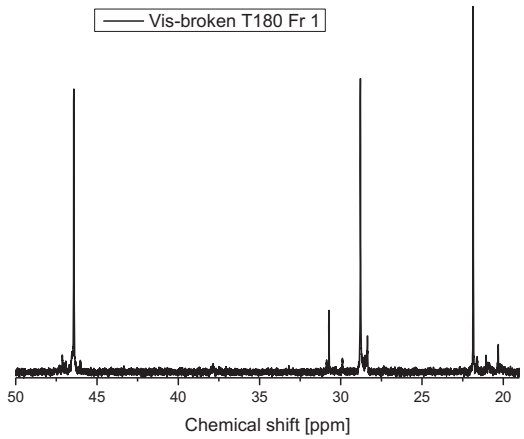

Figure A.11 Solution-state ^{13}C-NMR spectrum for fraction 1 of vis-broken T180

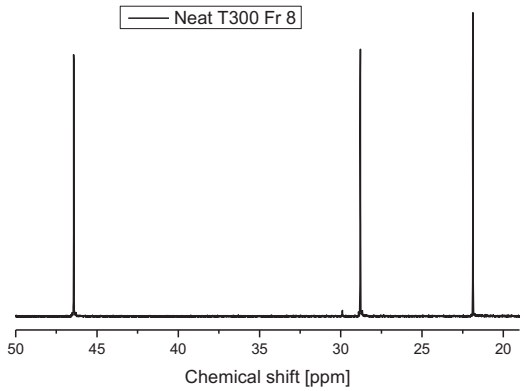

Figure A.12 Solution-state ^{13}C-NMR spectrum for fraction 8 of non vis-broken T300

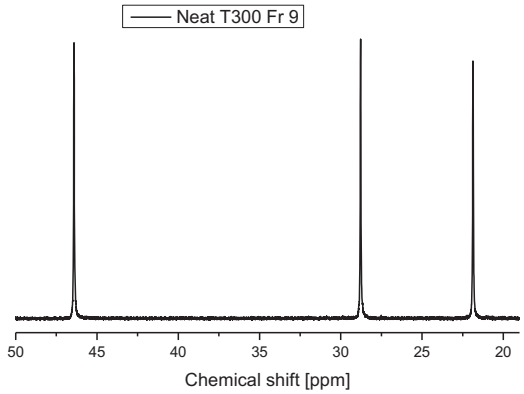

Figure A.13 Solution-state ^{13}C-NMR spectrum for fraction 9 of non vis-broken T300

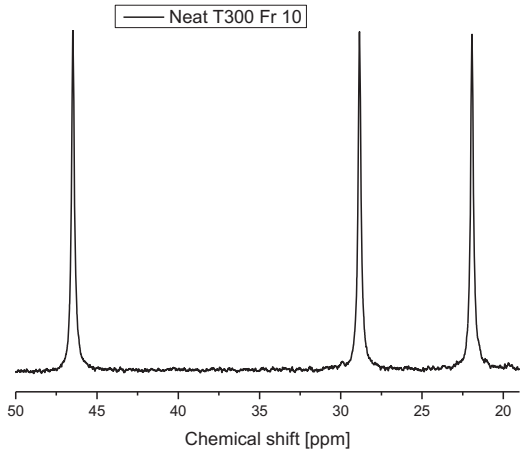

Figure A.14 Solution-state ^{13}C-NMR spectrum for fraction 10 of non vis-broken T300

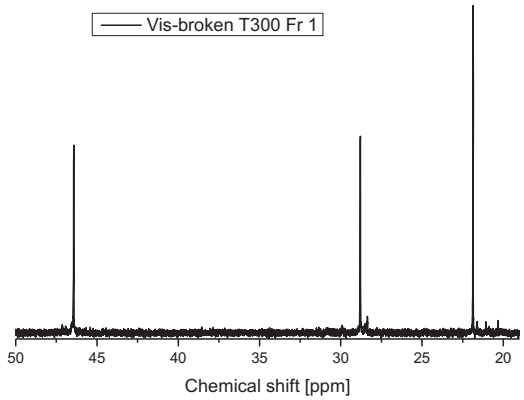

Figure A.15 Solution-state ^{13}C-NMR spectrum for fraction 1 of vis-broken T300

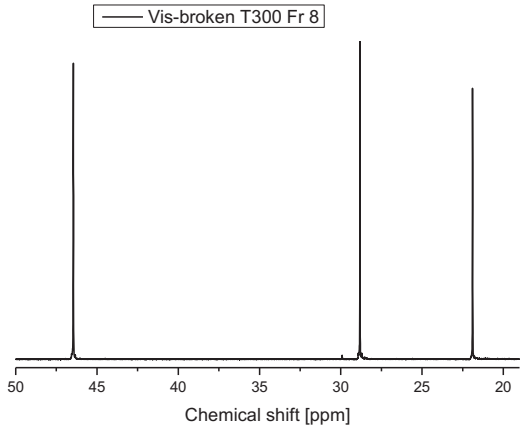

Figure A.16 Solution-state ^{13}C-NMR spectrum for fraction 8 of vis-broken T300

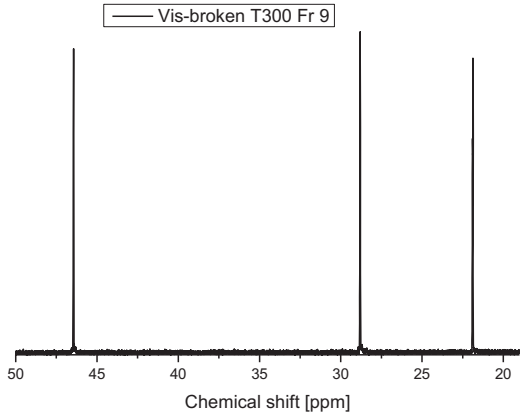

Figure A.17 Solution-state ^{13}C-NMR spectrum for fraction 9 of vis-broken T300

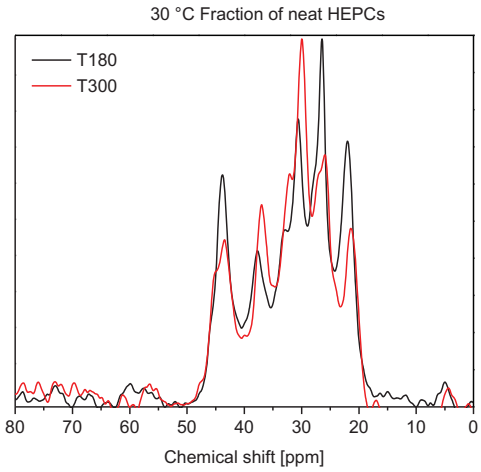

Figure A.18 CP-MAS profiles for the 30 °C fraction of non vis-broken T180 and T300

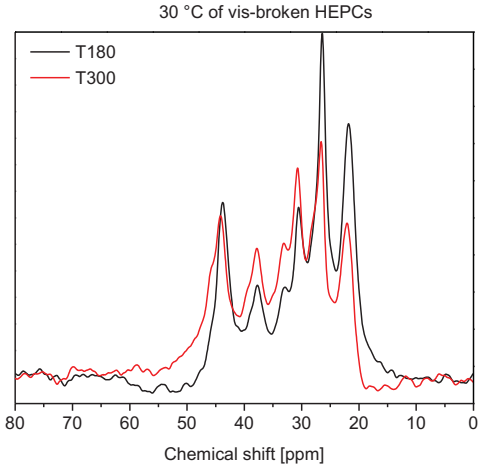

Figure A.19 CP-MAS profiles for the 30 °C fraction of vis-broken T180 and T300

Table A.1 SEC data of the bulk Neat T0 sample and TREF fractions

Fraction	Quantity [wt %]	Mp	Mn	Mw [g/mol]	Mz	PDI
30°C	1.26	26634	5032	46900	196262	9.34
60°C	1.55	2943	6535	78600	345380	12.04
80°C	3.89	209267	15242	185500	720466	12.17
90°C	3.7	15354	24143	218900	804929	9.07
100°C	7.8	32049	25850	122700	618704	4.75
110°C	60	205099	94435	337200	894673	3.57
120°C	20.7	214790	97150	331500	792239	3.41
130°C	1.1	205099	79915	306400	734841	3.84
Bulk	--	183742	46154	249700	633620	5.41

Table A.2 SEC data of the bulk Neat T180 sample and TREF fractions

Fraction	Quantity [wt %]	Mp	Mn	Mw [g/mol]	Mz	PDI
30°C	8.72	394896	7641	295800	1130960	38.7
60°C	3.17	218125	12935	305900	1051280	23.7
80°C	4.1	270943	12439	268600	1053360	21.6
90°C	11.3	33362	26625	97000	495054	3.65
100°C	2.21	15091	17393	200600	1174900	11.5
110°C	57	183362	99553	314100	871229	3.16
120°C	13	258593	156797	402300	917298	2.57
130°C	0.47	239305	41092	304800	658214	7.42
Bulk	--	194848	65022	295000	785478	4.54

Table A.3 SEC data of the bulk Neat T300 sample and TREF fractions

Fraction	Quantity [wt %]	Mp	Mn	Mw [g/mol]	Mz	PDI
30°C	15.5	138736	12176	142479	302706	11.7
60°C	3.53	126737	7924	101597	279329	12.82
80°C	3.7	6093	9799	92173	316891	9.41
90°C	2.87	12927	10834	56460	247161	5.21
100°C	8.55	28241	17708	62194	290656	3.51
110°C	64.8	109375	39250	144760	338079	3.69
120°C	0.717	112702	42679	142664	318120	3.34
130°C	0.32	98587	36407	105507	189553	2.9
Bulk	--	177130	52895	312199	967712	5.9

Table A.4 SEC data of the bulk Vis-broken T0 sample and TREF fractions

Fraction	Quantity [wt %]	Mp	Mn	Mw [g/mol]	Mz	PDI
30°C	1.4	25340	6147	32700	124218	5.33
60°C	2.64	56642	7438	43300	122076	5.82
80°C	3.58	7936	10247	45200	173805	4.42
90°C	4.95	18778	18549	62300	249050	3.36
100°C	17.3	53409	33084	84300	225457	2.55
110°C	64.4	117618	48772	151400	354166	3.1
120°C	5.6	139186	86773	195000	399191	2.25
130°C	0.0691	133004	82981	189500	407618	2.28
Bulk	--	117647	36105	146400	327650	4.06

Table A.5 SEC data of the bulk Vis-broken T180 sample and TREF fractions

Fraction	Quantity [wt %]	Mp	Mn	Mw [g/mol]	Mz	PDI
30°C	11.2	214790	4922	206300	689324	41.9
60°C	4.58	104766	8910	159000	585494	17.9
80°C	4.63	169883	13627	197800	829017	14.5
90°C	3.22	16168	14640	95600	542025	6.54
100°C	10	45797	32377	79900	251006	2.47
110°C	65.1	155056	99110	233600	499359	2.36
120°C	1.21	189060	88198	260000	545770	2.95
130°C	0.063	--	--	--	--	--
Bulk	--	87978	30387	104500	222303	3.44

Table A.6 SEC data of the bulk Vis-broken T300 sample and TREF fractions

Fraction	Quantity [wt %]	Mp	Mn	Mw [g/mol]	Mz	PDI
30°C	15.9	135519	11603	135658	327287	11.69
60°C	5.53	83607	9655	118882	466525	12.3
80°C	5.35	7420	11622	151255	786907	13.01
90°C	3.55	14508	12305	90601	957315	7.36
100°C	11.5	31066	17419	51734	151884	2.97
110°C	56.3	101896	40050	124992	248352	3.12
120°C	1.74	126215	39642	15319	395419	3.87
130°C	0.111	96361	21207	135156	453024	6.37
Bulk	--	86695	32885	100455	214011	3.05

Table A.7 SEC data of the bulk Neat T0 sample and SGEF fractions

Fraction	Vol. % Xylene	Quantity [wt %]	Mp	Mn	Mw [g/mol]	Mz	PDI
Fr 1	12.5	4.84	8167	6057	14300	29010	2.37
Fr 2	20	1.12	11657	8077	16300	28424	2.01
Fr 3	25	0.635	--	--	--	--	--
Fr 4	30	1.3	16929	17634	26500	40775	1.5
Fr 5	50	3.95	23575	24420	49700	215871	2.04
Fr 6	60	5.07	36526	37368	86500	401420	2.32
Fr 7	70	4.67	58975	58267	124600	369860	2.14
Fr 8	80	2.59	73300	69119	158100	518372	2.29
Fr 9	90	14.4	115121	97003	232900	596613	2.4
Fr 10	100	61.4	228459	164136	382200	856366	2.33
Bulk	--	--	183742	46154	249800	633620	5.41

Table A.8 SEC data of the bulk Neat T180 sample and SGEF fractions

Fraction	Vol. % Xylene	Quantity [wt %]	Mp	Mn	Mw [g/mol]	Mz	PDI
Fr 1	12.5	7.15	18004	9875	19200	30247	1.95
Fr 2	20	1.11	21490	11018	21100	32984	1.92
Fr 3	25	0.807	14746	12320	20000	30924	1.62
Fr 4	30	0.977	17852	16555	30900	51537	1.87
Fr 5	50	7.23	93014	37990	151300	508245	3.98
Fr 6	60	8.22	76571	43726	159200	708352	3.64
Fr 7	70	20.01	127148	75017	199700	514432	2.66
Fr 8	80	29.6	141272	71933	204200	487432	2.84
Fr 9	90	15.7	188443	92467	260600	586048	2.82
Fr 10	100	9.17	238008	104781	318200	734793	3.04
Bulk	--	--	194848	65022	295000	785478	4.54

Table A.9 SEC data of the bulk Neat T300 sample and SGEF fractions

Fraction	Vol. % Xylene	Quantity [wt %]	Mp	Mn	Mw [g/mol]	Mz	PDI
Fr 1	12.5	1.48	5857	5722	13300	29370	2.33
Fr 2	25	--	--	--	--	--	--
Fr 3	30	0.954	26847	17435	27200	41549	1.56
Fr 4	50	0.789	23501	20054	31200	47723	1.56
Fr 5	60	15.6	42107	45742	244600	1.14078E6	5.35
Fr 6	70	14.7	78935	84308	384500	1.35981E6	4.56
Fr 7	80	11.9	107952	88277	266400	1.04781E6	3.02
Fr 8	90	27.1	191979	140981	302500	695718	2.15
Fr 9	100	22	332004	218740	493700	1.03975E6	2.26
Fr 10	--	5.49	380589	222415	515000	1.06424E6	2.32
Bulk	--	--	177130	52895	312200	967712	5.9

Table A.10 SEC data of the bulk Vis-broken T0 sample and SGEF fractions

Fraction	Vol. % Xylene	Quantity [wt %]	Mp	Mn	Mw [g/mol]	Mz	PDI
Fr 1	12.5	4.66	8011	6677	54700	738073	8.2
Fr 2	20	0.823	11996	9058	47100	597958	5.2
Fr 3	25	0.356	--	--	--	--	--
Fr 4	30	0.161	--	--	--	--	--
Fr 5	50	5.62	23842	29911	69200	206316	2.32
Fr 6	60	5.85	30582	36042	86600	246160	2.4
Fr 7	70	3.59	91588	55830	138500	354716	2.48
Fr 8	80	44.8	122262	82203	175900	383761	2.14
Fr 9	90	29.9	127918	86117	178800	356889	2.08
Fr 10	100	4.19	133849	91510	190800	400519	2.09
Bulk	--	--	117647	36105	146400	327650	4.06

Table A.11 SEC data of the bulk Vis-broken T180 sample and SGEF fractions

Fraction	Vol. % Xylene	Quantity [wt %]	Mp	Mn	Mw [g/mol]	Mz	PDI
Fr 1	12.5	5.53	7500	4281	10200	20416	2.38
Fr 2	20	0.0146	--	--	--	--	--
Fr 3	25	0.0219	--	--	--	--	--
Fr 4	30	--	--	--	--	--	--
Fr 5	50	21.5	49268	29966	87700	223015	2.93
Fr 6	60	53.9	96167	51388	123300	261756	2.4
Fr 7	70	17.2	98701	55005	126600	252802	2.3
Fr 8	80	1.84	130433	69768	164500	336915	2.36
Fr 9	90	--	--	--	--	--	--
Fr 10	100	--	--	--	--	--	--
Bulk	--	--	87978	30387	104600	222303	3.44

Table A.12 SEC data of the bulk Vis-broken T300 sample and SGEF fractions

Fraction	Vol. % Xylene	Quantity [wt %]	Mp	Mn	Mw [g/mol]	Mz	PDI
Fr 1	12.5	4.93	7692	7021	15300	28301	2.19
Fr 2	20	1.28	12311	9787	18600	30359	1.9
Fr 3	25	0.373	24520	17483	25300	34568	1.45
Fr 4	30	0.508	30042	23448	33000	44840	1.41
Fr 5	50	15.7	29709	39668	108200	292581	2.73
Fr 6	60	14.9	46808	49756	150200	493530	3.01
Fr 7	70	13.2	93346	75085	199800	1.05421E6	2.66
Fr 8	80	38.1	120435	92377	170400	320792	1.84
Fr 9	90	11.1	126004	93988	172549	311941	1.84
Fr 10	100	--	--	--	--	--	--
Bulk	--	--	86695	32885	100500	214011	3.05

Table A.13 DSC data of the bulk Neat T0 and TREF fractions

Fraction	T_m [°C]	T_c [°C]
30°C	--	--
60°C	119.86	89.67
80°C	134.21	103.15
90°C	125.88 / 144.37 / 151.87	112.7
100°C	153.35 / 162.09	113.78
110°C	162.27	113.81
120°C	163.66	114.39
130°C	--	--
BULK	160.71	112.33

Table A.14 DSC data of the bulk Neat T180 and TREF fractions

Fraction	T_m [°C]	T_c [°C]
30°C	--	--
60°C	111.48	62.05/ 78.83
80°C	130.02 / 138.79	96.91
90°C	154.85 / 163.29	113.75
100°C	145.77 / 153.96	111.07
110°C	146.73 / 153.95 / 161.87	114.35
120°C	164	113.62
130°C	--	--
BULK	161.5	111.88

Table A.15 DSC data of the bulk Neat T300 and TREF fractions

Fraction	T_m [°C]	T_c [°C]
30°C	--	--
60°C	93.5 /123.3	74.9 /87.7
80°C	137 /143.5	93.7 / 105.1
90°C	147.1 / 154.1	112.84
100°C	153.7 / 161.9	114.6
110°C	160.4 / 166.8	113.2
120°C	163.4	115.6
130°C	162.4	114.4
BULK	160.9	112.3

Table A.16 DSC data of the bulk Vis-broken T0 and TREF fractions

Fraction	T_m [°C]	T_c [°C]
30°C	--	--
60°C	124.09	90.05
80°C	137.44 / 144.76	105.88
90°C	147.56 / 155.64	112.86
100°C	154.19 / 162.92	113.54
110°C	159.42 / 166.26	113.23
120°C	159.30 / 165.97	115.07
130°C	--	--
BULK	158.14 / 164.59	112.45

Table A.17 DSC data of the bulk Vis-broken T180 and TREF fractions

Fraction	T_m [°C]	T_c [°C]
30°C	--	--
60°C	118.34	80.53
80°C	132.98 / 141.21	101.29
90°C	146.38 / 154.44	112.2
100°C	155.15 / 163.53	113.59
110°C	161.01 / 166.99	113.61
120°C	161.4	114.69
130°C	--	--
BULK	155.11 / 163.53	112.46

Table A.18 DSC data of the bulk Vis-broken T300 and TREF fractions

Fraction	T_m [°C]	T_c [°C]
30°C	--	--
60°C	118.6	68.5 / 80.2
80°C	135.2 / 142.9	103
90°C	146.5 / 154.1	111.2
100°C	153.7 / 162.3	114.3
110°C	159.3 / 166.8	113.2
120°C	159.4 / 165.9	113.4
130°C	--	--
BULK	156.9 / 163.9	111.2

Table A.19 DSC data of the bulk Neat T0 and SGEF fractions

Fraction	T_m [°C]	T_c [°C]
Fr 1	142.3	110.55
Fr 2	144.91	115.37
Fr 3	--	--
Fr 4	--	--
Fr 5	153.9	121.06
Fr 6	156.3	121.43
Fr 7	159.32	120.92
Fr 8	160.1	120.81
Fr 9	162.37	119.41
Fr 10	164.92	116.35
Bulk	160.4	114.16

Table A.20 DSC data of the bulk Neat T180 and SGEF fractions

Fraction	T_m [°C]	T_c [°C]
Fr 1	140.17 / 146.11	107.56
Fr 2	144 / 150.62	113.15
Fr 3	146.82 / 153.97	114.69
Fr 4	145.63 / 154.36	114.75
Fr 5	148.49 / 159.45	115.37
Fr 6	155.84 / 164.30	117.5
Fr 7	161.23	117.11
Fr 8	162.51	117.16
Fr 9	162.88	116.06
Fr 10	163.4	114.84
Bulk	161.5	111.88

Table A.21 DSC data of the bulk Neat T300 and SGEF fractions

Fraction	T_m [°C]	T_c [°C]
Fr 1	142.88 / 152.37	113.8
Fr 2	--	--
Fr 3	151.21 / 158.08	120.17
Fr 4	151.42 / 157.85	120.64
Fr 5	156.12 / 162.61	119.45
Fr 6	161.43	89.25 / 119.23
Fr 7	163.11	97.86 / 120.74
Fr 8	165.88	119.42
Fr 9	166.14	118.52
Fr 10	165.98	119.17
Bulk	159.9	112.78

Table A.22 DSC data of the bulk Vis-broken T0 and SGEF fractions

Fraction	T_m [°C]	T_c [°C]
Fr 1	142.14 / 158.36	114.06
Fr 2	144.81 / 155.72	115.89
Fr 3	--	--
Fr 4	--	--
Fr 5	151.20 / 159.70	116.54
Fr 6	154.54 / 161.80	119.75
Fr 7	158.45	119.94
Fr 8	161	119.55
Fr 9	160.91	118.35
Fr 10	--	--
Bulk	157.85/ 164.59	112.45

Table A.23 DSC data of the bulk Vis-broken T180 and SGEF fractions

Fraction	T_m [°C]	T_c [°C]
Fr 1	138.14 / 145.51	109.11
Fr 2	--	--
Fr 3	--	--
Fr 4	--	--
Fr 5	152.22 / 161.53	117.45
Fr 6	160.71	119.54
Fr 7	161.82	121.32
Fr 8	162.33	122.71
Fr 9	--	--
Fr 10	--	--
Bulk	155.11 / 163.53	112.46

Table A.24 DSC data of the bulk Vis-broken T300 and SGEF fractions

Fraction	T_m [°C]	T_c [°C]
Fr 1	137.29 / 144.29	108.35
Fr 2	141.66 / 148.77	112.35
Fr 3	144.41 / 151.87	72.70 / 114.83
Fr 4		--
Fr 5	150.40 / 159.07	117.77
Fr 6	156.00 / 162.77	119.76
Fr 7	160.95	121
Fr 8	161.64	120.37
Fr 9	161.66	199.32
Fr 10	--	--
Bulk	164.7	111.12